Pablo de Olavide University
Department of Physiology, Anatomy and Cellular Biology

Carlos Andrés Sánchez León

Physiological mechanisms underlying transcranial direct-current stimulation effects on mice somatosensory and cerebellar cortices

Doctoral Thesis directed by
Javier Márquez Ruiz and José María Delgado García

Seville, Spain 2019.

Mr. Javier Márquez Ruiz, Associate Professor of the Physiology, Anatomy and Cellular Biology Department/Experimental Science Faculty at the Pablo de Olavide University, and Mr. José María Delgado García, Full Professor of the Physiology, Anatomy and Cellular Biology Department/Experimental Science Faculty at the Pablo de Olavide University, **DECLARE** that:

The present scientific work entitled "Physiological mechanisms underlying transcranial direct-current stimulation effects on mice somatosensory and cerebellar cortices" has been realized by Mr. Carlos Andrés Sánchez León under their direction and supervision, and it meets the requirements and scientific rigor to be presented and defended as Doctoral Thesis.

Seville, September 26, 2019

Fdo: Javier Márquez Ruiz

Fdo: José María Delgado García

***Partida y regreso: historia de un Hobbit*.**

Por Bilbo Bolsón.

Agradecimientos

En un pequeño pueblo de Extremadura, vivía un joven extremeño, que como tantos otros antes que él tuvo que emigrar para alcanzar sus ambiciones.

Han pasado 6 años desde que comenzara esta andadura científica, muchas personas han entrado a formar parte de mi vida durante todo este tiempo, por lo que considero que la tesis ha supuesto más que un trabajo, una experiencia vital. Entre todas ellas, hay una que destaca, mi director de tesis, no solo un jefe sino un mentor, un compañero y un amigo. Gracias Javier.

Por otra parte, mi más sincero agradecimiento para Javier Medina, por su mentoría durante la estancia y calidad científica, pero sobre todo por su calidad personal y su ayuda en los momentos donde más lo necesité. Un fuerte abrazo. Así mismo, desear lo mejor para mis compañeros durante la estancia, Olivia, Greg, Shane, Shogo, Keiko… espero que nuestros caminos vuelvan a cruzarse.

También me gustaría agradecer el apoyo prestado por mi co-director, José María Delgado, sin el cual hubiera sido imposible obtener los medios necesarios para la realización de este trabajo. Muchas gracias.

La tesis doctoral sirve como formación de los futuros científicos, una gran etapa profesional que representa muchísimos cambios en la forma de pensar y trabajar. Afortunadamente, durante esta transformación me he visto rodeado de una multitud de compañeros cuya amistad desearía mantener de por vida. En este ambiente tan cambiante que es la ciencia, continuamente unos vienen y otros se van, pero los hay que permanecen junto a ti de una u otra manera. Gracias Samuel, Ana, Mar, Flor, Sara, Teresa, José Antonio, Pier…

Junto a las experiencias personales, una de las cosas más maravillosas de este trabajo son los lazos que se crean con personas en una situación similar a la nuestra. El trabajo científico puede ser tan frustrante que sin este apoyo sería mucho más difícil, si no imposible, acabar con buen pie. Ahí estaba Claudia, mi madrina científica, la que me enseñó a dar los primeros pasos en este mundillo. Después me tocó el turno de enseñar a mí, lo que tuvieron que sufrir Bernardo, Laura Castro, Luis o Laura Lalaguna. Aunque

para sufrir, porque aún lo siguen haciendo, tengo que agradecerles todos y cada uno de los momentos juntos a Isa, Guille, Marta, Alejandro y Álvaro, ¡menuda cuadrilla! Finalmente, pero no por ello menos importante, a Alba, que, aunque no sigue haciendo waveform average, sigue junto a nosotros como una compañera más.

Pero no todo es el laboratorio, ni mucho menos. Todo este esfuerzo hubiera sido mucho más pesado sin el grandioso apoyo de mi familia, todos y cada uno de ellos, no solo por haberme hecho la persona que soy ahora sino por empujarme y ayudarme en todo lo que he necesitado para dedicarme a lo que más deseo. Gracias Mamá y Papá por enseñarme a cuestionarlo todo y a creer en mí mismo, sin saberlo habéis creado un mini científico. Gracias Hermana por ser un referente en la vida, tanto personal como profesionalmente, ojalá tuviera tu perseverancia y tenacidad para conseguir tus objetivos, y gracias por ayudarme en todos y cada uno de los pasos que voy dando. Y gracias al peque por… al peque no se le dan las gracias, se le quiere más que a nada, porque hace que cualquier día oscuro se desvanezca en cuanto le oyes reir y darte un besazo de los suyos. Pero, sobre todo, tengo que agradecérselo a una persona en especial, aquella que me hace ser mejor persona porque ella misma es mejor persona, aquella con las mismas ambiciones que yo y con la que hay un entendimiento mutuo. Gracias.

Y por último, agradecérselo a las personas que siempre están ahí, para lo bueno y para lo malo, los amigos de toda la vida, Pedro, Alex, Felipe… los que aparecieron más tarde pero suponen una parte fundamental, Jorge y Violeta, y por supuesto a los flooders del foro, esa amistad que comenzó virtualmente pero acabó formando parte de mi vida más personal.

Resumen

La estimulación transcraneal con corriente continua (tDCS, del inglés *transcranial direct-current stimulation*) es una de las técnicas de estimulación cerebral no invasivas más utilizadas y consiste en la aplicación de corrientes eléctricas débiles a través del cráneo. La técnica comenzó a ganar popularidad hace unos 20 años cuando se demostraron sus efectos neuromoduladores durante la administración del tDCS y, quizás incluso más relevante, permaneciendo durante varios minutos tras el cese de la estimulación. Gracias a los estudios realizados *in vitro*, se sabe que los efectos que se observan en la modulación neuronal de manera inmediata son causados por la polarización de los diferentes compartimentos neuronales (soma, dendritas, axón) causados a su vez por el desplazamiento y redistribución de cargas que el campo eléctrico produce. Por otra parte, los efectos a largo plazo se han relacionado con cambios en los receptores de membrana, modificación de proteínas y actividad glial. Sin embargo, aún existe un gran desconocimiento sobre los mecanismos fisiológicos que subyacen a estos efectos. Por este motivo, el objetivo principal de la presente Tesis Doctoral consistió en el estudio y caracterización de los efectos y mecanismos detrás de la neuromodulación que el tDCS ejerce sobre las cortezas somatosensorial (S1) y cerebelar (CrusI-II) en ratones despiertos. Primero, se comprobó la fuerza del campo eléctrico generado por el tDCS, observando una disminución logarítmica del mismo conforme nos alejamos del electrodo de estimulación cuando se aplica directamente sobre S1 (S1-tDCS) o el cerebelo lateral (Cb-tDCS). Además, el campo eléctrico generado en S1 cuando el tDCS se aplica sobre el cerebelo lateral resultó ser dos órdenes de magnitud inferior al campo eléctrico generado por la aplicación directa del tDCS sobre S1. Posteriormente, se caracterizaron los efectos del tDCS sobre la excitabilidad de S1 y CrusI-II mediante técnicas electrofisiológicas e inmunohistoquímicas. Sobre los resultados con S1-tDCS, hubo una modulación de los campos sensoriales evocados (SEPs, del inglés *sensory evoked potentials*) dependiente de la polaridad y la intensidad de estimulación, con anodal incrementando y catodal disminuyendo la excitabilidad de S1. Sin embargo, tras el cese de la estimulación, únicamente la polaridad catodal mantuvo una disminución de la excitabilidad durante al menos una hora. Estos resultados

concuerdan con el aumento observado en los niveles de GAD65-67 en el hemisferio estimulado tras 20 minutos con tDCS catodal. Con respecto a los resultados con Cb-tDCS, hubo un incremento inmediato de la amplitud de los SEPs registrados en cerebelo durante Cb-tDCS anodal y un descenso con catodal. No obstante, no se observaron efectos a largo plazo tras el cese del tDCS ni en los registros electrofisiológicos ni en los niveles de GAD65-67 o vGlut1. A continuación, se evaluó el impacto del Cb-tDCS sobre regiones distantes interconectadas (S1), mostrando una disminución de la excitabilidad de S1 durante el Cb-tDCS anodal y un aumento tras catodal. Significativamente, tras la disminución inmediata de la excitabilidad de S1 durante los primeros minutos del Cb-tDCS anodal, hubo una vuelta a los valores control en los últimos minutos de la estimulación, e incluso apareció un incremento de la excitabilidad justo al apagar la estimulación con Cb-tDCS anodal. No se observaron cambios tras el Cb-tDCS catodal y no se observaron cambios en los niveles de GAD65-67 o vGlut1 en S1 tras el Cb-tDCS anodal ni catodal. Por último, se exploraron los efectos del Cb-tDCS con un análisis más preciso mediante registros de actividad unitaria en animales despiertos, observándose una modulación heterogénea de la frecuencia de disparo espontánea tanto de células de Purkinje como no Purkinje, dependiente de la polaridad y la intensidad de estimulación. Para desenmascarar las causas de este comportamiento heterogéneo, se procedió a la tinción juxtacelular de las neuronas registradas en animales anestesiados. Los resultados obtenidos mostraron que la orientación del eje somatodendrítico con respecto al campo eléctrico generado por el tDCS fue el principal factor determinante de la modulación de las células de Purkinje. En conclusión, los resultados obtenidos proporcionan una medida directa de los diferentes efectos que el tDCS puede tener sobre diferentes regiones estimuladas y proporciona información sobre la importancia de los posibles efectos sobre regiones distantes que puede tener esta técnica neuromoduladora. Finalmente, los datos presentados en esta tesis constituyen los primeros resultados *in vivo* de la

importancia del eje somatodendrítico sobre los efectos polarizadores que el tDCS puede ejercer.

Abstract

Transcranial direct-current stimulation (tDCS) is one of the most commonly used non-invasive brain stimulation techniques consisting in the application of weak electrical currents through the scalp. The technique began to gain popularity about 20 years ago when its neuromodulatory effects were demonstrated during the administration of tDCS and, perhaps most importantly, lasting several minutes after stimulus cessation. It is known from *in vitro* studies, that immediate observed neuronal modulation is caused by the polarization of the different neuronal compartments (soma, dendrites, axon) caused by the displacement and redistribution of charges due to the electric field. On the other hand, long-term effects have been related with membrane receptors changes, protein modifications and glial activity. However, there are still huge gaps of knowledge about the physiological mechanisms underlying its effects. For this reason, the main objective of the present Doctoral Thesis was to examine and characterize the effects and mechanisms behind the neuromodulation of tDCS in somatosensory (S1) and cerebellar (CrusI-II) cortices in the alert mice. First, the strength of the electric field generated by tDCS was assessed, observing a decay with distance from the electrode in a logarithmic manner when applied over S1 (S1-tDCS) or lateral cerebellum (Cb-tDCS). In addition, the actual electric field generated in S1 when tDCS was applied over lateral cerebellum was two orders of magnitude lower than the electric field generated by tDCS directly applied over S1. After that, tDCS effects on S1 and CrusI-II excitability were characterized by means of electrophysiological and immunohistochemical measures. For S1-tDCS, there was a polarity and intensity-dependent modulation of sensory evoked potentials (SEPs) during the application of transcranial currents with anodal increasing and cathodal decreasing S1 excitability. Nonetheless, after tDCS cessation, just cathodal stimulation maintained a decreased excitability for up to one hour. This result was in accordance with an increase in GAD65-67 levels observed in the stimulated hemisphere after 20 minutes of cathodal tDCS. With respect to Cb-tDCS, there was also an immediate increase with anodal and decrease with cathodal Cb-tDCS of the cerebellar SEPs during the application of the current. Nevertheless, no long-term effects were observed after tDCS cessation for both electrophysiological nor GAD65-67 or vGlut1 levels. After that,

the impact of Cb-tDCS on interconnected distant regions (S1) was evaluated, showing a decrease in S1 excitability during anodal and an increase during cathodal Cb-tDCS. Interestingly, after the instant decrease in S1 excitability observed during the first minutes of anodal Cb-tDCS, there was a return to control levels in the last minutes of stimulation and, intriguingly, an increase in excitability appeared just after anodal Cb-tDCS was switched off. No changes were observed after cathodal Cb-tDCS, and no changes were observed for GAD65-67 or vGlut1 levels in S1 after anodal nor cathodal Cb-tDCS. Lastly, a more detailed analysis of Cb-tDCS effects was explored by single-cell recordings in awake mice, showing a polarity and intensity-dependent modulation of ongoing firing activity of Purkinje and non-Purkinje cells in a heterogeneous manner. To unravel the causes of this heterogeneous behaviour, juxtacellular labelling of the recorded neurons in anesthetized mice was performed. The observed results indicate that the somatodendritic axis orientation with respect to the tDCS-generated electric field was the main factor determining the modulation of the Purkinje cells. In conclusion, present results show direct evidence of the different effects that tDCS may have on different stimulated regions, providing evidence of the importance of potential distant effects induced by this neuromodulatory technique. Finally, the data presented in this thesis constitutes the first *in vivo* experimental evidence of the fundamental role of the somatodendritic axis orientation on tDCS polarizing effects.

Abbreviations:

AC, alternating-current; **CBI**, cerebellar-brain inhibition; **Cb-tDCS**, cerebellar transcranial direct current stimulation; **CS**, complex spike; **DC**, direct-current; **DCN**, deep cerebellar nuclei; **DCS**, direct current stimulation; **ERP**, event-related potential; **GABA**, γ-aminobutyric acid; **M1**, motor cortex; **MMN**, mismatch negativity; **MRS**, magnetic resonance spectroscopy; **NIBS**, non-invasive brain stimulation; **PC**, purkinje cell; **S1**, somatosensory cortex; **SEP**, sensory-evoked potential; **SS**, simple spike; **tACS**, transcranial alternating current stimulation; **tDCS**, transcranial direct current stimulation; **tES**, transcranial electrical stimulation; **TMS**, transcranial magnetic stimulation; **tRNS**, transcranial random-noise stimulation

Index

1 Introduction

In the last decades, several non-invasive brain stimulation (NIBS) techniques have shown their ability to modulate neuronal excitability. Among them, transcranial magnetic stimulation (TMS) and transcranial electrical stimulation (tES) are the most commonly used (Huang et al., 2017). TMS consists in the application of a strong time-varying magnetic field that elicit an electric current (~150 V/m, (Rossi et al., 2009)) inside the brain, whereas tES directly apply weak electric currents (~1 V/m (Opitz et al., 2016)) through the scalp. In contrast to TMS, which is delivered through a sophisticated and expensive device, tES is affordable and readily accessible by non-trained individuals (Brunoni et al., 2012). Besides, even easier and cheaper NIBS techniques have appeared in the last decade, investigating cortical excitability changes by means of static magnetic field (magnets) stimulation (Oliviero et al., 2011; Carrasco-López et al., 2017; Matsugi and Okada, 2017).

Regarding tES, there are several protocols depending on the temporal patterns of applied electric currents. Thus, transcranial direct-current (DC), alternating-current (AC) and random-noise stimulation (commonly known as tDCS, tACS, and tRNS, respectively) have been used to neuromodulate different regions of the brain (Fig. 1.1) (Reed and Cohen Kadosh, 2018; Sánchez-León et al., 2018b, 2018a; Bikson et al., 2019a).

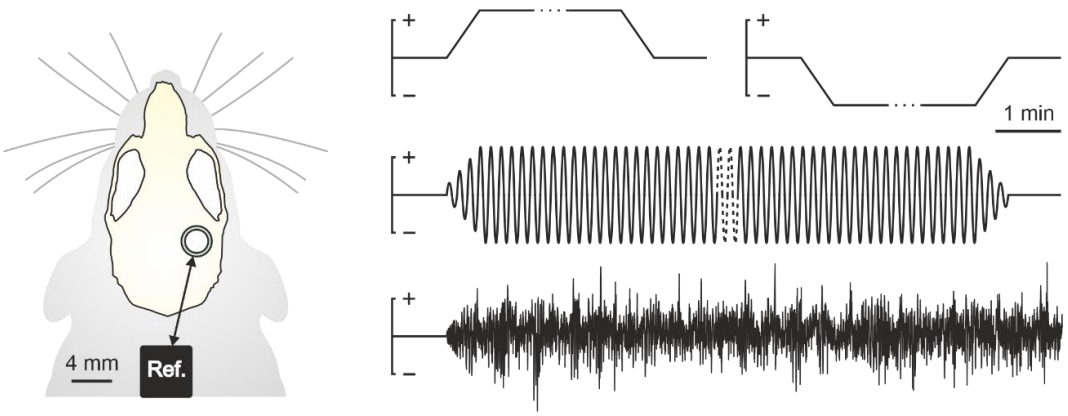

Figure 1.1. Conventional tES protocols. From top to bottom, traces corresponding to transcranial direct-current stimulation (tDCS) (Anodal: left, cathodal: right), transcranial alternating-current stimulation (tACS) and transcranial random-noise stimulation (tRNS). Weak electric currents are applied between an active electrode placed over the region of interest and a distant reference electrode (Ref.) (From Sánchez-León et al., 2018b).

Since the first evidence of Priori (Priori et al., 1998), and the seminal work of Nitsche and Paulus (Nitsche and Paulus, 2000) demonstrating its modulatory effects over motor cortex (M1) excitability, tDCS has gained increasing popularity (Nitsche et al., 2008) and it is now being used in a wide range of neurological and psychiatric conditions (Grimaldi et al., 2016; Reed and Cohen Kadosh, 2018; Stagg et al., 2018; Miterko et al., 2019). Nonetheless, the use of electric currents for the treatment of medical conditions has a long-lasting history dating back a few hundreds of years (Wu, 1984; Sarmiento et al., 2016).

1.1 History of neurostimulation.

The history of electrical stimulation is accompanied by the discovery of electricity itself. Much of the first approaches to understand electricity came from animals able to generate electric discharges, specifically by electric fishes. The earliest records of electric fishes are depictions of the Nile catfish (*Malopterurus electricus*) by ancient Egyptians (Fig. 1.2left), but it is not known if (and how) they experimented with them for clinical purposes. The first reported evidence of electrical stimulation appears a few centuries later (43–48 AC) in the Roman Empire (Fig. 1.2right), when Scribonius Largus in his *De compositionibus medicamentorum* described the headache relieve in a patient by placing a live torpedo fish (*Torpedo torpedo*) over his scalp (Scribonius Largus, 1529). He also prescribes it for the treatment of gout as follows: *"For any type of gout a live black torpedo should, when the pain begins, be placed under the feet. The patient must stand on a moist shore washed by the sea and he should stay like this until his whole foot and leg up to the knee is numb"*. These and similar remedies were copied and recopied by Western medical authorities as Pliny the Elder (23–79 AD) and the Greek physician Claudius Galen (131–401 AD) (Kellaway, 1946).

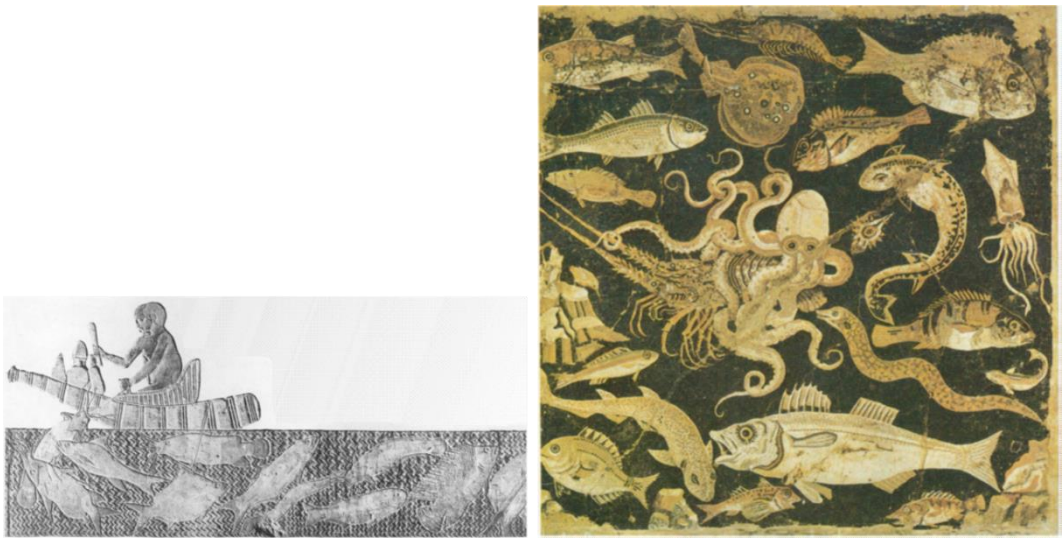

Figure 1.2. Left: Ancient Egyptians knew about the effects of electricity through the Nile catfish (in the picture directly below the rear of the boat), as shown in this bas-relief from the tomb of Ti of the Fifth Dynasty at Saqqarah (~2750 B.C.) (From Gaillard, 1923). Right: Also, the torpedo fish (near the top in the middle of the picture, directly above the tentacles of the octopus) was well known in the classical Roman world, as is indicated by this mosaic found among the ruins of Pompeii (1st century A.D.) (From Feder, 1978).

This kind of stimulation was also known in Persia, where the 11th century Muslim physician Ibn-Sidah suggested the use of torpedo fishes to treat epilepsy (Priori, 2003), and also in South America, where the early explorers and colonists reported that the native Indians treated gout with the powerful electric eel (*Electrophorus electricus*) (Keynes, 1956). However, the scientific method was not stablished in these days, so the effectivity of these treatments is doubtful.

In 1660, the German scientist Otto von Guericke invented the first electrostatic generator (Comroe and Dripps, 1976), and a century later, in 1745, Ewald Georg von Kleist developed the first capacitor in history, the Leyden jar (Keithley, 1999). This device could store electric charge produced from an electrostatic generator, so for the first time in history, experimenters vastly increased the amount of electricity that could be employed in their research. Intriguingly, those who experienced shocks from both, the electric fish and the Leyden jar, were immediately struck by their great similarity (Fig. 1.3).

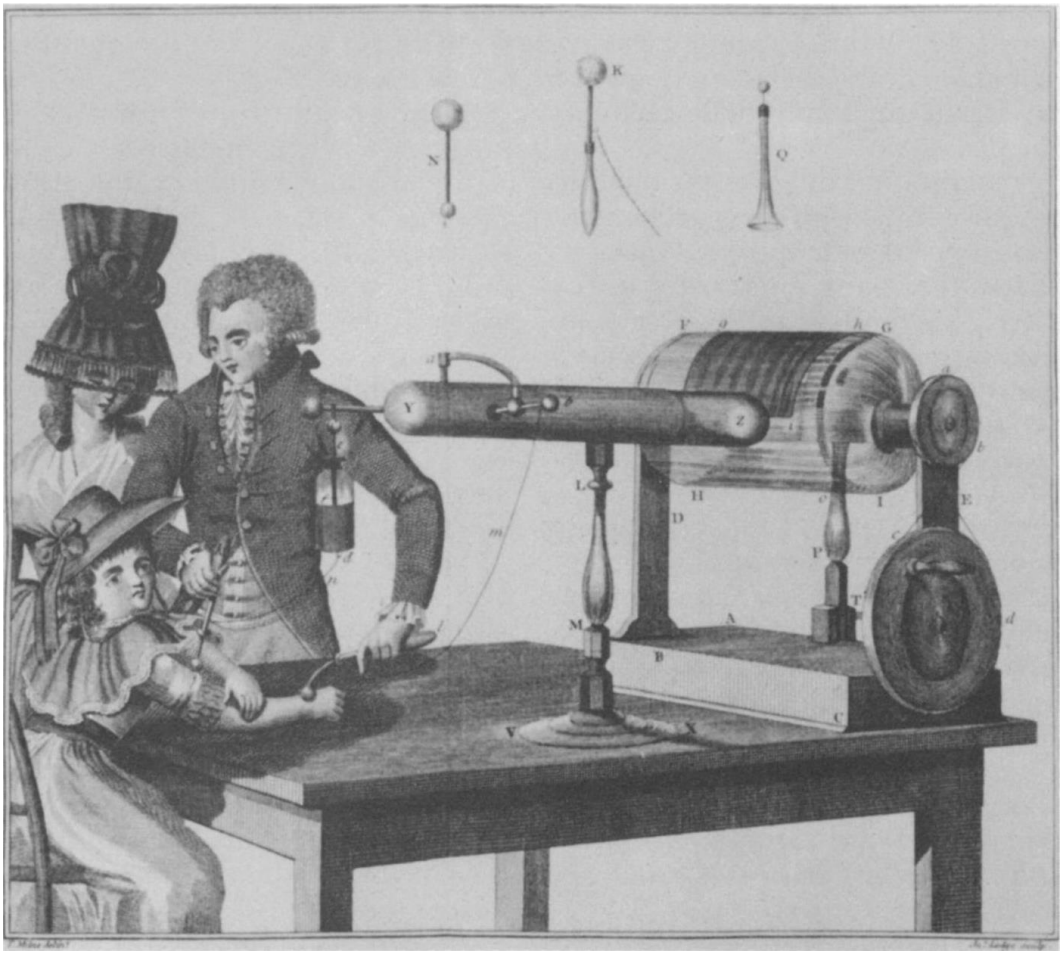

Figure 1.3. Depiction of the apparatuses employed for the first experiments with electric currents in humans. The Leyden jar (labelled "d", below the man's left shoulder) is being used to store electricity generated by the electrostatic machine, at the right (From Adams, 1799).

These discoveries together with the reports in the same years of the existence of the powerful South American eel, led to a scientific battle to determine if the effects of the electric fishes and the Leyden jar were of the same nature (Wu, 1984). In the end, the experiments resolving the dispute were made in 1776 by John Walsh (a member of English Parliament and a fellow of the Royal Society), demonstrating the production of a spark by the electric eel, and laying down the full acceptance of the electrical nature of the discharge. The general acceptance of Walsh's discoveries led to experimenters of the time like Anton de Haen in 1755 (Priestley, 1767) and Benjamin Franklin in 1757 (Franklin, 1757), to use the electric currents for therapeutically purposes again, but instead of electricity from unreliable animal sources, they started working with artificially generated currents.

It was in this environment that Luigi Galvani made his milestone announcement (Galvani, 1791), the observation that frog legs contract under electrical stimulation, thus starting the famous discussion between him and Alessandro Volta about the electrical properties of nerves and muscles. Such discussion led to the establishment of the new science known as Electrophysiology, and to the creation of the first electric battery by mimicking the electric organ of electric fishes (Fig. 1.4).

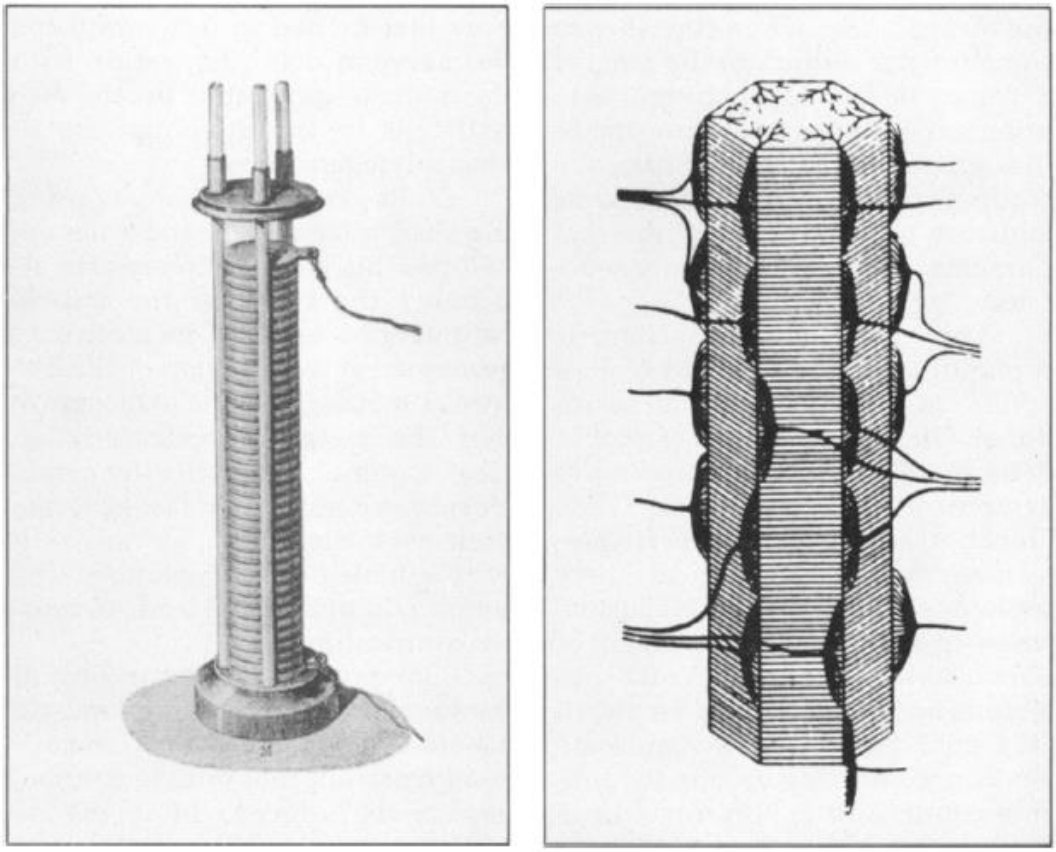

Figure 1.4. Comparison between the first electric battery, the Alessandro Volta's "pile'' (left), and schematic drawing of the vertical columns composing the electric organ of the torpedo (right). Volta named his new apparatus an "artificial electric organ" because it mimicked "the natural electric organ of the torpedo or electric eel" (Volta, 1800) (Figure at left from Dibner, 1952; figure at right from Fritsch, 1890).

In 1804, Giovanni Aldini (1762 – 1834), Galvani's nephew, was one of the first persons to utilize direct current (DC) for clinical applications (but first testing the effects of galvanic currents on his own head (Aldini, 1794), assessing the effects of galvanic currents applied over the head of a patient suffering from melancholy madness (major

depression) and reporting complete recovering after several weeks of treatment (Aldini, 1804) (Fig. 1.5).

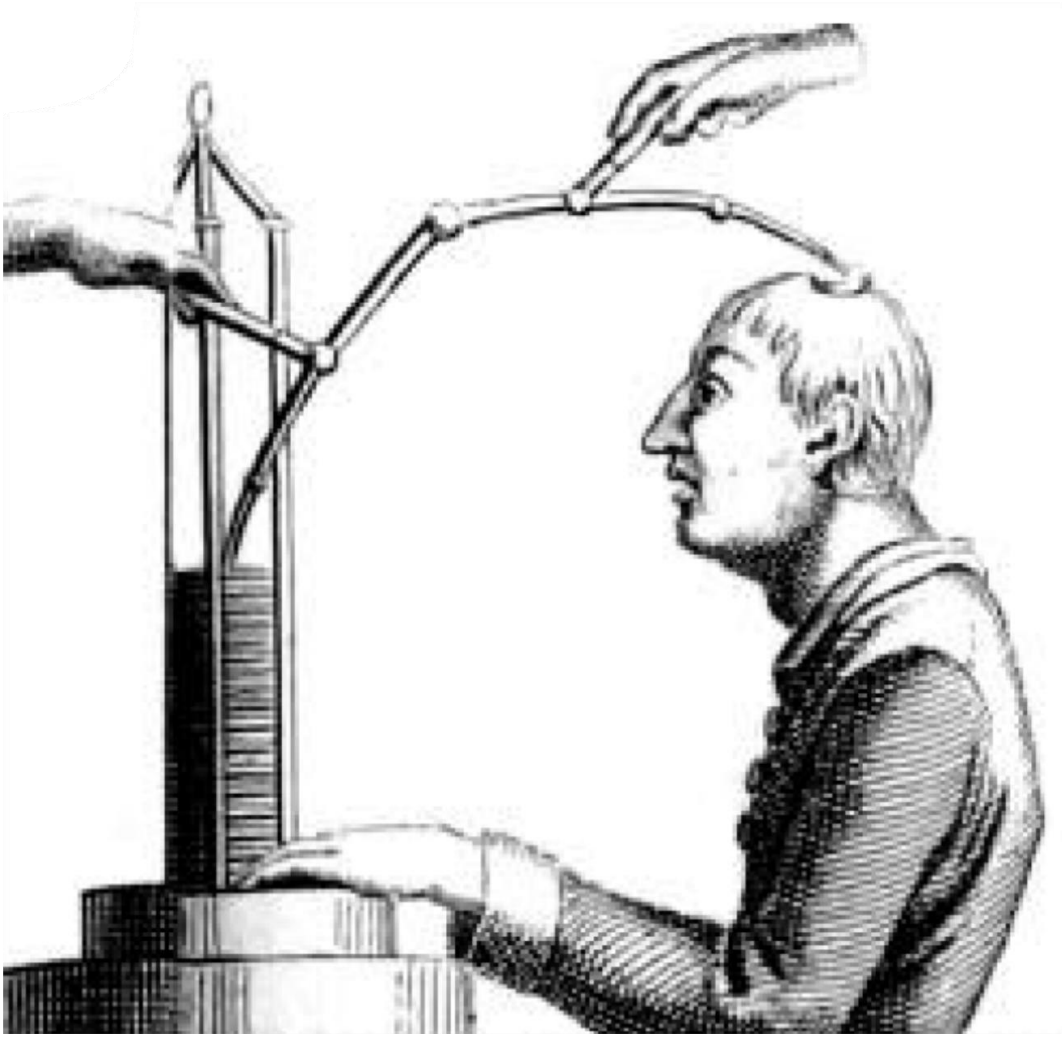

Figure 1.5. Details from plate V in Aldini J, *Essai théorique et experimental sur le galvanisme*. It depicts the application of galvanic currents to Luigi Lanzarini's head (From Parent, 2004).

Aldini's work marked the beginning of a new era for neurostimulation, and around 1880, German psychiatrists, the pioneers in electrotherapy at that time, tried to establish clear rules on the most beneficial application methods and doses. Between 1870 and 1920, electrical medicine was so popular in the United States and Europe that the period is often referred to as the "golden age of electrotherapy" (Geddes, 1984; de la Peña, 2005). During this time, electricity was administered by medical practitioners (both mainstream and alternative) in offices and clinics but it was also widely used by consumers for self-treatment in their own homes (de la Peña, 2003). Just in the United

States, at least 150 different companies sold their own brand of medical battery in this period (Wexler, 2017) (Fig. 1.6).

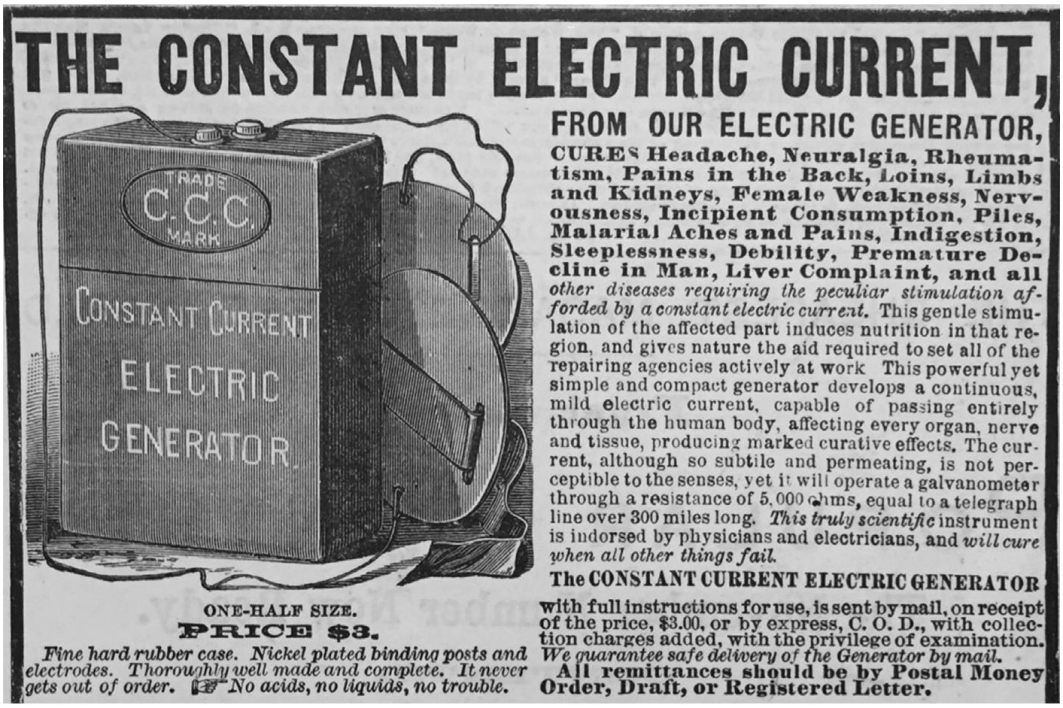

Figure 1.6. An advertisement (1881, Frank Leslie's Newspaper) of a medical battery showing the price (3 $) and a wide variety of diseases that could be cured (From Wexler, 2017).

However, the variation of procedures, the misunderstood effect of polarization and the variable results, led to the decline of the technique, and after the discovery of electroconvulsive therapy in the 1930s, fewer studies focused on weak DC currents. A brief return of subconvulsive stimulation took place between 1957 and late 60's with the discovery of electroanesthesia and electrosleep (Kuzin et al., 1965; Brown, 1975), but side effects and probably the introduction of new psychiatric drugs led once again to the abandonment of the technique. However, after the influence of DC in the cerebral cortex was tested using transcranial magnetic stimulation (Priori et al., 1998; Nitsche and Paulus, 2000), the development of tES and the research about the mechanisms rocketed. Once again, Italians and Germans neuroscientists were the pioneers in electrostimulation.

1.2 Transcranial electrical stimulation (tES) nowadays.

During the last 20 years, more than 5.000 studies have appeared regarding tDCS (PubMed), and the interest in the technique is even increasing (Fig. 1.7). The objective of the present introduction is not to cover all the reported applications related with this technique, but to discuss some of the most relevant aspects related to this non-invasive technique as its neuromodulatory effects or associated brain mechanisms.

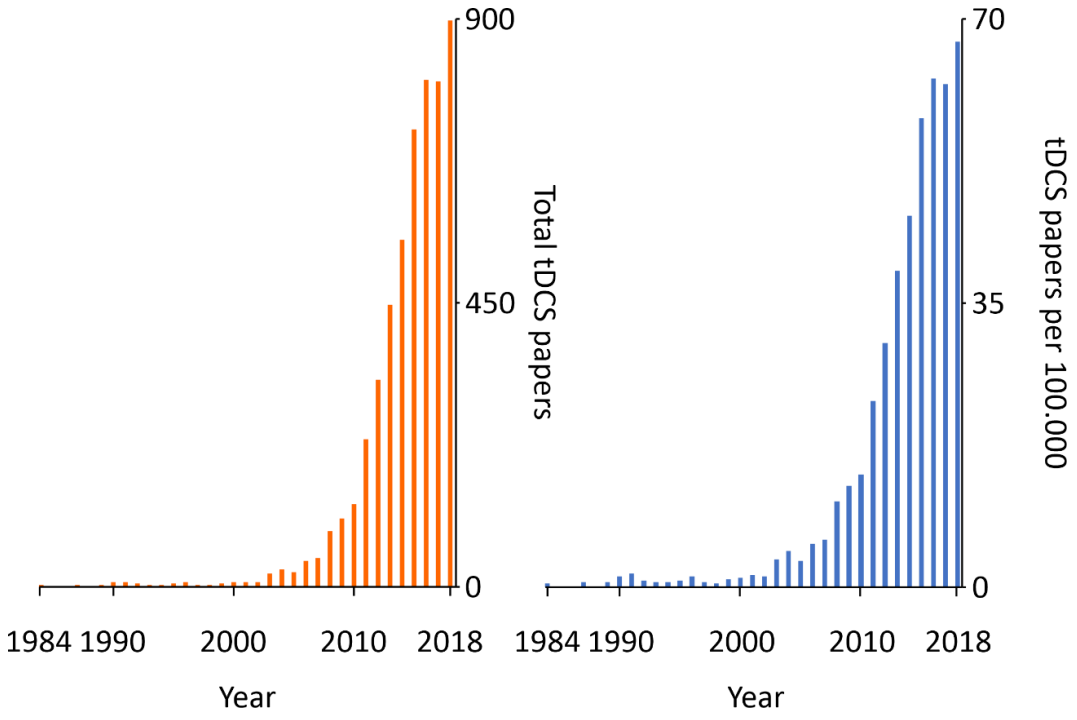

Figure 1.7. Results of a PubMed search for the term "tDCS" at September 10th, 2019. Left: Total articles published per year. Right: Proportion of "tDCS" articles over 100.000 published papers in every year.

Currently, it exists a wide variety of tES techniques (Bikson et al., 2019a), with tDCS and tACS being the most extended. In these two tES techniques, an electrode is placed over the region of interest (termed *active electrode*) and another in a distant region (termed *reference electrode*). For tDCS, the current can be applied in two different polarities, denominated as anodal and cathodal stimulation depending if the active electrode positioned over the stimulated region act as an anode or as a cathode, respectively. Once the capacity of anodal and cathodal tDCS to modulate cortical excitability in a polarity-dependent manner was demonstrated (Priori et al., 1998;

Nitsche and Paulus, 2000), several studies explored the open possibilities by changing the site of stimulation (Grimaldi et al., 2016), electrode positions (Batsikadze et al., 2019), intensity (Jamil et al., 2017), duration (Bikson et al., 2017) or number of electrodes acting as active or reference (Hill et al., 2017). Also, promising experimental results about tDCS are showing its capacity to improve a variety of neurological and psychiatric conditions such as epilepsy (Berenyi et al., 2012; Gschwind and Seeck, 2016; Regner et al., 2018), recovery after stroke (Notturno et al., 2014; Braun et al., 2016; Pikhovych et al., 2016), attention deficit hyperactivity disorder (ADHD) (Salehinejad et al., 2019), schizophrenia (Andrade, 2013; Reinhart et al., 2015a, 2015b; Pinault, 2017), ataxia (Grimaldi et al., 2014b; Benussi et al., 2015), autism (D'Urso et al., 2014; Gómez et al., 2017; Stoodley et al., 2017; Esse Wilson et al., 2018) and even creativity (Hertenstein et al., 2019). The wide range of combinations explored in the literature has the counterpart that, sometimes, it difficult the comparison between studies. For this reason, the standardization of methods and nomenclature become much necessary to increase reproducibility of the results (Bikson et al., 2019a).

Among the cortical areas under investigation, we will focus on primary somatosensory (S1) and cerebellar (CrusI-II and Vermis) cortices modulation. S1 has been modulated with tES in an attempt to modulate sensory perception, thus, several studies have revealed that after cathodal S1-tDCS there is an increase of sensory and pain thresholds (Vaseghi et al., 2015), and during and after cathodal S1-tDCS there is a decrease in tactile discrimination (Rogalewski et al., 2004). Also, an improvement in tactile spatial acuity can be achieved after 20 min of 1 mA anodal S1-tDCS (Ragert et al., 2008) and an improvement of tactile discrimination in stroke patients for dual-hemisphere tDCS over S1 and S2 (Fujimoto et al., 2016). Animal studies also reported the ability of S1-tDCS to potentiate or depress the acquisition of classical eyeblink conditioning by the application of anodal or cathodal stimulation, respectively, suggesting that tDCS modulates the sensory perception process necessary for associative learning (Márquez-Ruiz et al., 2012). Besides, tACS was able to cause sub- or supra-threshold effects depending on the frequency of the applied current, thus frequencies between 30-200 Hz were able to induce motor evoked responses when applied over M1, and to substitute a natural stimulus on the whisker for an artificial

stimulus evoked directly in S1 (Márquez-Ruiz et al., 2016). Summarizing, tES have shown promising results as a tool able to modulate sensory processing.

Apart from cerebral cortex, other regions of the brain have been tested. Among them, the cerebellum is receiving increasing attention as an opportunity to modulate motor (Ammann et al., 2016) but also cognitive functions (Miterko et al., 2019). Celnik's group have demonstrated the ability of cerebellar tDCS (Cb-tDCS) to improve motor skill learning by improving accuracy in the sequential visual isometric pinch task (Cantarero et al., 2015), or by fastening adaptation in a visuomotor transformation task (Galea et al., 2011). Also, Zuchowski and colleagues were able to increase and decrease conditioned response acquisition with anodal and cathodal tDCS, respectively, during eyeblink conditioning (Zuchowski et al., 2014), and other groups revealed the contribution of the cerebellum in verbal working memory (Boehringer et al., 2013) and predictive language processing (Miall et al., 2016; D'Mello et al., 2017) by means of Cb-tDCS.

Furthermore, tDCS es being used to indirectly modulate functionally connected regions of the brain. One of these circuits connect the cerebellum through the thalamus with the cerebral cortex. The Purkinje cells (PC) in the cerebellum exerts an inhibitory tone over M1 cortex that can be assessed with TMS in humans, a phenomenon termed cerebellar-brain inhibition (CBI). Human studies have shown that cathodal tDCS over the cerebellum resulted in a decrease of the inhibition whereas anodal tDCS increased it (Galea et al., 2009; Batsikadze et al., 2019). These results could be explained by the fact that the solely output from cerebellar cortex are the inhibitory PC. Thus, cathodal tDCS could decrease PC activity allowing deep cerebellar nuclei (DCN) to increase its firing rate, hence boosting the glutamatergic di-synaptic connection with the brain cortex, and vice versa for anodal tDCS. Other study measured the mismatch negativity (MMN), an evoked potential recorded in cerebral cortex in response to a rare "oddball" sensory stimuli, while tDCS was applied in the right cerebellar hemisphere, finding an increase in peak amplitude of somatosensory MMN after anodal tDCS and a reduction after cathodal tDCS (Chen et al., 2014). In addition, studies using functional magnetic resonance imaging (fMRI) have shown the ability of Cb-tDCS to modulate functional

connectivity of distant regions connected to the stimulated cerebellum (D'Mello et al., 2017; Stoodley et al., 2017). Together, these studies demonstrate the capacity of tDCS to modulate interconnected regions of the brain.

In addition to the stablished protocols, new tES methods are trying to improve some of the limitations with currently available techniques, demonstrating the feasibility to reach deeper structures or to increase stimulation intensity without proportionally increase scalp sensation. One approach consisted in the use of temporal interfering stimulation, allowing the modulation of hippocampal neurons without affecting the overlying tissue (Grossman et al., 2017), and another uses multiple pairs of electrodes sequentially applying short pulses that converge at specific brain regions, focusing the strongest modulatory effects in a spatially confined area (Vöröslakos et al., 2018).

1.3 Transcranial direct current stimulation (tDCS) mechanisms.

As we have seen, electrical stimulation has been used from long time ago, but despite brief sprouts in popularity its use has not been widely accepted, probably due to the variability observed in the results (Horvath et al., 2015, 2016), and the gaps in knowledge about the mechanisms behind its effects. The simplicity of the technique led many clinical studies using tDCS to employ a simplistic dose strategy where excitability is always increased under the anode and decreased under the cathode, but the diffusion of electric currents across the different body tissues (Miranda et al., 2006) and the interaction with cellular activity has proven to be much more complex (Jackson et al., 2016). For this reason, fine control over the variables affecting neuronal modulation must be achieved to understand how to properly modulate brain activity and associated behaviours. In order to manage this variability, animal model studies are usually needed.

Animal models, including *in vitro* slice preparations, "encéphale isolé" preparations, and *in vivo* anesthetized or awake animal preparations, can cover a wide range of experiments with exquisite control of the variables and more or less proximity to human applications. Furthermore, they boost the possibilities to explore the different

mechanisms underlying tES immediate effects (1) observed in neural activity when the external electric field is simultaneously applied, and the long-term effects (2) that persists when tES is no longer present.

Early works applying weak DC stimulation directly over the brain surface indicated that anodal and cathodal stimulation lead to an increase and a decrease of neuronal excitability, respectively, and showed that the effects were related to changes in membrane potential (Creutzfeld et al., 1962; Purpura and McMurtry, 1964). At the same time, evidence appeared regarding long-term effects after 5 minutes or more of

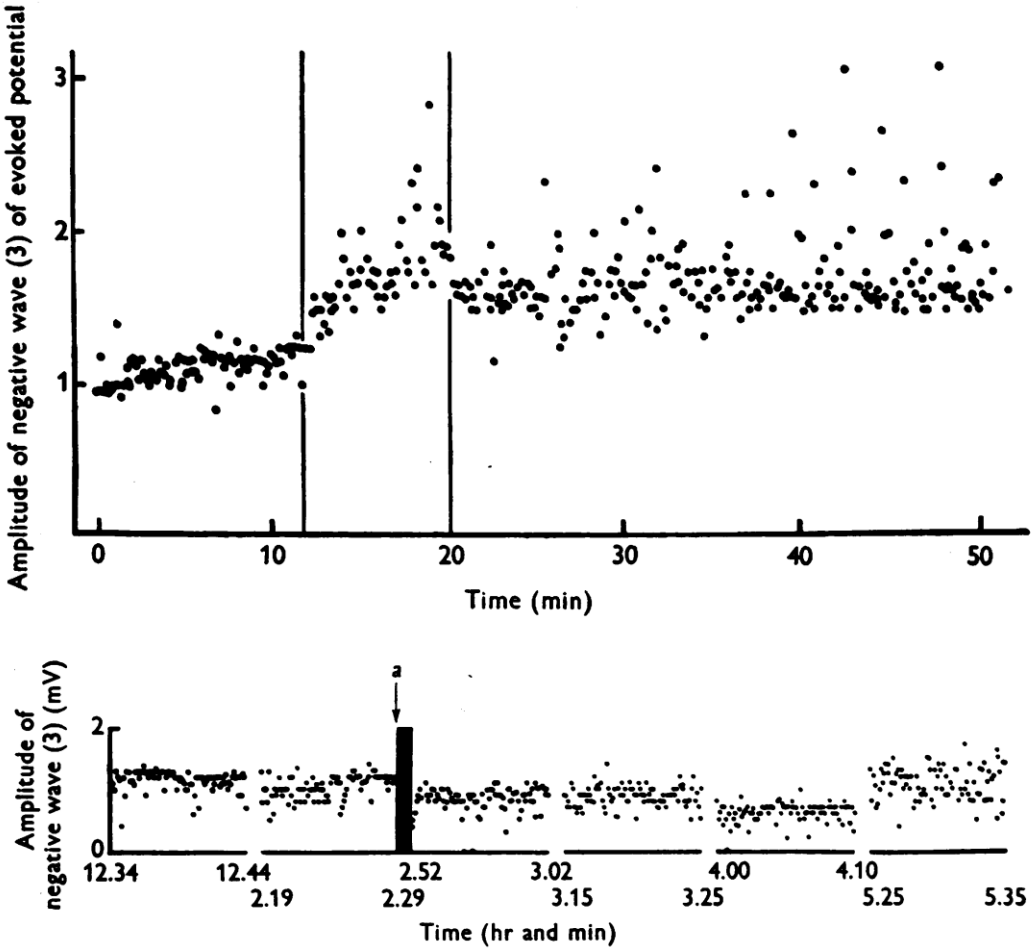

Figure 1.8. Long-term effects observed in peak amplitude of the evoked potential in urethane-anaesthetized rat S1. Increase (top) and decrease (bottom) in amplitude observed after anodal or cathodal epidural stimulation, respectively (From Bindman et al., 1964).

cortical electrical stimulation (Bindman et al., 1964), when no external currents were already affecting membrane potential (Fig. 1.8).

Soon after that, by means of turtles isolated cerebellum, a characterization of the relationship between the applied electric field, cellular morphology and the effects of DC was made (Chan and Nicholson, 1986; Chan et al., 1988), showing that the electric field can modulate different compartments of the same neuron in different ways (i.e. depolarizing the soma but hyperpolarizing the dendrites). Then, several studies appeared in the 90's showing the relevance of Calcium levels and AMPc, through adenosine receptors, for the long-term effects (Hattori et al., 1990; Islam et al., 1995a), and the relevance of NMDA receptors (Islam et al., 1995b).

When the influential papers of Priori (Priori et al., 1998), and Nitsche and Paulus (Nitsche and Paulus, 2000) were published, a renovated interest in tDCS emerged and the knowledge of its mechanisms rapidly expanded (Jackson et al., 2016). *In vitro* studies revealed the basic principles of DC modulation, stating that externally applied electric currents lead to a current flow across the brain, resulting in local membrane hyperpolarization when the current goes into a membrane compartment (positive charges are repelled so the inner part of the membrane has more negative charges resulting in lower membrane potential), and current out of a membrane compartment results in local membrane depolarization (positive charges are attracted so the inner part of the membrane has more positive charges resulting in higher membrane potential) (Bikson et al., 2004; Kabakov et al., 2012; Kronberg et al., 2017). Also, several studies showed that different neuronal features such as the orientation of the somatodendritic axis with respect to the electric field (Bikson et al., 2004), the neuronal morphology (Radman et al., 2009) or the axonal orientation (Kabakov et al., 2012) are going to determine the overall modulation (Fig. 1.9), showing that purely depolarizing or purely hyperpolarizing DCS does not exist.

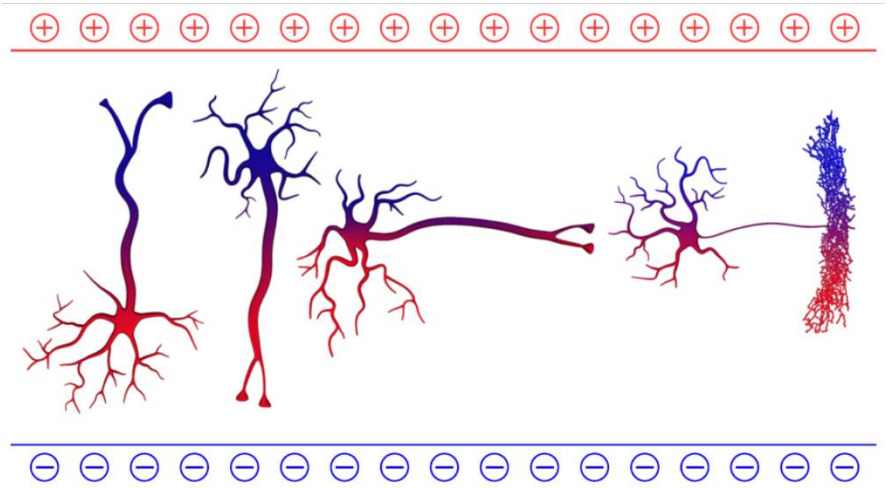

Figure 1.9. Idealized neurons representing the relationship between different neuronal features and tES impact on membrane polarization. The orientation and morphology of the different neuronal compartments (soma, dendrites and axon) with respect to the electric field determine whether the neuron will be net depolarized or hyperpolarized (From Liu et al., 2018).

Furthermore, the complexity of the interaction between externally applied electric fields and neuronal activity has emerge due to *in vitro* and *in vivo* studies demonstrating the modulation of vesicle release probability at presynaptic terminals (Kabakov et al., 2012; Márquez-Ruiz et al., 2012; Bolzoni et al., 2013), and the implication of glial cells (Monai et al., 2016), neurotrophic BDNF (Ranieri et al., 2012), different receptors such as NMDA (Fritsch et al., 2010), mGluR5 (Sun et al., 2016), AMPA (Stafford et al., 2018; Martins et al., 2019) and adenosine (Márquez-Ruiz et al., 2012), together with the activation of early genes participating in protein synthesis (Holmes et al., 2016).

Regarding long-term effects, measurement of neurotransmitters levels in humans with magnetic resonance spectroscopy (MRS) have repeatedly shown a decrease in GABA concentration after anodal M1-tDCS (Stagg et al., 2009; Bachtiar et al., 2018; Patel et al., 2019) and the involvement of GABA and glutamatergic concentrations after cathodal M1-tDCS (Stagg et al., 2009; Bachtiar et al., 2018; Patel et al., 2019). Meanwhile, no changes in neurotransmitters levels have been found after tDCS applied over posterior superior temporal gyrus nor cerebellum (Jalali et al., 2018; Dwyer et al., 2019), a difference that could be due to different parameters of stimulation

or to distinct mechanisms supporting the long-term effects depending on the stimulated region.

Interestingly, a recent paper (Asamoah et al., 2019) even challenge the notion of tES directly affecting cortical neurons, at least for alternating currents (tACS). Instead, they propose a modulation of peripheral nerves as a presumable cause of the observed effects. This work stands out the idea that tES is so easy to apply that we need to know the mechanisms in depth to properly use it.

In addition to the information about the mechanisms, animal models also provide an opportunity to define the safety limits of tES, validate computational models or explore new tES protocols and applications (Sánchez-León et al., 2018a). Although low-intensity currents are applied in humans, concerns about the technique may arise, especially when protocols try to increase intensity or duration, the number of stimulating sessions or when studies are performed in susceptible individuals (e.g., children). Several human trials have been conducted regarding this issue (Nitsche et al., 2004; Kessler et al., 2013; Pirulli et al., 2014; Guarienti et al., 2015), however, the establishment of safety parameters for tES requires characterization of a lesion threshold, a dose-response curve, and the impact of electrical fields on molecular markers that mediate neuroinflammatory processes, for what human experiments cannot be done. It was not until 2009 that the first systematic study about safety aspects of tES was published. In this work, Liebetanz and colleagues evaluated the minimum current density (intensity/electrode surface area), as well as the minimum charge density (current density × time) necessary to cause tissue damage by epicranial tDCS in rats (Liebetanz et al., 2009). The authors estimated a charge density threshold of 52.400 C/m^2 for histological damage, two orders of magnitude above the charge densities usually applied in human studies (171 – 480 C/m^2). Also, no detectable tissue lesion was observed below a current density of 28.6 A/m^2, or between 142.9 and 287.0 A/m^2 when the charge density was set below 52.400 C/m^2, again very far away from current densities usually applied in humans (2 A/m^2). A more recent study (Jackson et al., 2017) in rats reported similar results, with a histological lesion threshold for a current density of 20 A/m^2 and a charge density of 72.000 C/m^2. Nonetheless, neuroinflammatory

responses with density currents below established lesion thresholds have been observed, consisting of an upregulation of the innate immune response after both anodal and cathodal stimulation, as well as an increased number of neural stem cells (Rueger et al., 2012), highlighting the relevance of animal models to understand all possible effects of tES.

1.4 Sensory evoked potentials (SEPs) in animal models.

Besides tDCS promising results, the variability usually observed in human studies reflects the need for a better understanding about the mechanisms governing tDCS effects *in vivo*. For this reason, the work performed in the present Doctoral Thesis aims to bridge the gap between the highly controlled experiments of *in vitro* studies and the highly variable results from human studies. In this regard, event-related potentials (ERPs), which represent an evoked extracellular measure of neuronal activity generated by a population of nearby neurons, allow comparison between human and animal experiments (Modi and Sahin, 2017).

We will focus in sensory evoked potentials (SEPs) which are ERPs evoked by sensory stimulation (Woodman, 2010). When different parts of the body are stimulated (touch, vibration, electricity…) tactile information is send to the central nervous system where it reaches a wide variety of regions in which it will be processed (Bosman et al., 2011). Some of the regions receiving abundant sensory information are the S1 and cerebellar CrusI-II region.

1.4.1 Somatosensory cortex (S1).

In rodents, the whisker-related S1 has received considerable attention. The region receiving whisker information is arranged in a well-defined shape called “barrel cortex”, which occupy a large portion of the rodent brain and is somatotopically organized in an almost identical fashion to the distribution of the whiskers on the snout (Woolsey and Van der Loos, 1970; Petersen, 2007) (Fig. 1.10). Furthermore, rodent experiments allow an in-depth analysis of its functional role in sensory processing (Peron

et al., 2015), goal-directed behaviours (Yamashita and Petersen, 2016) or the crucial issue of its state-dependency of sensory processing (Castro-Alamancos, 2004).

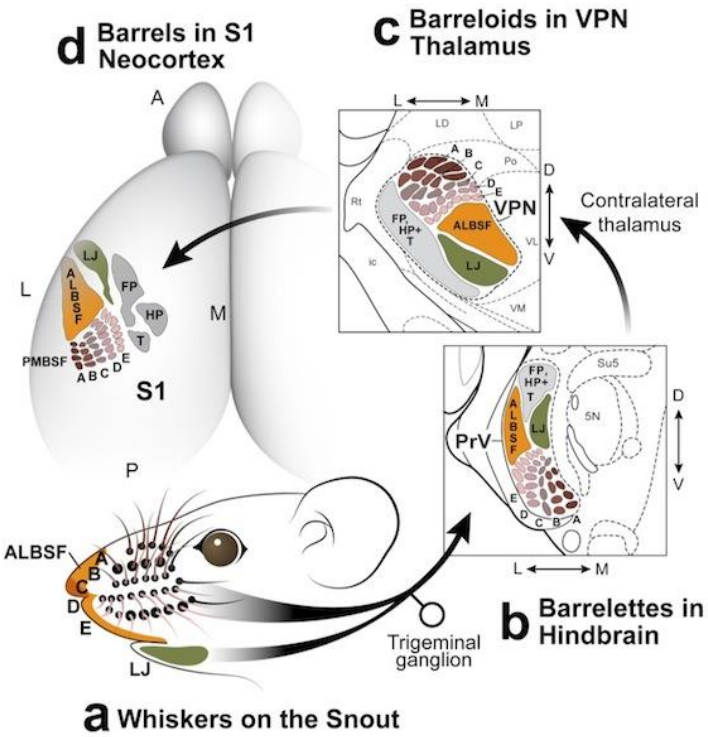

Figure 1.10. Schematic representation of mice whiskers somatosensory system. a) Neurons whose cell bodies reside in the trigeminal ganglion transmit sensory information from each individual whisker (a) to the rostral principal nucleus (PrV, a part of the trigeminal nucleus) in the hindbrain (b). The whiskers somatotopic map is arranged in barrelettes in the hindbrain that send their axons to contralateral sensory thalamus to innervate the ventroposterior nucleus (VPN) forming the barreloids (c). Finally, thalamocortical axons innervate S1 barrel cortex maintaining the somatotopy (d) (From Zembrzycki et al., 2013).

In behaving animals, SEPs in S1 can be recorded after tactile or electrical stimulation of the whiskers (Castro-Alamancos and Oldford, 2002; Márquez-Ruiz et al., 2012; Le Merre et al., 2018) and tDCS have shown its ability to modulate the amplitude of this SEP in a polarity and intensity-dependent manner (Márquez-Ruiz et al., 2012, 2016). This results have also been confirmed in humans, where an increase of SEP amplitude is observed after anodal stimulation of S1 (Sugawara et al., 2015) or M1 (Matsunaga et al., 2004), and a decrease in amplitude is observed after cathodal tDCS over S1 (Dieckhöfer et al., 2006; Vaseghi et al., 2015). Furthermore, the studies by Dieckhöfer and col. And Matsunaga and col. assessed the effects of both polarities, but

they reported SEP amplitude changes just for anodal (Matsunaga et al., 2004) or cathodal (Dieckhöfer et al., 2006) tDCS. Nonetheless, the measures of cortical excitability are explored after tDCS and not during stimulation, so it cannot be ruled out the possibility of an immediate effect of tDCS with absence of long-term changes after stimulation.

1.4.2 Cerebellum.

The basic cellular composition of the cerebellum was determined well over a century ago (Ramon y Cajal, 1909), and its structural and functional organization it is well-stablished (Voogd and Glickstein, 1998; Cerminara et al., 2015; Eccles, 1976), pointing to the PC as a fundamental part of the network and the solely output from cerebellar cortex. The adult mammalian cerebellum is anatomically segmented into ten primary lobules separated from one another by a series of fissures (Larsell, 1952) (Fig. 1.11). However, although all lobules contain the same canonical microcircuit, each part of the cerebellum is related with different regions of the cerebral cortex (Buckner et al., 2011).

The cerebellum have been traditionally associated with motor learning and coordination (Ito, 2002), but the evidence accumulated points to an involvement in sensorimotor and cognitive functions too (Schmahmann and Sherman, 1998; Schmahmann, 2001; Ramnani, 2006; Bostan and Strick, 2018). Particularly, CrusI-II lobules of the cerebellar cortex have been associated with sensory processing (Bower and Woolston, 1983; Bengtsson and Jörntell, 2007; Márquez-Ruiz and Cheron, 2012) in a close relation with prefrontal and S1 cortices (Ramnani, 2006; Miall et al., 2016; Stoodley et al., 2017), and fMRI studies have shown some evidence that anodal tDCS increase activity in right Crus I-II (D'Mello et al., 2017; Stoodley et al., 2017).

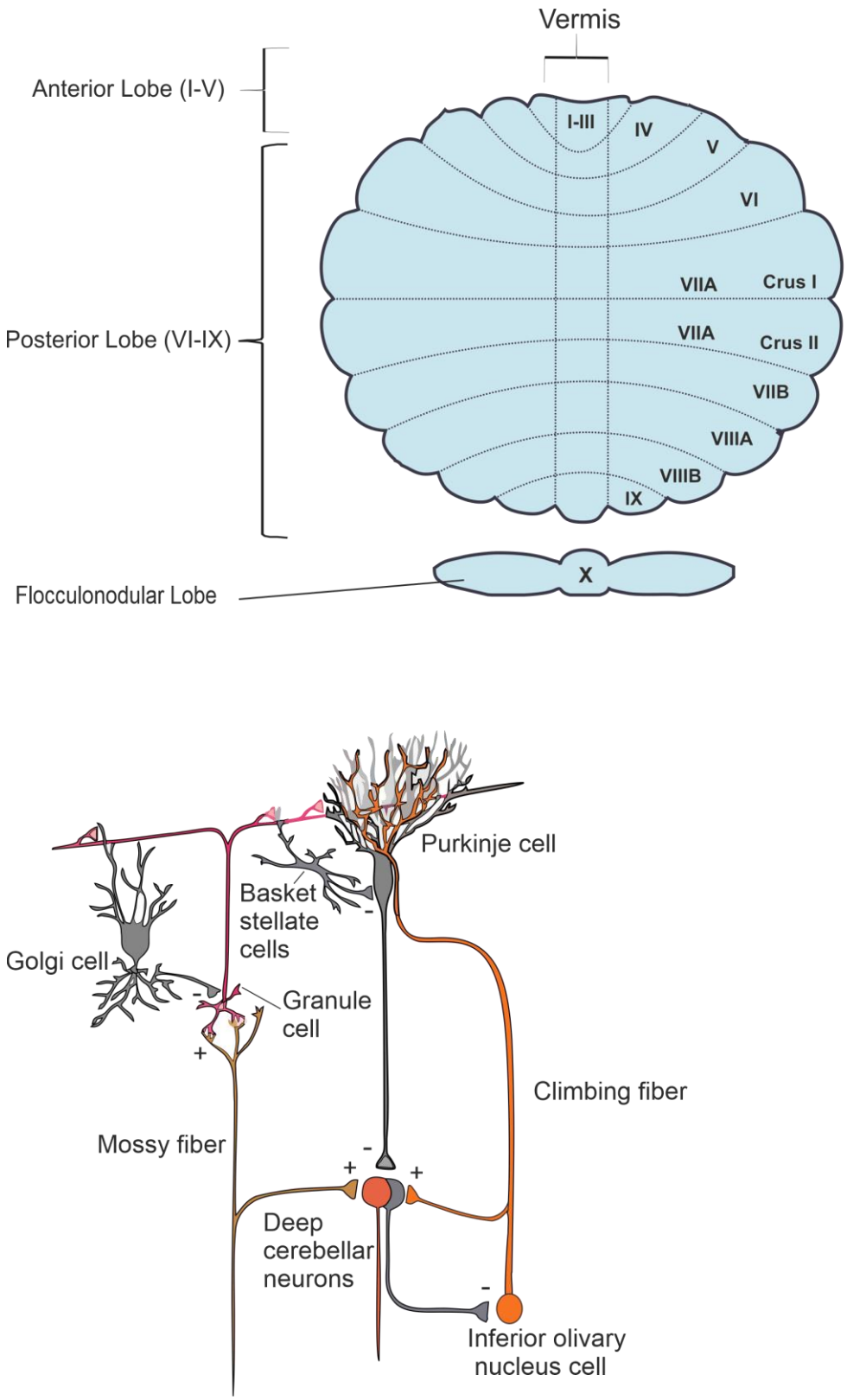

Figure 1.11. Schematic representation of cerebellar lobules (left) and main cerebellar circuit (right). (From Fernández et al., 2019).

In behaving animals, after tactile or electrical stimulation of the whiskers, a SEP is also recorded in CrusI-II (Mapelli and D'Angelo, 2007; Roggeri et al., 2008; Márquez-Ruiz and Cheron, 2012) with several components that reflect inputs from the trigeminal ganglion and from cerebral cortex (Morissette and Bower, 1996; Brown and Bower, 2002) (Fig. 1.12).

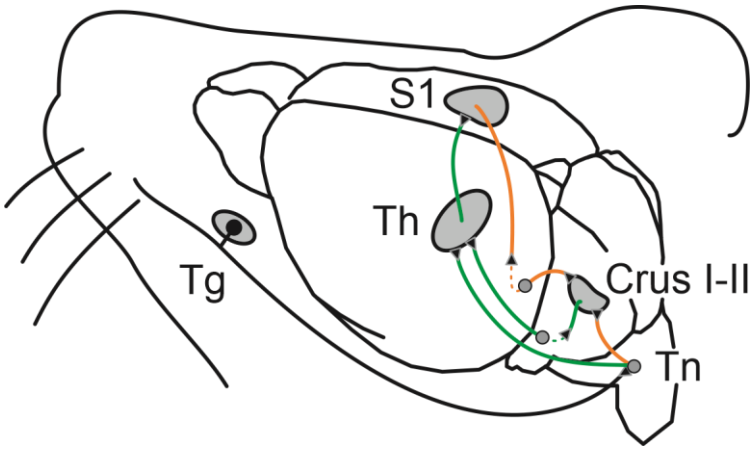

Figure 1.12. Schematic simplification of the mice whisker circuit connecting somatosensory and cerebellar cortices. Sensory information from whiskers is conveyed through Tn in the midbrain (black trace) to cerebellar CrusI-II by two different pathways (orange traces); a direct input comes from Tn and an indirect afference arrives from S1 (through pontine nucleus (orange dotted line), not showed in the figure). Also, CrusI-II projects back to S1 through deep cerebellar nuclei (not showed in the figure (green dotted line)) and Th. Abbreviations: Somatosensory cortex (S1), thalamus (Th), trigeminal ganglion (Tg) and trigeminal nucleus (Tn).

Also, it is known that S1 is highly interconnected with the cerebellum (Schmahmann, 2001; Ramnani, 2006; Buckner et al., 2011). S1 information can reach the cerebellar cortex by its two inputs, from the mossy fibers through the pontine nucleus (Allen et al., 1979; Leergaard et al., 2000; Nagao, 2004; Odeh et al., 2005) and from the climbing fibers through the inferior olive (Swenson et al., 1989; Lawrenson et al., 2016). Also, the cerebellum projects to S1 through the thalamus (Proville et al., 2014), closing the loop between this two areas.

For these reasons, in the present Doctoral Thesis we will mainly focus in the analysis of SEPs evoked in S1 and CrusI-II and the ability of tDCS to modulate them directly and indirectly through the stimulation of the other. Also, a characterization of

neurotransmitters levels will be carried out by the analysis of GAD65-67 (enzyme that catalyzes the decarboxylation of glutamate to GABA) and vGlut1 (protein bound to vesicles transporting glutamate) levels, and the detailed effects of tDCS will be explored by means of single-cell recordings during tDCS.

2 Objectives

tDCS is a non-invasive neuromodulation technique that is being applied to induce changes in neuronal excitability. Typical protocols consist in the application of several minutes of non-invasive weak electric currents to the scalp through strategically positioned electrodes. The technique began to gain popularity about 20 years ago when its neuromodulatory effects over the human motor cortex were demonstrated, consisting in an increase or a decrease (depending on the electrodes polarity) of cortical excitability during the administration of tDCS and, perhaps most importantly, lasting several minutes after stimulus cessation. Since then, there have been an increasing interest from clinicians and neuroscientists and it have been used to alter psychological, motor, and behavioural processes, as well as clinical symptoms in neurological and psychiatric diseases. However, despite promising results, a lot of variability is observed in human experiments, with subjects showing no response or even contradictory results. Thus, for tDCS to be used effectively, it is crucial to properly understand the physiological mechanisms of action. These have been increasingly elucidated during the last years, but it is still necessary to address several critical gaps in our knowledge. In this way, animal models can help to disentangle the physiological mechanisms associated to this type of neuromodulation.

For these reasons, the **general aim** of this study was to examine and characterize the effects and mechanisms behind the neuromodulation of tDCS in S1 and cerebellar cortices in mice. For this purpose, the following **specific objectives** were addressed experimentally:

1- Characterize the effects of tDCS applied over S1 by electrophysiological and immunohistochemical analysis of S1.

2- Determine the effects of tDCS applied over lateral cerebellum by electrophysiological and immunohistochemical analysis of the cerebellar cortex.

3- Investigate the immediate effects of tDCS on single-cell activity, focusing on the relationship between somatodendritic axis orientation and modulation of firing activity.

4- Explore the effects of tDCS applied over lateral cerebellum by electrophysiological and immunohistochemical analysis of S1.

3 Materials and methods

3.1 Animals.

Experiments were carried out on adult males C57 mice (University of Seville, Spain) weighing 28–35 g. Before and after surgery, the animals were kept in the same room but placed in independent cages. The animals were maintained on a 12-h light/12-h dark cycle with continuously controlled humidity (55 ± 5%) and temperature (21 ± 1 °C). All experimental procedures were carried out in accordance with European Union guidelines (2010/63/CE) and following Spanish regulations (RD 53/2013) for the use of laboratory animals in chronic experiments. In addition, these experiments were submitted to and approved by the local Ethics Committee of Pablo de Olavide University (Seville, Spain).

3.2 Experimental groups.

A total of four sets of experiments were carried out in the present doctoral thesis. The first set (**Set 1, n = 43**) consisted on the characterization of tDCS effects over S1 cortex by electrophysiological and immunohistochemical methods. In the second set (**Set 2, n = 111**) tDCS was applied over lateral cerebellum and the modulation of the cerebellar cortex was assessed by electrophysiological and immunohistochemical means. The next group was very similar to Set 2, but with tDCS being applied over cerebellar Vermis (**Set 3, n = 27**) for single-cell recordings and juxtacellular labeling. Finally, tDCS was applied over lateral cerebellum but the electrophysiological and immunohistochemical analysis were carried out in S1 (**Set 4, n = 66**).

3.3 Surgery.

Animals were anesthetized with a ketamine–xylazine mixture (Ketaset, 100 mg/ml, Zoetis, NJ., USA; Rompun, 20 mg/ml, Bayer, Leverkusen, Germany) at an initial dosage of 0.1 ml / 20 g. Animals were prepared for chronic electrophysiological recordings in cerebral (S1) and cerebellar (CrusI-II and Vermis) cortices during simultaneous tDCS.

Under aseptic conditions, an anteroposterior (AP) incision in the skin along the midline of the head, from the front leading edge to the lambdoid suture, was performed. The skull covering the cerebellum was exposed by retracting the muscles over the occipital bones. Subsequently, the periosteum of the exposed surface of the skull was removed and washed with saline. The animal's head was correctly positioned to mark the position of Bregma as stereotaxic cero.

For tDCS administration in Set 1, 2 and 3 experiments, custom-made silver ring-electrodes were manufactured. A silver wire (ø: 635 µm; A-M Systems, WA., USA) was cut into pieces of 1 cm length and one end was curved and welded to form a close loop. Subsequently, this end was pressed with pliers to flatten the surface and create a 2.5 mm inner ø, 3.5 mm outer ø stimulation surface that was chlorinated. In order to insulate the wire, the electrode was introduced into a flexible tubing (inner ø: 0.508 mm; outer ø: 0.939 mm; wall thickness: 0.215 mm; Silicone Tubing, A-M Systems), exposing both ends. The silver ring-electrode was soldered to a connector pin.

Depending on the experiment, the silver ring-electrode, which acted as the active electrode for tDCS, was placed over the skull centered on the right S1 barrel cortex (antero-posterior = − 0.9 mm; Lateral = -3 mm; relative to bregma (Paxinos and Franklin, 2004) (Set 1, Fig. 3.1*A*)), on the left CrusI-II (antero-posterior = − 6 mm; Lateral = +2 mm; relative to bregma (Paxinos and Franklin, 2004) (Set 2, Fig. 3.1*B*)) or on the cerebellar Vermis (Antero-posterior = − 6 mm; Lateral = 0 mm; relative to bregma (Paxinos and Franklin, 2004) (Set 3, Fig. 3.1*C*)). The tDCS active electrode was covered with dental cement (DuraLay, Reliance dental Mfg. Co., Ill., USA) making sure not to pour it between the electrode and the skull. After that, a hole (2 mm ø) was drilled in the bone inside the ring-electrode to expose the cortex. The dura mater surface was sealed with wax bone (Ethicon, Johnson & Johnson, NJ., USA) until recording sessions.

For Set 4 (Fig. 3.1*D*) and those experiments where the brains had to be processed for immunohistochemical analysis, the active electrode for tDCS was a polyethylene

tubing (inner ø: 2.159 mm; outer ø: 0.325 mm; wall thickness: 0.546 mm; A-M Systems) placed over the stimulated region. No trepanation was made to avoid tissue damage.

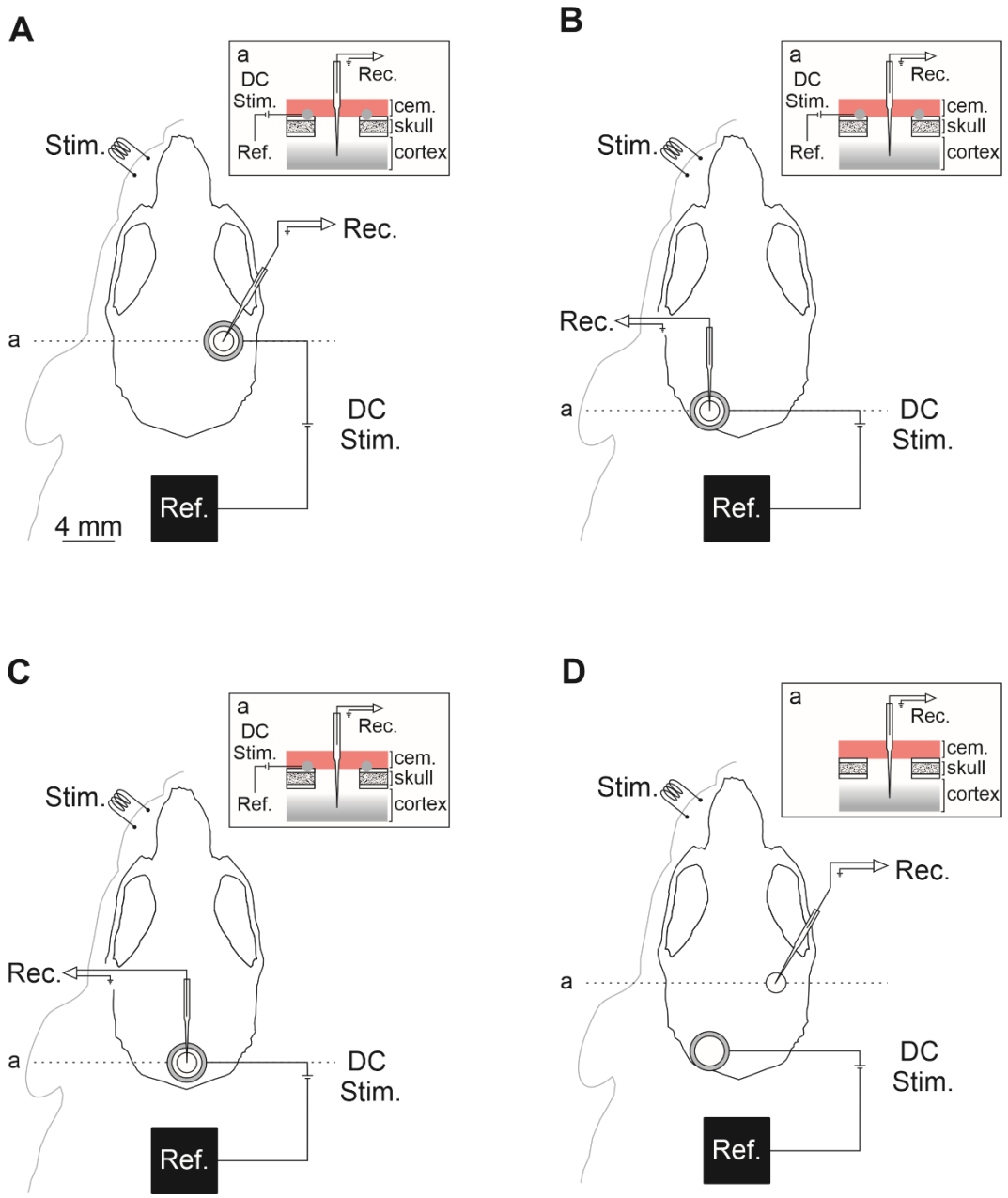

Figure 3.1. Experimental design for *in vivo* electrophysiology in the awake mice. *A*) Preparation for experiments of Set 1 with concurrent tDCS and recordings on S1 cortex. *B*) Preparation for experiments of Set 2 with concurrent Cb-tDCS and recordings on CrusI-II. *C*) Preparation for experiments of Set 3 with concurrent Cb-tDCS and single-cell recordings on Vermis. *D*) Preparation for experiments of Set 4 with Cb-tDCS over lateral cerebellum and recordings on S1 cortex.

A silver electrode (ø: 381 µm, A-M Systems) was used as electrical reference for all the experiments. It was cut into pieces of 1 cm length, a loop (2 mm ø) was made at one end to facilitate posterior grasping by the amplifier equipment and the opposite end of the electrode was braided and filed to avoid damaging the dura mater. Then, it was placed over the dura surface under the left parietal bone (Antero-posterior = − 0.9 mm; Lateral = + 3 mm; relative to bregma (Paxinos and Franklin, 2004)).

Finally, a head-holding system consisting of three bolts screwed to the skull and a bolt placed over the skull upside down and perpendicular to the frontal plane was implanted to allow the head fixation during the experiments. All the holding system was cemented to the skull.

3.4 *In vivo* experiments.

3.4.1 Head immobilization.

Recording sessions began at least two days after surgery. The animals were placed over a treadmill with an infrared sensor that enable the measurement of locomotion activity, and the head was fixed to the recording table by means of the implanted head-holding system. Bone wax was removed with the aid of a surgical microscope (SMZ-140, Motic, Barcelona, Spain) and the cortical surface was carefully cleaned with super fine forceps (Dumont #5, FST, Heidelberg, Germany) and cotton swab without damaging the dura mater.

3.4.2 Whiskers stimulation.

To elicit the whisker stimulation, an electrical shock was subcutaneously delivered by a pair of flexible steel electrodes (Strand ø: 50.8 µm; Coated ø: 228.6 µm; A-M Systems) inserted under the skin of the left whisker pad with the help of a needle (25 G) and with a separation between them of 2-3 mm. The electrical stimulus consisted on a single square pulse (0.2 ms; 0.5-3 mA) delivered by an isolation unit (CS20, Cibertec, Madrid, Spain) connected to a stimulator device (CS420, Cibertec).

3.4.3 Recordings.

All experiments were carried out with an amplifier (BVC-700A, Dagan corporation, MN., USA) connected to a dual extracellular-intracellular headstage (8024). The recording electrodes consisted on glass micropipettes (Outside ø: 2.0 mm; Inner ø: 1.6 mm; length: 15 cm, with inner filament; A-M Systems, WA., USA) manufactured by pulling the glass capillary with a vertical pipette puller (Model PE-22, Narishige, Japan) and, subsequently, breaking the tip under an optical microscope to obtain tips with an appropriate diameter.

For SEP recordings, a micropipette with a tip diameter between 8-10 µm was filled with 3 M NaCl, mounted on a micromanipulator (MO-10, Narishige) and placed over the recording area. In order to map the SEP, the electrical stimulus was delivered at the whisker pad every 10 ± 2 s, the micropipette was lowered, and the current intensity adjusted until the maximum amplitude SEP was achieved. Then, the current intensity of whisker electrical pulses was decreased as to elicit a SEP with half of the maximum amplitude to allow the observation of an increase or decrease of its components during and after tDCS intervention.

For single-cell activity, a micropipette with a tip diameter between 1-2 µm was filled with 3 M NaCl, mounted on a micromanipulator (MO-10, Narishige) and placed over the recording area. The electrode was slowly lowered at ~2 µm/s and spikes were detected based on visual (2002C and 2004C, Tektronix, OR., USA) and auditory (Audio monitor 3300, A-M Systems, WA., USA) cues. Once the spiking activity was detected, the micropipette tip was advanced very slowly to properly isolate and identify just one neuron in the recorded signal.

3.4.4 Juxtacellular labeling.

The procedure was similar to that of single-cell recordings except that the micropipette was filled with 2% Neurobiotin (SP-1120, Vector Laboratories, CA., USA) in 0.5 M NaCl, the tip was immersed in Dil (Vybrant Dil cell-labeling, V22885, Thermo Fisher Scientific, Mass., USA) and the impedance was periodically checked to assure that it was

between 4–12 MΩ. With the headstage in extracellular mode (because of the higher gain) and after single-cell activity was isolated, the micropipette tip was advanced until the negative spikes (extracellular recording) became positive spikes (juxtacellular recording) with an amplitude of at least 600 µV. Then, the headstage was switched to intracellular mode to juxtacellularly label the neuron following the method described by Pinault (Pinault, 1996) (Fig. 3.2). Briefly, the technique consists in the modulation of the firing rate by passing positive current pulses (200 ms ON/OFF) of increasing intensities (1-10 nA) through the micropipette tip. After a delay of a few seconds, the electrical properties of the recorded neuron suddenly and significantly change, increasing its firing rate and broadening the spike waveform. From this critical moment, pulse intensity is lowered to prevent cellular damage and the modulation was maintained from several seconds to minutes in order to fill the neuron with neurobiotin.

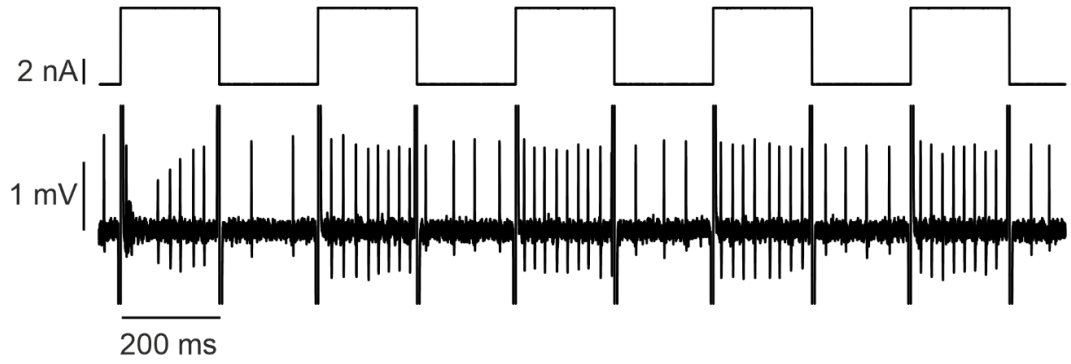

Figure 3.2. Experimental protocol for juxtacellular labeling. Spontaneous activity of an isolated cerebellar neuron (lower trace) showing the firing rate modulation during the current pulses delivered through the micropipette tip (top trace).

3.5 tES.

The different protocols for transcranial currents were designed in Spike2 (Cambridge Electronic Design (CED), Cambridge, U.K.) and sent to a battery-driven linear stimulus isolator (WPI A395, World Precision Instruments, FL., USA) through an analog output from the acquisition board (CED micro1401-3; CED). They were applied between the active electrode (custom-made ring-electrode or polyethylene tubing) over the scalp (S1, lateral cerebellum or Vermis) and a reference electrode consisting on a rectangle

rubber (6 cm^2) attached to the back of the mice and moisten with electrogel (E10, Electro-Cap International, OH., USA) (Fig. 3.3).

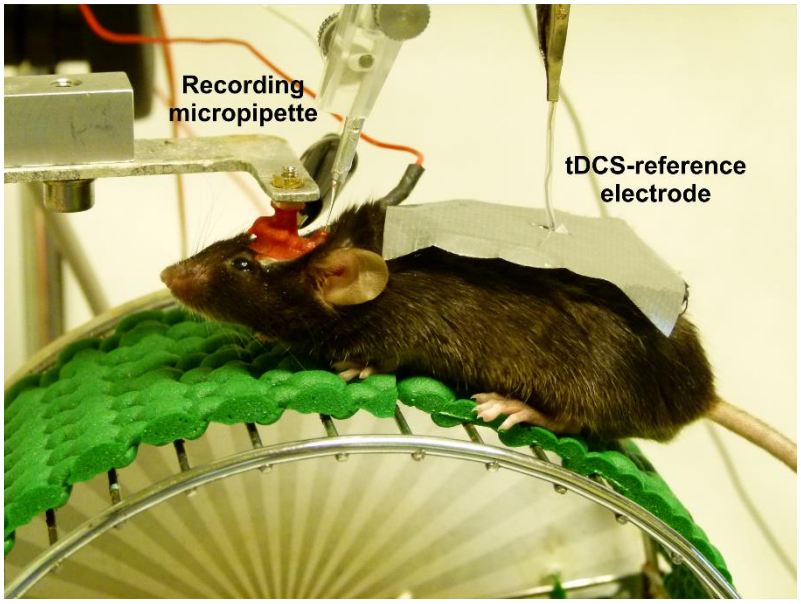

Figure 3.3. Representative picture of the experimental set-up showing the glass micropipette over cerebellum and the reference electrode for tDCS in the back of the animal (attached with adhesive tape).

In experiments where the polyethylene tubing was used as tDCS active electrode, the tubing was filled with electrogel and the electrode from the stimulus isolator was directly immersed on it.

3.5.1 Measurement of intracranial electric fields.

To measure the actual voltage changes intracranially elicited, sinusoid waves of 1 Hz alternating current were delivered at ± 2, ± 20 and ± 200 µA (current densities: ± 0.0426, ± 0.426 and ± 4.26 mA/cm^2). Every sinusoid wave lasted 10 seconds and was randomly repeated three times. Measurements with glass micropipette were repeated at different depths, ranging from cortical surface until 4 mm below, in 1 mm steps.

3.5.2 tDCS immediate effects.

To characterize the direct effects of the electric current and avoid plasticity changes, alternating trials of 5-10 s anodal and cathodal tDCS at different intensities (50,

100, 150, 200 or 300 μA), with an additional 5 s ramp-up and 5 s ramp-down, were applied, separated by 10 s of non-stimulation. When more than one intensity was used, trials with different intensities were randomly distributed.

3.5.3 tDCS long-term effects.

To index long-lasting changes, tDCS was delivered during 20 min at 200 μA for cathodal and 150 μA for anodal stimulation (due to amplifier noise issues with higher currents) over S1 for Set 1, during 20 min at 200μA for cathodal and anodal over lateral cerebellum for Set 2, and during 20 min at 300 μA for cathodal and anodal over lateral cerebellum for Set 4.

3.6 Tissue processing.

For fluorescence immunohistochemistry, mice received 20 minutes of stimulation at 200 μA (either anodal, cathodal or sham), and were deeply anesthetized 15 min after tDCS cessation with ketamine–xylazine mixture (Ketaset, 100 mg/ml; Rompun, 20 mg/ml) and perfused transcardially with 0.9% saline followed by 4% paraformaldehyde (PanReac, Barcelona, Spain) in PBS. The brains were removed and stored in 4% paraformaldehyde for 24 hours, cryoprotected in 30% sucrose in PBS the next 48 hours, and then cut in coronal sections (50 μm) with a freezing microtome (CM1520, Leica, Wetzlar, Germany). Sections were processed “free-floating” and passed through all procedures simultaneously to minimize differences in immunohistochemical staining. After three washes of 10 min with PBS, sections were blocked with 10% Normal Donkey Serum (NDS, 566460, Merck, Darmstadt, Germany) in PBS with 0,2% Triton X-100 (Sigma-Aldrich, Mo., USA) (PBS-Tx-10% NDS) and then incubated overnight at room temperature in darkness with the primary antibody solution containing mouse anti-vesicular Glutamate Transporter 1 (vGlut1, 1:1000, MAB5502, Merck) or rabbit anti-Glutamate Decarboxylase 65&67 (GAD65-67, 1:1000, AB1511, Merck). After three washes with PBS, sections were incubated for 1 hour at room temperature in darkness with appropriate secondary antibodies: Alexa Fluor 488 donkey anti-mouse IgG (H+L) (1:400, A21202, Thermo Fisher Scientific) or Alexa Fluor 555 donkey anti-rabbit IgG (H+L) (1:400, A31572, Thermo Fisher Scientific), in PBS-Tx-5% NDS. After three washes with

PBS, sections were mounted on glass slides and coverslipped using Dako Fluorescence Mounting Medium (Dako North America, CA., USA).

For neurobiotin-labeled neurons, brains were equally processed as for fluorescence immunohistochemistry, but the coronal sections were 60-70 µm width. After three washes, sections containing neurobiotin-labelled neurons were blocked with 10% NDS and then incubated overnight at room temperature in darkness with Streptavidin (1:200, Streptavidin DyLight 488 conjugated, Thermo Fisher Scientific) in PBS with 1% Tx. After three washes with PBS, sections were mounted on glass slides and coverslipped using Dako Fluorescence Mounting Medium.

For confocal imaging, an *in vivo* confocal microscope (A1R HD25, Nikon, Tokyo, Japan) was used. Z-series of optical sections (usually 0.5 µm apart) were obtained using the sequential scanning mode.

3.7 Data analysis.

3.7.1 *In vivo* electrophysiology.

Recording and monitoring signals from the amplifier, tDCS converted signals, infrared sensor signals from wheel motion and 1-V rectangular pulses corresponding to whisker electrical stimulation presented during the different experiments were digitally stored on a computer for quantitative off-line analysis. Collected data were sampled at 25 kHz for SEP and unitary recordings, with an amplitude resolution of 16 bits (CED micro1401-3; CED, Cambridge, U.K.). The remaining non-neuronal signals were sampled at 5 kHz.

Spike2 (CED) and Matlab 2015a (MathWorks Inc., MA., USA) software was used to quantify peak-amplitude and latency of SEPs components. These measurements were used as an index of the synaptic response.

SEP amplitude was computed by the Spike2 command peak-to-peak measurements, where the maximum negative voltage value of every trough was subtracted from the maximum positive voltage value of the preceding peak. SEP latency was determined as the time from whisker stimuli to the maximum negative peak value. Given the dramatic decrease in some SEP's components amplitude while the animal was running, the SEPs coincident with animal running were removed, as well as those coincident with electrical artifacts.

3.7.2 Analysis of intracranial electric fields.

To estimate the electric field strength during tDCS, "DC remove" process from Spike2 was applied (with a time constant of 0.5 s) to correct for possible baseline drifts unrelated to stimulation and set the channel offset to zero. From every sinusoid wave, the peak-to-peak value (electric potential) from the LFP evoked by tES was measured and averaged for a given intensity and depth. Finally, the electric field strength (differences between potentials) for every intensity was calculated by computing the difference in peak-to-peak values between two consecutive depths (1 mm in distance).

3.7.3 tDCS immediate effects.

For tDCS immediate effects experiments, SEPs induced by left whisker-pad stimulation were recorded 1 s before tDCS ramp-up (control) and 1 s before tDCS ramp-down (immediate effects). For every tDCS trials, amplitude values during tDCS were normalized (dividing them by the immediately preceding control value and multiplying by 100) , and latency values were normalized subtracting them by the latency value of the preceding control SEP. These data were averaged per tDCS polarity and per intensity and compared.

3.7.4 tDCS long-term effects.

For tDCS long-term effects experiments, SEPs induced by left whisker-pad stimulation (delivered every 10 ± 2 s) were applied for 20 min before (control), 20 min during, and 60 min after tDCS. SEPs waveform were averaged every 5 minutes intervals

and, for comparison between animals, amplitude values were normalized dividing them by the mean of the baseline values (control condition, before tDCS) and multiplying by 100. Using this normalization, the baseline values are always close to 100 % but the variance is the same as in the raw data. For latency normalization, latency values before, during and after tDCS were subtracted by the mean of the baseline (control period) values.

3.7.5 Single-cell activity.

For single-cell recordings analysis, only well isolated spikes, with high signal-to-noise ratios were considered. A "DC remove" process (time constant (s): 0.001-0.0004) was applied to reduce DC level drifts, and spikes were detected based on threshold-crossing algorithm of Spike2 software. All spikes were visually confirmed and PC were identified as such if complex spikes (CS) were observed and had at least a 10-40 ms pause in simple spikes (SS) after CS occurrence. Subsequently, each neuron was analyzed as follow:

- Averaged waveforms were obtained from unprocessed data. For control condition, the 5 s before tDCS ramp-up were considered, and for tDCS condition the 5 s before anodal or cathodal tDCS ramp-down were computed.

- Peristimulus time histograms showing the number of spikes per bin (bin size: 0.1 s) were aligned with tDCS ramp-up and expressed as frequency in Hz. Frequency was normalized and standardized (Z-score= $\frac{X-\mu}{\sigma}$) with respect to the average frequency of the five seconds before anodal and cathodal tDCS ramp-up.

- Average frequency in five second windows were computed before tDCS ramp-up, during tDCS (5 s before tDCS ramp-down begins) and after tDCS (5 s after tDCS ramp-down ends) for statistical analysis.

- All neurons that showed statistical differences during anodal or cathodal tDCS with respect to control period were sorted in different groups based on the direction of modulation. One group gathered all non tDCS-modulated neurons, other 4 groups were made for neurons modulating with anodal and cathodal tDCS and another 4 groups for neurons modulating with anodal or cathodal tDCS (Table 1).

Table 1. Groups gathering all kind of neuronal modulation observed		
tDCS	**Anodal**	**Cathodal**
AND groups	Increase	Decrease
	Decrease	Increase
	Increase	Increase
	Decrease	Decrease
Or groups	Increase	No-modulation
	Decrease	No-modulation
	No-modulation	Increase
	No-modulation	Decrease
No-modulation group	No-modulation	No-modulation

- To compare the strength of the modulation for the same neuron with different tDCS intensities, the firing frequency in a 5 s window during tDCS was divided by the firing frequency in a 5 s window before tDCS ramp-up, for every intensity.

- For neurobiotin-labeled neurons, the deviation of the somatodendritic axis with respect to the active electrode was calculated by measuring the angle between the neuronal axis and an imaginary line perpendicular to the active electrode.

3.7.6 Fluorescence immunohistochemistry.

Confocal images were processed in ImageJ (https://imagej.nih.gov/ij/) with the image processing package Fiji (http://fiji.sc/Fiji) using a custom-built macro. The process consisted on:

- Subtract fluorescence background noise: five square regions of interest (ROI) of 30x30 pixels (26.22 μm^2) were placed over unlabeled nuclei in each image, and the obtained maximum brightness average was set as the minimum value for “setTreshold”, so the pixels with values lower than the average are considered as non-fluorescent. Then, a copy of the image is converted to binary to visually validate the procedure, and all the process is repeated until the threshold properly discriminate our signal from the noise.

- Analyze particles: five square ROIs of 100x100 pixels (291.31 μm^2) were randomly placed over regions absent of nuclei or unspecific noise (as for example blood vessels). Each image inside the ROI was converted to binary and the "Analyze Particles" command was used to count and measure aggregates of vGlut1 and GAD65-67. Particles were sorted as small (size = 10-25), medium (size = 26-46) or big (size = 47-100) and averaged together to obtain one value per hemisphere per animal.

3.7.7 Statistical analysis.

SigmaPlot 11.0 (Systat Software Inc, CA., USA) or Matlab 2015a (MathWorks Inc.) were used for statistical analysis. For tDCS immediate effects experiments, statistical significance of differences between groups was inferred by unpaired Student's t-test in Set 2 and Set 4. The non-parametric Wilcoxon Signed Rank test was applied for comparison when data did not permit normality assumption. For Set 1, because all animals received all treatments, a two-way repeated-measures analysis of variance (ANOVA) was performed, with CURRENT INTENSITY (50, 100, 150 or 200 µA) and POLARITY (Anodal or Cathodal) as within-subject factors, and the post hoc Holm-Sidak test for multiple comparisons.

For tDCS long-term effects experiments, the comparisons were made within tDCS conditions (anodal, cathodal or sham) and between tDCS conditions. A one-way repeated-measures ANOVA was performed to infer statistical differences within groups with TIME (temporal periods of 5 minutes each: one time point for control, four time points during tDCS/sham and twelve time points after tDCS/sham) as main factor, and the post hoc Holm-Sidak test for multiple comparisons versus control group. The non-parametric Friedman Repeated Measures Analysis of Variance on Ranks was applied for comparison when data did not permit normality assumption. For comparisons between conditions, statistical significance of differences was inferred by unpaired Student's t-test between each pair of temporal periods (5 minutes). The non-parametric Mann Whitney U test was applied for comparison when data did not permit normality assumption.

For single-cell recordings, statistical comparison was inferred by paired Student's t-test. Neural activity of each neuron was binned in 100 ms epochs, and statistical comparisons were made between a firing frequency baseline window of 5 s before tDCS ramp-up, during 5 s windows before tDCS ramp-down begins and 5 s windows after tDCS ramp-down ends. The non-parametric Wilcoxon signed-rank test was applied for comparisons when data did not permit normality assumption.

For immunohistochemical experiments, statistical comparison for fluorescence levels was inferred by a two-way mixed ANOVA with BRAIN HEMISPHERE (non-stimulated vs stimulated hemisphere) and tDCS POLARITY (anodal, cathodal or sham) as within-subject factors in Set 1 experiments, and two-way repeated-measures ANOVA with BRAIN HEMISPHERE (non-stimulated vs stimulated hemisphere) and tDCS POLARITY (anodal, cathodal or sham) as within-subject factors in Set 2 and Set 4 experiments. The post hoc Bonferroni test was applied for multiple comparisons.

Statistical significance was set at $p < 0.05$ in all cases.

4 Results

4.1 tDCS modulation of S1.

In the first set of experiments (Set 1), we characterize the effects of tDCS on S1. For that, the following experiments were performed:

- Firstly, the SEP recorded in S1 in response to whisker electrical stimulation was characterized: defining its components, assessing its variability across cortical layers and the relationship with the current intensity applied to the whisker.
- Then, the electric field imposed in the brain by tES was determined, and the electric field strength in the recording area was extrapolated.
- After that, the modulation produced by tDCS on SEPs was evaluated to test the immediate effects (15 s of tDCS, including 5 s ramp-up and 5 s ramp-down) and the long-term effects (during 20 minutes of tDCS and 1 hour after).
- Finally, the long-term impact of tDCS on excitation/inhibition balance was assessed by immunohistochemical methods, measuring GAD65-67 and vGlut1 levels.

4.1.1 SEPs characterization in S1.

To get a representative electrophysiological marker of neuronal excitability, S1-SEPs were characterized in alert mice (Fig. 4.1*A*). Electrical whisker stimulation evokes a SEP in the contralateral S1 barrel cortex (Fig. 4.1*B*) that mainly consists of three well defined components: the first positive component (P1) peaking at 3.8 ± 0.2 ms (mean ± SEM, n = 10 mice), followed by a negative deflection (N1) at 12.6 ± 1.2 ms (mean ± SEM, n = 10 mice), and finally a positive component (P2) peaking at 26.2 ± 2.8 ms (mean ± SEM, n = 10 mice).

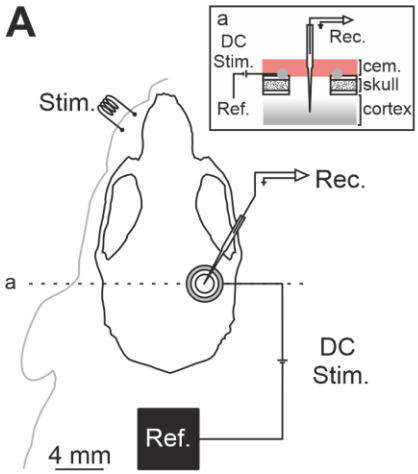
A
a
DC
Stim.
Rec.
cem.
skull
cortex
Ref.
Stim.
Rec.
a
DC
Stim.
Ref.
4 mm

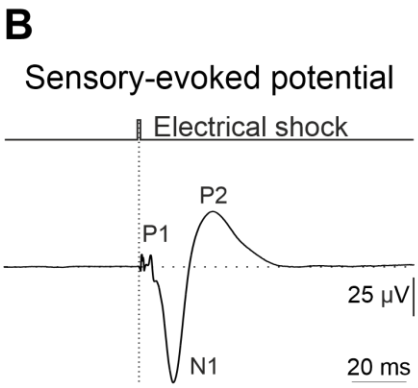
B
Sensory-evoked potential
Electrical shock
P1
P2
N1
25 µV
20 ms

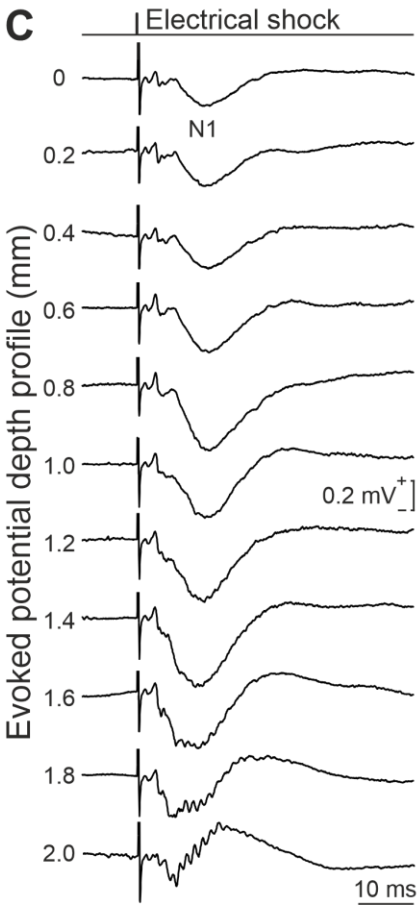
C
Electrical shock
N1
Evoked potential depth profile (mm)
0
0.2
0.4
0.6
0.8
1.0
1.2
1.4
1.6
1.8
2.0
0.2 mV
10 ms

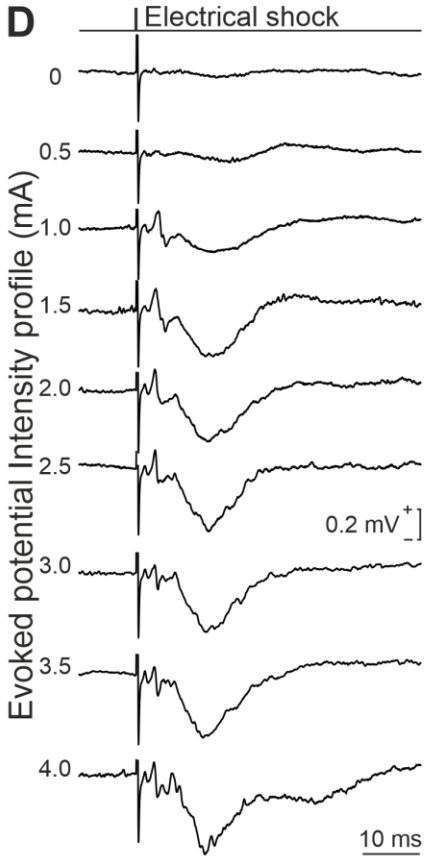
D
Electrical shock
Evoked potential Intensity profile (mA)
0
0.5
1.0
1.5
2.0
2.5
3.0
3.5
4.0
0.2 mV
10 ms

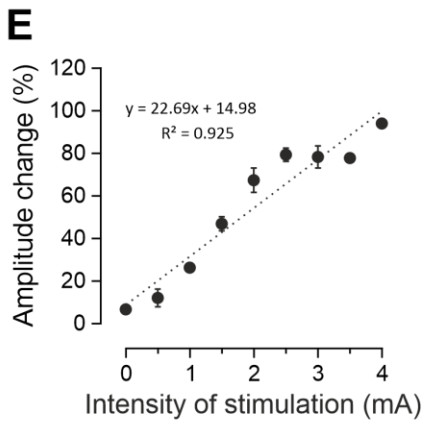
E
Amplitude change (%)
y = 22.69x + 14.98
R² = 0.925
0
20
40
60
80
100
120
0
1
2
3
4
Intensity of stimulation (mA)

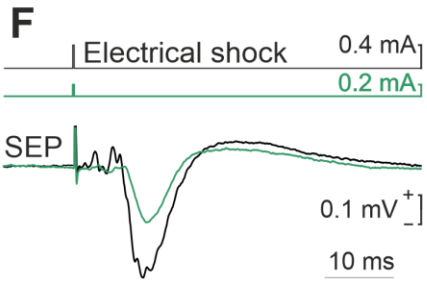
F
Electrical shock
0.4 mA
0.2 mA
SEP
0.1 mV
10 ms

Figure 4.1. Characterization of SEPs in S1 cortex. *A*) Experimental design of Set 1 experiments with concurrent tDCS and recordings on S1 cortex. *B*) Profile of sensory evoked potential by whisker electrical stimulation (n = 10 mice) showing the different components (P1, N1 and P2). *C*) S1-SEP depth profile. Every trace corresponds to an average of 10 SEPs recorded at different depths for a representative mouse. *D*) S1-SEP intensity profile. Every trace corresponds to an average of 10 SEPs recorded at the same location (0.8 mm depth) but with different intensities of whisker electrical stimulation for a representative mouse. *E*) Quantification of the amplitude change in N1 component of SEPs regarding intensities applied to whisker electrical stimulation. Data normalized with respect maximum amplitude recorded at 4 mA (n = 3 mice). *F*) Comparison of S1-SEPs for different intensities applied to whisker stimulation obtaining maximum N1-amplitude (black trace, n = 10), and 50% of the maximum N1-amplitude (green trace, n = 10).

The amplitude and latency of these components varied along the recording site across cortical layers (Fig. 4.1*C*) reaching a maximum amplitude between 0.8 – 1.4 mm depth (layers V-VI) and a polarity inversion at deeper recording sites. For this reason, during experimental sessions depth profile was obtained from all the participating mice selecting those recording sites where the amplitude of N1 was maximum. The final amplitude of N1 linearly depended on the intensity of the electrical stimuli applied to the whiskers (R^2 = 0.925; n = 3 mice, Fig. 4.1*D, E*). For the experiments, the current intensity of whisker electrical pulses was adjusted to elicit a SEP with half of the maximum amplitude to allow an increase or decrease of its components during and after tDCS intervention (Fig. 4.1*F*). Finally, it was observed that N1 amplitude decreased or even disappeared when the animal was running, so those events were discarded from the analysis, as well as those coincident with electrical artifacts.

4.1.2 Intracranial electric fields induced by S1-tDCS.

tDCS effects are supposed to depend on the strength of the electric field gradient imposed along the brain tissue. For that, in a series of experiments, the actual electric field gradient was determined. Animals (n = 6) were prepared for chronic recording of S1-LFPs in alert condition during simultaneous application over S1 of low-frequency tACS (1 Hz) at different intensities (± 2, ± 20 and ± 200 µA). Differential recordings were obtained between the glass micropipette and a silver reference electrode placed over the contralateral dura and were sequentially performed every 1 mm from cortical surface to 4 mm depth with a 20° lateral angle (Fig. 4.2*B*). The figure 4.2 (*B*) shows the grand average obtained from recordings (unprocessed data) at different depths including data from all the animals in the study. Under the active electrode the electric

field decreased it magnitude in depth in a logarithmic manner for all intensities tested. The recorded electric field for all the animals is represented in figure 4.2 (*C*).

To calculate the electric field imposed by tES at different intensities (50, 100, 150 and 200 µA) in the recording site (S1-layer V-VI, 1 mm) we used a linear regression equation extracted from the relation between tACS-intensity and voltage difference (y = -0.4473 X - 0.731; R^2 = 0.9949) for each depth (Fig. 4.2*D*). The calculated electric field strength induced by 50, 100, 150 and 200 µA at the recording site was 23.1, 45.5, 67.8 and 90.2 V/m, respectively.

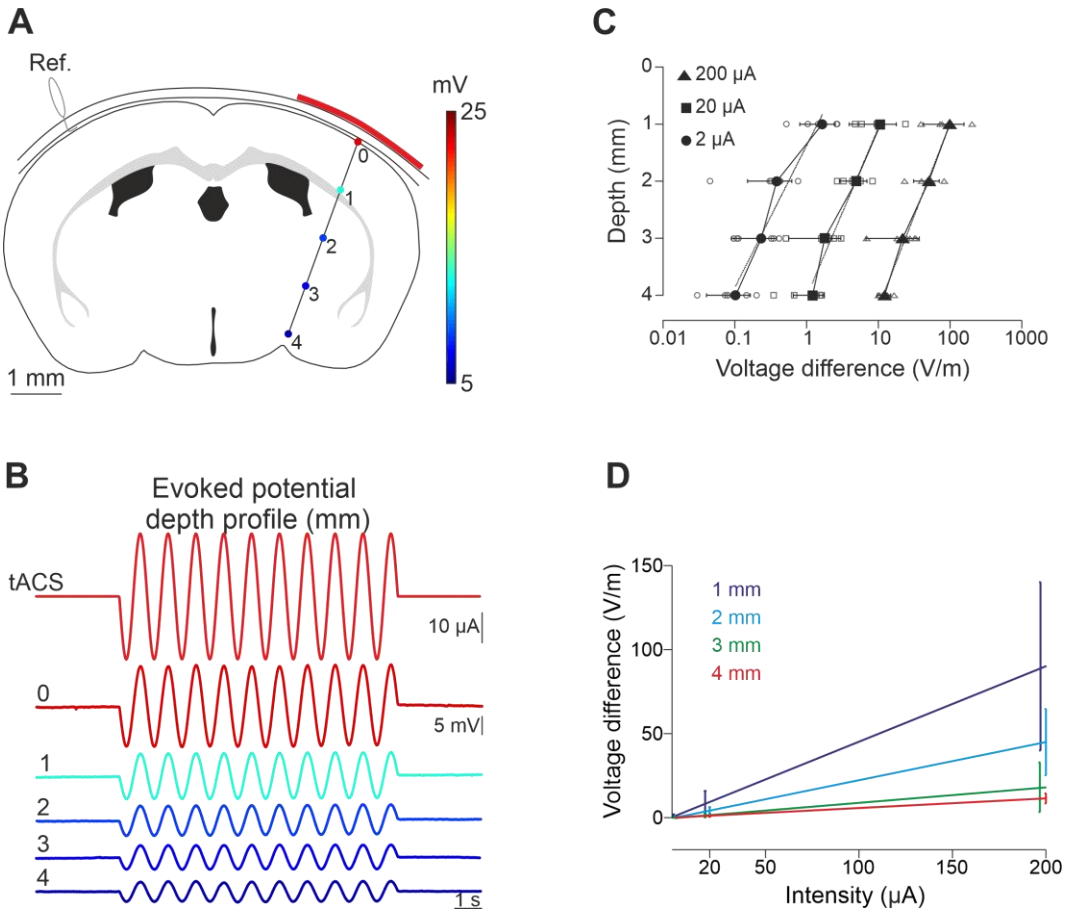

Figure 4.2. Intracranial electric fields induced by S1-tDCS. *A*) Schematic representation of electric potentials recorded in S1 at different depths. *B*) tACS stimulation (top trace) applied over the scalp and grand average (n = 6 mice, unprocessed data) of the actual potentials generated at different depths (from 0 to 4 mm). *C*) Average (filled symbols) and individual (empty symbols) electric fields recorded at different depths for ± 2 (circles), ± 20 (squares) and ± 200 µA (triangles) tACS. *D*) Linear regression applied to the relation between tACS-intensity and voltage difference for each depth.

4.1.3 S1-tDCS immediate effects on S1-SEPs.

To test the immediate effects of tDCS over neuronal activity and avoid the expression of long-term effects, SEPs were tested just before and during short-duration pulses (15 s, including 5 s ramp-up and 5 s ramp-down) of anodal and cathodal tDCS at different randomly distributed intensities (50, 100, 150 and 200 μA).

For S1-SEPs during S1-tDCS, figure 4.3 (*A*) shows the averaged SEP (n = 30) during control (black trace), anodal (red trace) and cathodal (blue trace) tDCS applied at 50, 100, 150 and 200 μA (density currents = 1.06 mA/cm^2, 2.13 mA/cm^2, 3.19 mA/cm^2 and 4.26 mA/cm^2, respectively) for a representative animal. Mean data obtained from the group of animals participating in the experiment (n = 14) are represented in figure 4.3 (*B*, amplitude; *C*, latency). Thus, anodal tDCS progressively increased the N1 amplitude of simultaneously recorded SEPs with increasing current intensity to a maximum of 41.5 ± 5.3 % at 200 μA whereas cathodal tDCS decreased the N1 amplitude a maximum of 26.8 ± 4.4 % at 200 μA (Fig. 4.3*B*). The normalized amplitudes of N1 were entered in a two-way repeated-measures analysis of variance (ANOVA) with CURRENT INTENSITY and POLARITY as within-subjects factors. The analysis showed a significant effect of CURRENT INTENSITY ($F_{3,39}$ = 3.316, p = 0.030) and POLARITY ($F_{1,13}$ = 51.081, p < 0.001). Interaction CURRENT INTENSITY X POLARITY was also significant ($F_{3,39}$ = 27.818, p < 0.001). Post hoc analysis confirmed that there was a significant difference between the normalized amplitude of N1 during anodal and cathodal tDCS for each one of the applied intensities (n = 14 animals, p < 0.05, Holm-Sidak post hoc test). In summary, the effects of tDCS on simultaneously recorded SEPs were dependent of the applied polarity and intensity.

As shown in figure 4.3 (*C*) there were differences on N1 latencies for the higher intensities used (100, 150 and 200 μA). Thus, anodal decreased the latency up to 0.3 ± 0.2 ms at 100 μA whereas cathodal increased it up to 0.4 ± 0.1 ms at 150 μA. The normalized latencies of N1 were entered in a two-way repeated-measures analysis of variance (ANOVA) with CURRENT INTENSITY and POLARITY as within-subjects factors, showing a significant effect of POLARITY ($F_{1,13}$ = 8.411, p = 0.012). Post hoc analysis

confirmed that there was a significant difference between the normalized latency of N1 during anodal and cathodal tDCS for each one of the three higher intensities (n = 14 animals, $p < 0.05$, Holm-Sidak post hoc test).

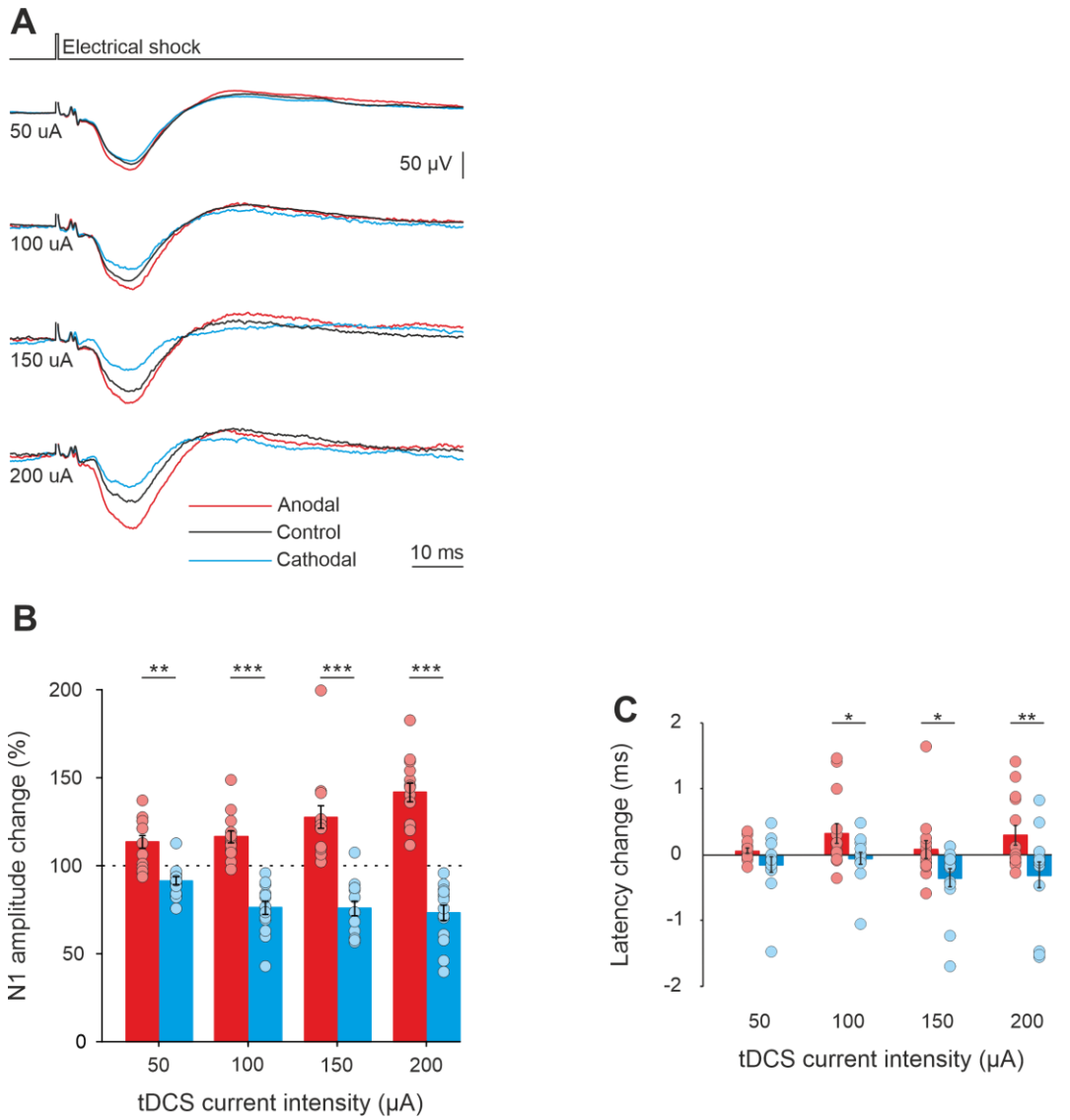

Figure 4.3. tDCS immediate effects over SEPs in S1 cortex. *A*) SEPs (n = 30) from a representative animal during control (black trace), anodal (red trace) and cathodal (blue trace) tDCS applied at 50, 100, 150 and 200 µA. *B*) Quantification and statistical results of tDCS effects on SEPs amplitude. Mean (bars) and individual amplitude data (circles) for all the animals are represented as percentage of change with respect to control values. n = 14 mice, two-way repeated-measures ANOVA, CURRENT INTENSITY effect, $F_{3,39} = 3.316$, $p = 0.030$, POLARITY effect, $F_{1,13} = 51.081$, $p < 0.001$, CURRENT INTENSITY X POLARITY Interaction, $F_{3,39} = 27.818$, $p < 0.001$, Holm-Sidak post hoc test. **p < 0.0.1; ***p < 0.001. *C*) Quantification and statistical results of tDCS effects on SEPs latency. Mean for all the animals are represented as the difference with respect to control values. n = 14 mice, two-way repeated-measures ANOVA, POLARITY effect, $F_{1,13} = 8.411$, $p = 0.012$, Holm-Sidak post hoc test. *p < 0.05; **p < 0.01. Error bars represent SEM.

4.1.4 S1-tDCS long-term effects on S1-SEPs.

To test the potential long-term effects of tDCS over S1 cortex excitability we recorded SEPs induced by whisker pad stimulation (every 10 ± 2 s) in three different experimental conditions. Animals were prepared for SEP recording and simultaneous tDCS and randomly assigned to anodal (n = 10), cathodal (n = 10) or sham (n = 10) groups. During experimental sessions SEPs were recorded along 20 min before tDCS, during simultaneous anodal (150 µA, 20 min), cathodal (-200 µA, 20 min) or sham (150 µA, 30 s) tDCS, and for 1 hour after tDCS.

As observed in figure 4.4 (*B*) tDCS has a significant effect on the normalized amplitude of N1 component of SEPs for both anodal ($F_{19,171} = 5.433$, $p < 0.001$, one-way repeated-measures ANOVA) and cathodal ($F_{19,171} = 12.839$, $p < 0.001$, one-way repeated-measures ANOVA) polarity. Interestingly, the post hoc analysis showed that significant differences are found during and after tDCS application in the cathodal group (n = 10 animals, $p < 0.05$, Holm-Sidak post hoc test) but only during tDCS in the anodal one (n = 10 animals, $p < 0.05$, Holm-Sidak post hoc test). Thus, anodal tDCS significantly increased the amplitude of SEPs (up to a maximum of 58.2 ± 11.0 %, n = 10) with respect to control values but only during simultaneous transcranial stimulation (red filled diamonds in Fig. 4.4*B*). On the other hand, cathodal tDCS decreased the amplitude of SEPs with respect to control values reaching its maximum effects (maximum of 36.1 ± 7.9 %, n = 10) during simultaneous transcranial stimulation and remaining significantly decreased for 1 hour after tDCS removal (blue filled squares in Fig. 4.4*B*). Accordingly, we found significant differences along time when values from anodal and cathodal groups were compared with values from sham group (black triangles in Fig. 4.4*B*). As expected, significant differences between anodal and sham groups were restricted to the tDCS period (n = 10 animals, $p < 0.05$, unpaired t-test) whereas significant differences were maintained during and after tDCS when comparing cathodal and sham groups. No significant effects were observed in the amplitude of N1 component of SEPs between the sham group ($F_{19,171} = 1.412$, $p = 0.127$, one-way repeated-measures ANOVA).

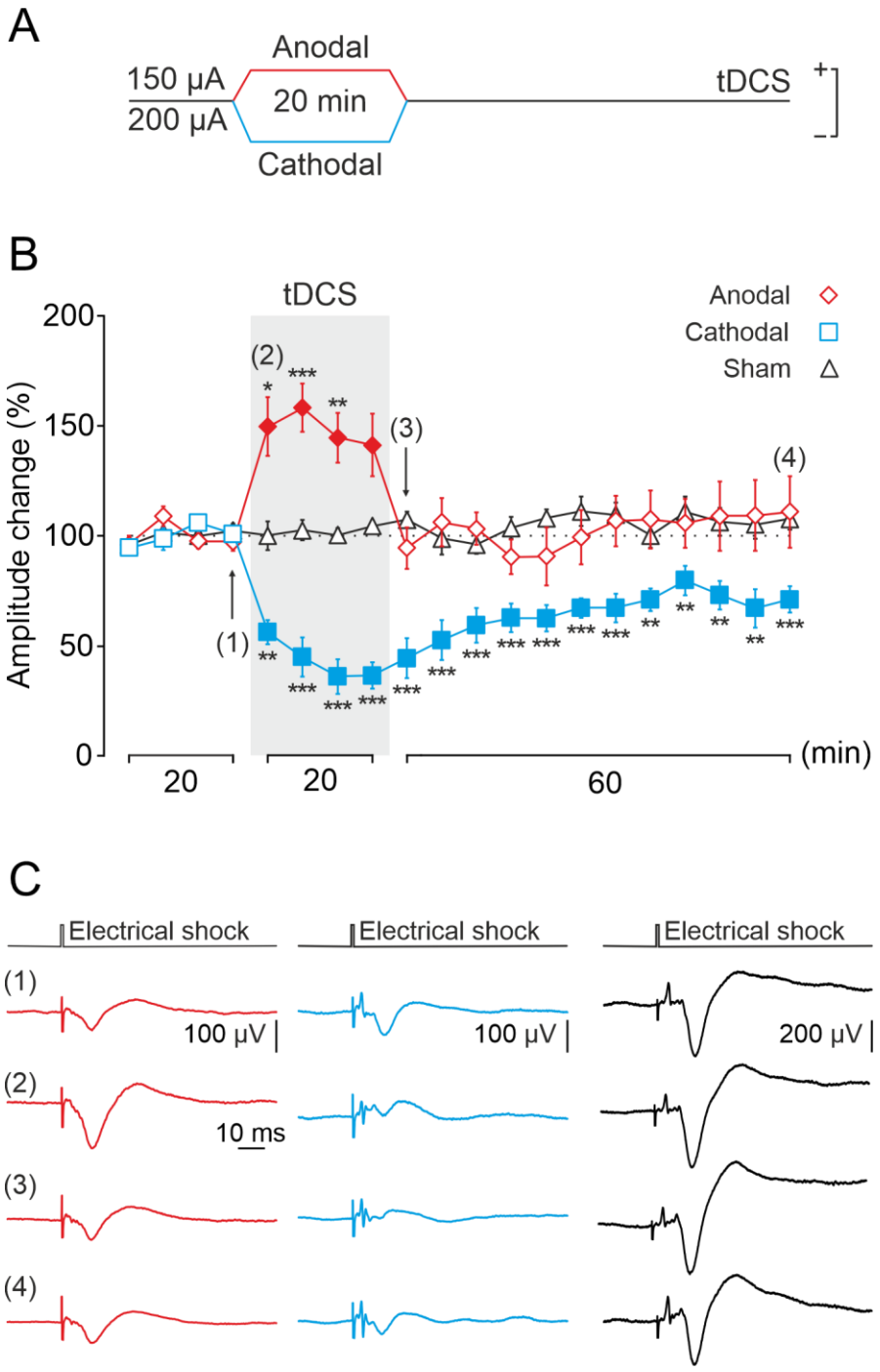

Figure 4.4. tDCS long-term effects over SEPs in S1 cortex. *A*) tDCS protocol used in the long-term effect experiment. *B*) Normalized amplitude change of N1 averaged every 5 min for 20 min of anodal (red diamonds), cathodal (blue squares) or sham (black triangles) tDCS. Filled symbols represent statistical differences with the last control period (n = 10 mice, $p < 0.05$, Holm-Sidak post hoc test). Asterisks mark statistical differences between the same temporal period for anodal or cathodal with sham tDCS (n = 10 animals, *$p < 0.05$; **$p < 0.01$; ***$p < 0.001$, unpaired t-test). *C*) Averaged SEPs from a representative mouse taken 5 minutes before (1) and after tDCS ramp-up (2), and just after (3) or 1 hour after (4) tDCS ramp-down. Error bars represent SEM.

Latency values were entered into a one-way repeated-measures ANOVA but no differences were found for any temporal period for anodal, cathodal nor sham tDCS.

4.1.5 GAD65-67 and vGLUT1 levels in S1 after 20 minutes of S1-tDCS.

To elucidate the molecular changes underlying the long-term effects observed, vGlut1 and GAD65-67 levels were used to assess possible modifications of the excitation/inhibition balance. For that, we prepared a group of animals for tDCS application during whisker stimulation (no electrophysiological recordings were carried out in these experiments) and randomly assigned to anodal (n = 5), cathodal (n = 4) or sham (n = 4) condition.

The number of GAD65-67 (Fig. 4.5*A*) and vGLUT1 (Fig. 4.5*B*) positive clusters of puncta in the stimulated and non-stimulated S1 were analyzed in the sham, anodal and cathodal groups. For that, BRAIN HEMISPHERE (non-stimulated vs stimulated hemisphere) and tDCS POLARITY (anodal, cathodal or sham) conditions were included in a two-way mixed ANOVA. There was no significant difference in vGLUT1 between the stimulated and non-stimulated hemispheres in any of the tested stimulation conditions ($F_{2,10}$ = 0.12, p = 0.888, Fig. 4.5*B*). Nevertheless, there was a significant general main effect on the GAD65-67 positive clusters for the interaction BRAIN HEMISPHERE x tDCS POLARITY ($F_{2,10}$ = 5.163, p = 0.029, Fig. 4.5*B*). Post hoc analysis showed a significant difference between the stimulated vs non-stimulated hemisphere in the cathodal tDCS condition (n = 4 animals, p = 0.005, Bonferroni post hoc test, Fig. 4.5*B*) indicating higher GAD65-67 positive clusters in the stimulated S1 hemisphere than in non-stimulated control S1. No other significant differences were found in anodal nor sham condition.

Finally, to know more about potential spreading effects of cathodal tDCS in the mice cortex we also tested GAD65-67 and vGLUT1 positive clusters in the adjacent primary motor cortex (M1). No significant effects were found in any GAD65-67 and vGLUT1 positive clusters ($F_{2,10}$ = 0.06, p = 0.942, Fig. 4.5*C*) suggesting a focalized histological long-term effect of cathodal tDCS on the stimulated region.

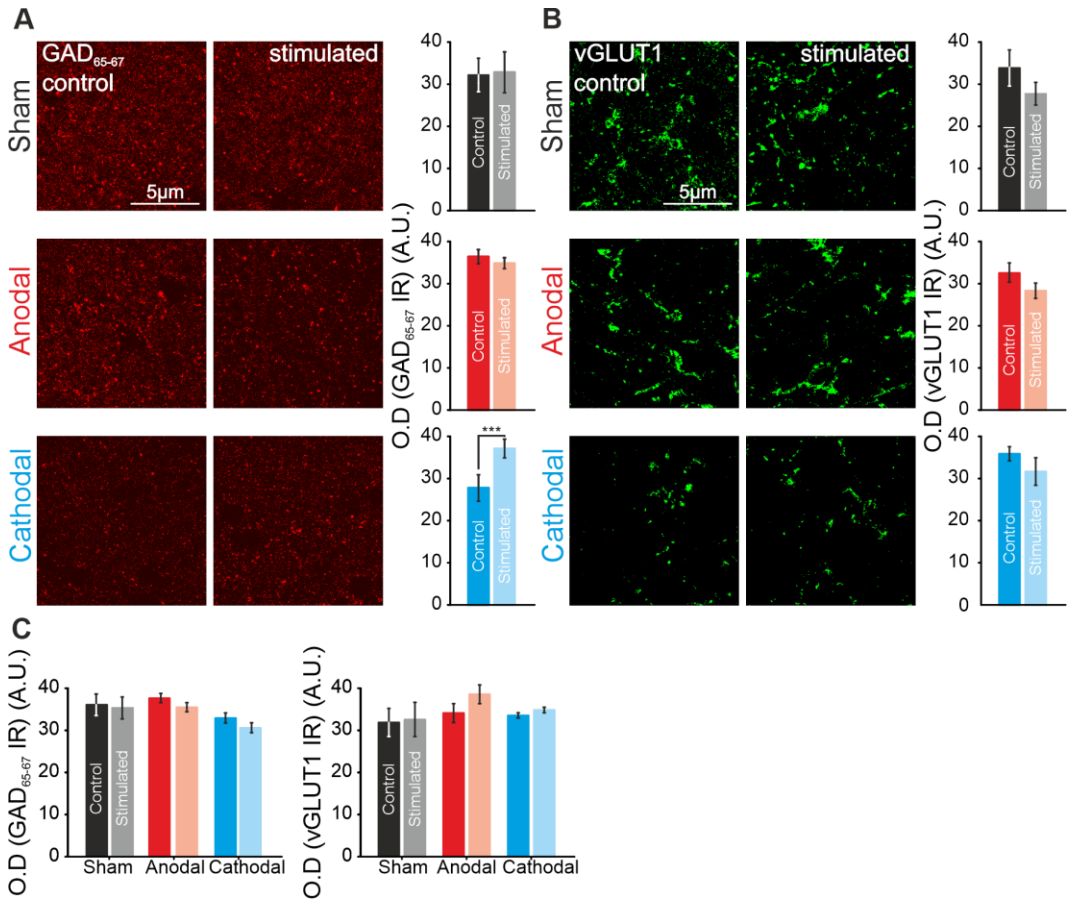

Figure 4.5. Immunohistochemical changes after 20 minutes of tDCS over S1. *A* and *B*) Confocal photomicrographs (images), quantification and statistics (bars charts) of GAD65-67 expression (*A*) or vGlut1 expression (*B*) in S1 after 20 min of Sham condition (upper row, n = 4 mice), after 20 min of Anodal tDCS (middle row, n = 5 mice) and after 20 min of Cathodal tDCS (lower row, n = 4 mice, two-way mixed ANOVA, $F_{2,10} = 5.163$, ***$p < 0.001$) . *C*) Same analysis but for adjacent motor cortex. Error bars represent SEM. GAD65-67: Glutamic acid decarboxylase isoforms 65 and 67; vGLUT1: vesicular glutamate transporter 1; OD: optical density; IR: immunoreactivity; A.U: arbitrary units.

In summary, these results provide a robust evidence of the effects that tDCS have over S1. The validation of SEPs as a measure of cortical excitability allow us to ascertain that anodal and cathodal tDCS can increase and decrease, respectively, cortical excitability immediately and for 20 minutes of continuous electrical stimulation, but these effects are maintained after tDCS just for cathodal polarity, with no long-term effects observed after anodal polarity. Furthermore, immunohistochemical analysis performed after 20 min of tDCS account for the long-term effects, with GAD65-67 levels increasing after cathodal stimulation, thus providing a mechanism to decrease cortical excitability through increased GABA levels after tDCS cessation.

4.2 tDCS modulation of cerebellar cortex.

Once characterized the effects of tDCS on S1, we explore the effects of Cb-tDCS. In the second and third sets of experiments (Set 2 and 3), the characterization of tDCS effects on cerebellar cortex was evaluated. For that, tDCS was first applied over laterall cerebellum (Set 2) and a similar approach than in Set 1 was carried out:

- Firstly, the SEP recorded in CrusI-II in response to whisker electrical stimulation was characterized: defining its components and the relationship with current intensity applied to the whisker.
- Then, the electric field imposed in the cerebellum by tES was determined, and the electric field strength in the recording area was extrapolated.
- After that, the modulation produced by Cb-tDCS on SEPs was evaluated to test the immediate effects (15 s of Cb-tDCS, including 5 s ramp-up and 5 s ramp-down) and the long-term effects (during 20 minutes of Cb-tDCS and 1 hour after).
- Additionally, the long-term impact of Cb-tDCS on excitation/inhibition balance was assessed by immunohistochemical methods, measuring GAD65-67 and vGlut1 levels.
- Finally, single-cell recordings in awake and anesthetized mice were made during the administration of short pulses of Cb-tDCS (15 or 20 s, including 5 s ramp-up and 5 s ramp-down) of varying intensities (100, 200 and 300 μA). In addition, some of the recorded neurons were filled with neurobiotin for further morphological reconstruction.

For experiments of Set 3, single-cell recordings and neurobiotin labeling were made as in Set 2, but in Vermis and just in anesthetized mice.

4.2.1 SEPs characterization in CrusI-II.

To get a representative electrophysiological marker of neuronal excitability, SEPs in CrusI-II were characterized in alert mice (Fig. 4.6*A*). Electrical whisker stimulation evokes a SEP in the ipsilateral CrusI-II region consisting in two mayor negative waves corresponding to trigeminal (T) and cortical (C) responses (Fig. 4.6*B*). The T component could be subdivided in N1 and N2, the first one being an early small negative wave with

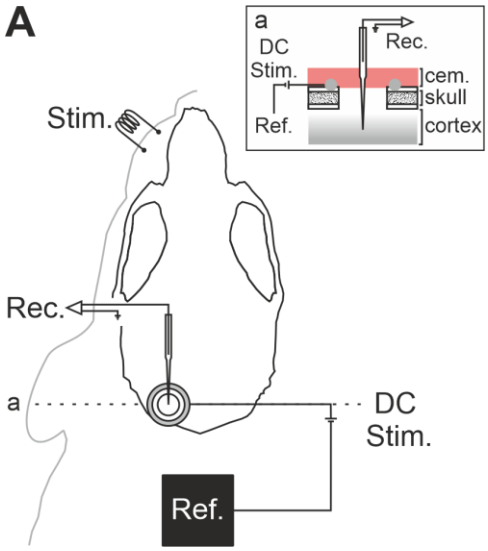
A
a
DC
Stim.
Rec.
cem.
skull
cortex
Ref.
Stim.
Rec.
a
DC
Stim.
Ref.

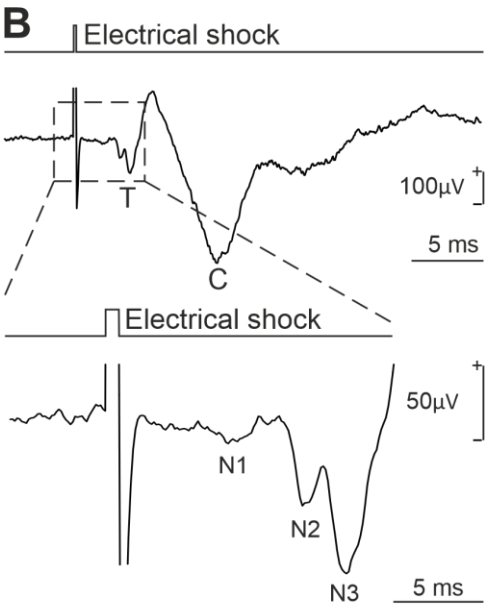
B
Electrical shock
100µV
5 ms
T
C
Electrical shock
50µV
N1
N2
N3
5 ms

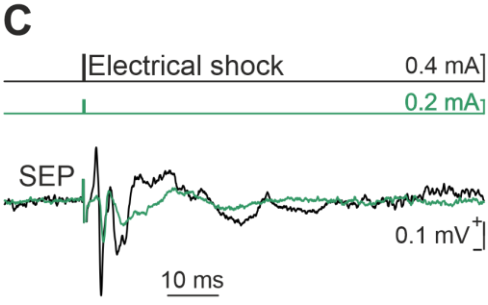
C
Electrical shock
0.4 mA
0.2 mA
SEP
0.1 mV
10 ms

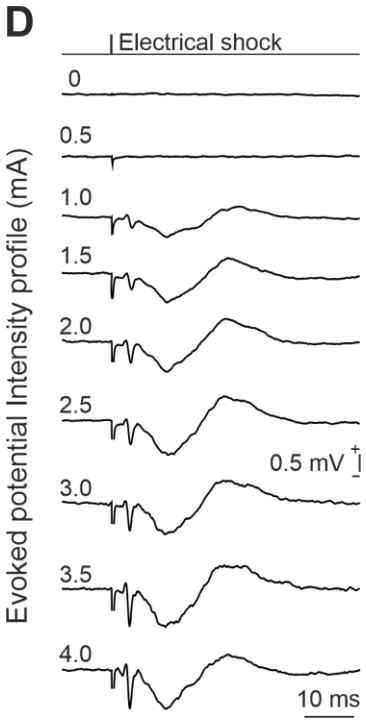
D
Electrical shock
0
0.5
1.0
1.5
2.0
2.5
0.5 mV
3.0
3.5
4.0
10 ms
Evoked potential Intensity profile (mA)

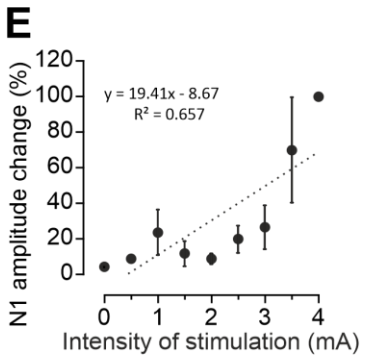
E
y = 19.41x - 8.67
R² = 0.657
N1 amplitude change (%)
Intensity of stimulation (mA)

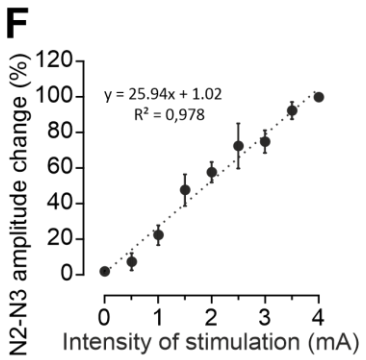
F
y = 25.94x + 1.02
R² = 0,978
N2-N3 amplitude change (%)
Intensity of stimulation (mA)

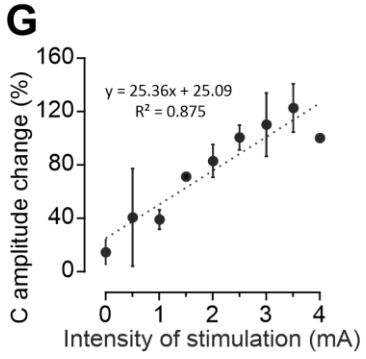
G
y = 25.36x + 25.09
R² = 0.875
C amplitude change (%)
Intensity of stimulation (mA)

Figure 4.6. Characterization of SEPs in CrusI-II. *A*) Experimental design for Set 2 experiments with concurrent Cb-tDCS and recordings on CrusI-II. *B*) Profile of SEP induced by whisker electrical stimulation (n = 30 SEPs from one mouse) showing the different components (trigeminal component (T) N1, N2 and N3; cortical component (C)). *C*) Comparison of CrusI-II-SEPs for two different intensities applied to whisker stimulation obtaining maximum N2-N3 amplitude (black trace, n = 10), and 50% of the maximum N2-N3 amplitude (green trace, n = 10). *D*) CrusI-II-SEP intensity profile. Every trace corresponds to an average of 5 SEPs recorded at the same location but with different intensities of whisker electrical stimulation. *E*-*G*) Quantification of the amplitude change in N1 (*E*), N2-N3 (*F*) and C (*G*) components regarding intensity applied to whisker electrical stimulation. Data normalized with respect maximum amplitude recorded at 4 mA (n = 2 mice).

very short latency of 1.75 ± 0.23 ms (n = 14 mice) from whisker stimulus, and the second a bigger negative wave with a latency of 3.79 ± 0.69 ms (n = 14 mice) (Fig. 4.6*B*, lower figure). As previously reported (Márquez-Ruiz and Cheron, 2012), in some recordings the N2 component appeared subdivided in two different waves (termed as N2 and N3), but this differentiation was not reliable across time and mice, so the analysis were performed just considering N2-N3 complex. Finally, the cortical component (C) peaked at 12.57 ± 1.12 ms (n = 14 mice) and its amplitude decreased when the animal was running, so those events were discarded from the analysis, as well as those coincident with electrical artifacts.

The final amplitude of the different components linearly depended on the intensity of the electrical stimuli applied to the whiskers (N1 component: R^2 = 0.657, Fig. 4.6*E*; N2 component: R^2 = 0.978, Fig. 4.6*F*; C component: R^2 = 0.875, Fig. 4.6*G*; n = 2 mice), so for the experiments the current intensity of whisker electrical pulses was adjusted as to elicit a N2-N3 component with half of the maximum amplitude to allow an increase or decrease of the SEP components during and after Cb-tDCS intervention (Fig. 4.6*C*).

4.2.2 Intracranial electric fields induced by Cb-tDCS in cerebellar cortex.

To know the actual electric field gradient imposed by Cb-tDCS on cerebellar cortex, the same procedure as for S1 experiments was performed. Animals (n = 9) were prepared for chronic recording of cerebellar cortex-LFPs in alert condition during simultaneous application over lateral cerebellum of low-frequency tACS (1 Hz) at different intensities (± 2, ± 20 and ± 200 μA). Differential recordings were obtained

between the glass micropipette in cerebellar cortex and a silver reference electrode placed over the dura in the ipsilateral parietal cortex. LFP recordings were sequentially performed every 1 mm from cortical surface to 3 mm depth with a 15° rostro-caudal angle (Fig. 4.7*A*).

The figure 4.7 (*B*) shows the grand average obtained from recordings (unprocessed data) at different depths including data from all the animals in the study. Under the active electrode the electric field decreased it magnitude in depth in a logarithmic manner for all intensities tested. The recorded electric field for all the animals is represented in figure 4.7 (*C*).

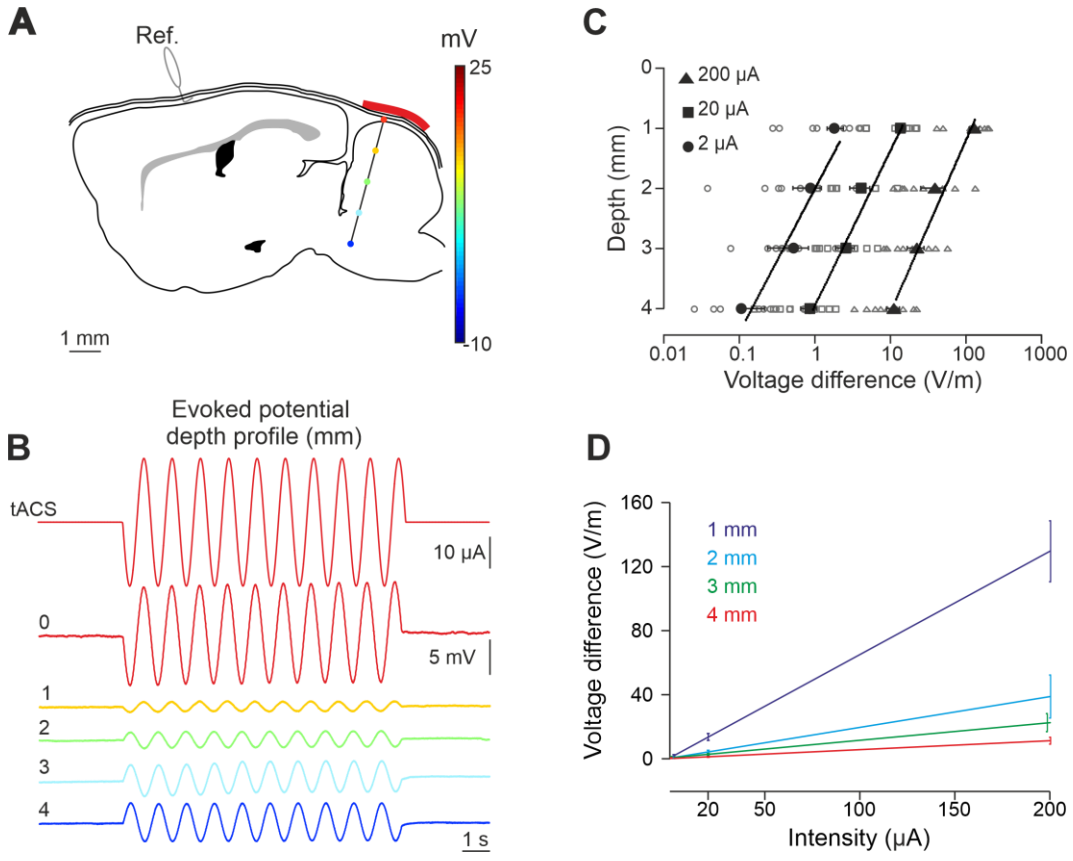

Figure 4.7. Intracranial electric fields induced by Cb-tDCS. *A*) Schematic representation of electric potentials recorded in lateral cerebellum at different depths. *B*) tACS stimulation (top trace) applied over the scalp and grand average (n = 9 mice, unprocessed data) of the actual potentials generated at different depths (from 0 to 4 mm). *C*) Average (filled symbols) and individual (empty symbols) electric fields recorded at different depths for ± 2 (circles), ± 20 (squares) and ± 200 µA (triangles) tACS. *D*) Linear regression applied to the relation between tACS-intensity and voltage difference for each depth.

To calculate the electric field imposed by tES at 200 µA over CrusI-II, we used a linear regression equation extracted from the relation between tDCS-intensity and voltage difference (y = 0.6436 X + 0.8036; R^2 = 0.9952) for each depth (Fig. 4.7*D*). The calculated electric field strength induced by 200 µA at the recording site (around 1 mm) was 129,52 V/m.

4.2.3 Cb-tDCS immediate effects on CrusI-II-SEPs.

For CrusI-II-SEPs during Cb-tDCS, figure 4.8 (*A*) shows the averaged SEPs (n = 15) during the control just before anodal (light-red trace), during anodal (red trace), before cathodal (light-blue trace) and during cathodal (blue trace) Cb-tDCS applied at 200 µA (density current = 4.26 mA/cm^2) for a representative animal. Mean data obtained from the group of animals participating in the experiment (n = 11) are represented in figure 4.8 (*B*, amplitude; *C*, latency). During 5 seconds of stimulation the amplitude of N1 and N2-N3 were significantly increased and decreased in response to anodal and cathodal Cb-tDCS, respectively. The C component did not show a significant modulation, but it showed a tendency to being modulated in the opposite direction of N1-N2 (Fig. 4.8*A*). The average N1 and N2-N3 amplitude increase for 200 µA of anodal stimulation was 47.77 ± 17.91 % and 13.74 ± 4.16 %, respectively, and a decrease for cathodal stimulation of 15.51 ± 7.24 % and 10.20 ± 4.91 % (Wilcoxon Signed Rank Test for N1, p = 0.019; paired t-Test for N2-N3, p < 0.001) (Fig. 4.8*B*). The average C amplitude was reduced a 10.69 ± 6.72 % for anodal stimulation and increased a 3.55 ± 5.38 % after cathodal stimulation (Wilcoxon Signed Rank Test for C, p = 0.147) (Fig. 4.8*B*).

Latency values were entered into a paired Student's t-test but no differences were found on T nor C latencies for anodal nor cathodal Cb-tDCS (N1: p = 0.895; N2: Signed Rank Test, p = 0.465; C: p = 0.411).

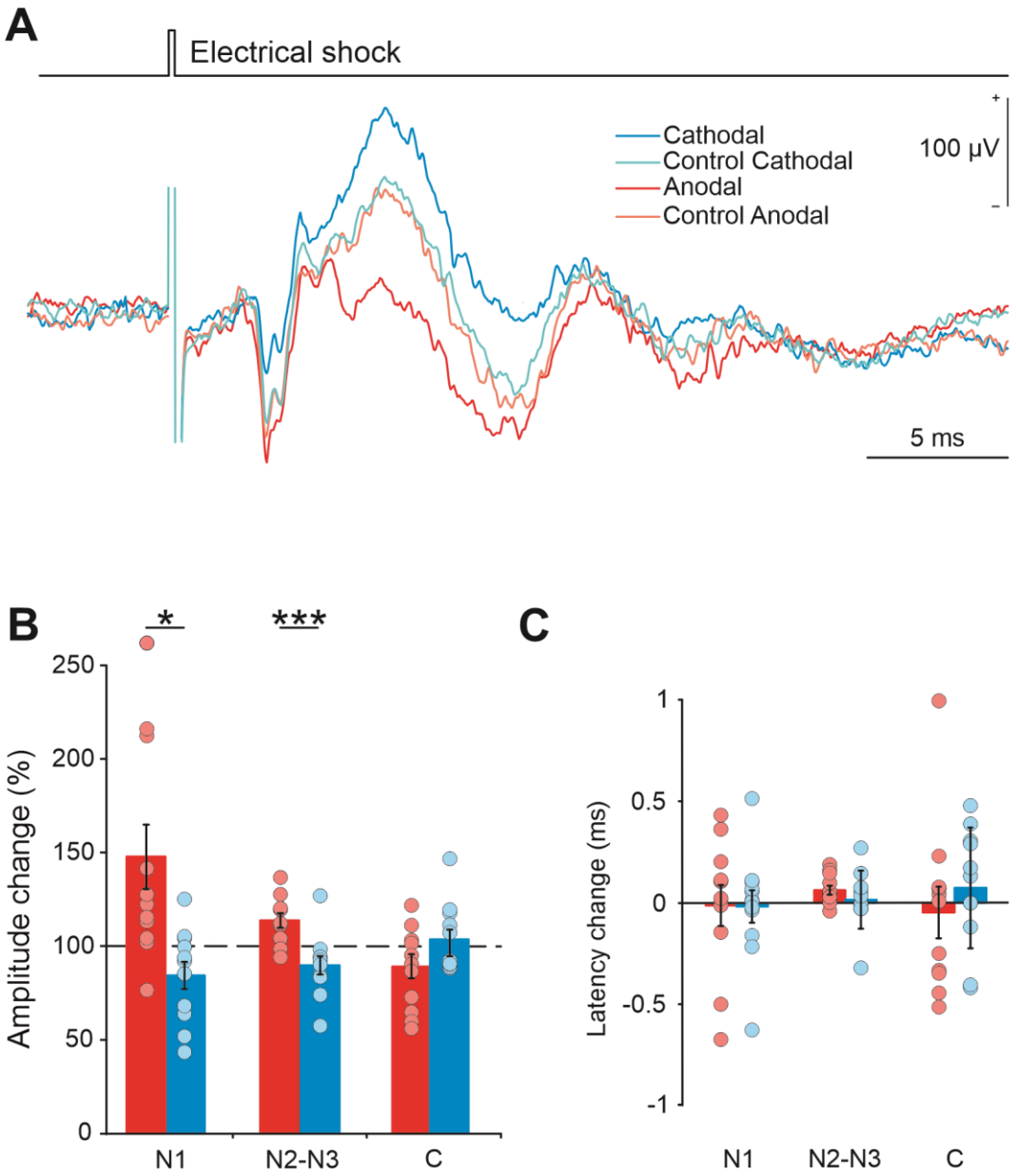

Figure 4.8. Cb-tDCS immediate effects over SEPs in CrusI-II. *A*) CrusI-II-SEPs (n = 15) from a representative animal during control before anodal (light-red trace), anodal (red trace), control before cathodal (light-blue trace) and cathodal (blue trace) Cb-tDCS applied at 200 µA. *B*) Quantification and statistical results of Cb-tDCS effects on the different components of CrusI-II-SEPs amplitude. Mean (bars) and individual amplitude data (circles) for all the animals are represented as percentage of change with respect to control values. n = 11 mice, Wilcoxon Signed Rank Test for N1, *p = 0.012; paired t-Test for N2, ***p < 0.001. *C*) Quantification and statistical results of Cb-tDCS effects on SEP-components latency. Mean for all the animals are represented as the difference with respect to control values. Error bars represent SEM.

4.2.4 Cb-tDCS long-term effects on CrusI-II-SEPs.

To test the potential long-term effects of Cb-tDCS over CrusI-II excitability we recorded SEPs induced by whisker pad stimulation (every 10 ± 2 s) in three different experimental conditions. Animals were prepared for SEP recording and simultaneous Cb-tDCS and randomly assigned to anodal (n = 12), cathodal (n = 11) or sham (n = 7) groups. During experimental sessions SEPs were recorded along 20 min before Cb-tDCS, during simultaneous anodal (200 µA, 20 min), cathodal (-200 µA, 20 min) or sham (200 µA, 30 s) Cb-tDCS, and for 1 hour after Cb-tDCS.

As observed in figure 4.9 (*B*) Cb-tDCS has a significant effect on the normalized amplitude of N2-N3 component of SEPs for both anodal ($p < 0.001$, Friedman Repeated Measures Analysis of Variance on Ranks) and cathodal ($p < 0.001$, Friedman Repeated Measures Analysis of Variance on Ranks) polarity. The post hoc analysis showed that significant differences are found just during the last 10 minutes of Cb-tDCS application in the anodal and cathodal groups (Anodal: n = 12 mice, $p < 0.05$, Dunnett's post hoc test; Cathodal: n = 11 mice, $p < 0.05$, Dunnett's post hoc test). Thus, anodal Cb-tDCS significantly increased the amplitude of N2-N3 component (up to a maximum of 38.58 ± 9.86 %, n = 12) with respect to control values (red filled diamonds in Fig. 4.9*B*), and cathodal Cb-tDCS decreased the amplitude of N2-N3 component (maximum of 14.66 ± 3.68 %, n = 11) with respect to control values (blue filled squares in Fig. 4.9*B*). Once Cb-tDCS was switched off, no differences were found in the amplitude of N2-N3 after anodal nor cathodal stimulation. Also, no differences were found for C component in any temporal period for anodal ($p = 0.64$, Friedman Repeated Measures Analysis of Variance on Ranks) nor cathodal ($p = 0.981$, Friedman Repeated Measures Analysis of Variance on Ranks) Cb-tDCS. N1 component was so small that the resolution for the amplitude measurements cannot give a reliable result, yielding and incredibly high dispersion. For this reason, N1 amplitude was not computed for this analysis.

In addition, we found significant differences along time when values from anodal group were compared with values from sham group. As expected, significant differences

in N2-N3 amplitude were restricted to the Cb-tDCS period (n = 7 mice for Sham, n = 12 mice for Anodal and n = 11 mice for Cathodal, $p < 0.05$, unpaired t-test). No differences were found in the amplitude of the C component between anodal, cathodal and sham groups. Besides founded differences between control period before cathodal Cb-tDCS and during cathodal Cb-tDCS, no differences were found for any of the components when cathodal and sham groups were compared. Between the sham group, as expected, no significant effects were observed in the amplitude of T or C components (N2-N3: $F_{19,114} = 0.563$, $p = 0.925$, repeated-measures ANOVA, black triangles in Fig. 4.9*B*; C: $F_{19,76} = 0.815$, $p = 0.683$, repeated-measures ANOVA).

Latency values were entered into a one-way repeated-measures ANOVA but no differences on N2-N3 nor C components were found for any temporal period for anodal, cathodal nor sham Cb-tDCS.

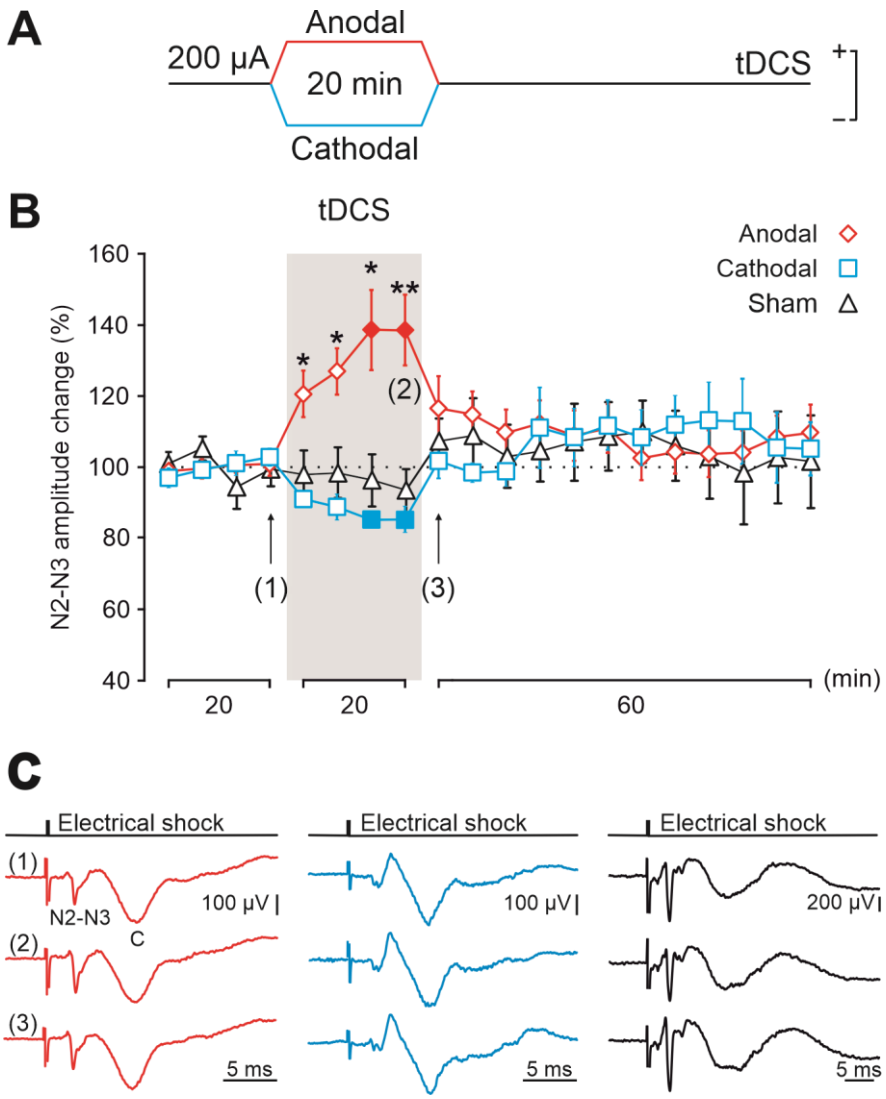

Figure 4.9. Cb-tDCS long-term effects over SEPs in CrusI-II. *A*) Cb-tDCS protocol applied for long-term experiments. *B*) Normalized amplitude change of N2-N3 averaged every 5 min for 20 min of anodal (red diamonds), cathodal (blue squares) or sham (black triangles) Cb-tDCS. Filled symbols represent statistical differences with the last control period (n = 12 mice for anodal, n = 11 for cathodal, n = 7 mice for sham, $p < 0.05$, Holm-Sidak post hoc test). Asterisks mark statistical differences between the same temporal period for anodal or cathodal with sham Cb-tDCS (n = 12 mice for anodal, n = 11 for cathodal, n = 7 mice for sham, *$p < 0.05$; **$p < 0.01$; ***$p < 0.001$, unpaired t-test). *C*) Averaged SEPs from a representative mouse taken 5 minutes before Cb-tDCS ramp-up (1), before (2) and just after (3) Cb-tDCS ramp-down. Error bars represent SEM.

4.2.5 GAD65-67 and vGLUT1 levels in CrusI-II after 20 minutes of Cb-tDCS.

To explore potential molecular changes after Cb-tDCS, vGlut1 and GAD65-67 levels were used to assess possible modifications of the excitation/inhibition balance. For that, we prepared a group of animals for Cb-tDCS application during whisker

stimulation (no electrophysiological recordings were carried out in these experiments) and randomly assigned to anodal (n = 7), cathodal (n = 7) or sham (n = 7) condition.

The number of GAD65-67 (Fig. 4.10*A*) and vGLUT1 (Fig. 4.10*B*) positive clusters of puncta in the stimulated and non-stimulated CrusI-II region were analyzed in the sham, anodal and cathodal groups. For that, BRAIN HEMISPHERE (non-stimulated vs stimulated hemisphere) and tDCS POLARITY (anodal, cathodal or sham) conditions were included in a two-way repeated-measures ANOVA. According with the lack of long-term effects observed in the electrophysiological recordings, there were no differences in GAD65-67 nor vGLUT1 levels in CrusI-II after 1 session of 20 minutes of cathodal or anodal Cb-tDCS.

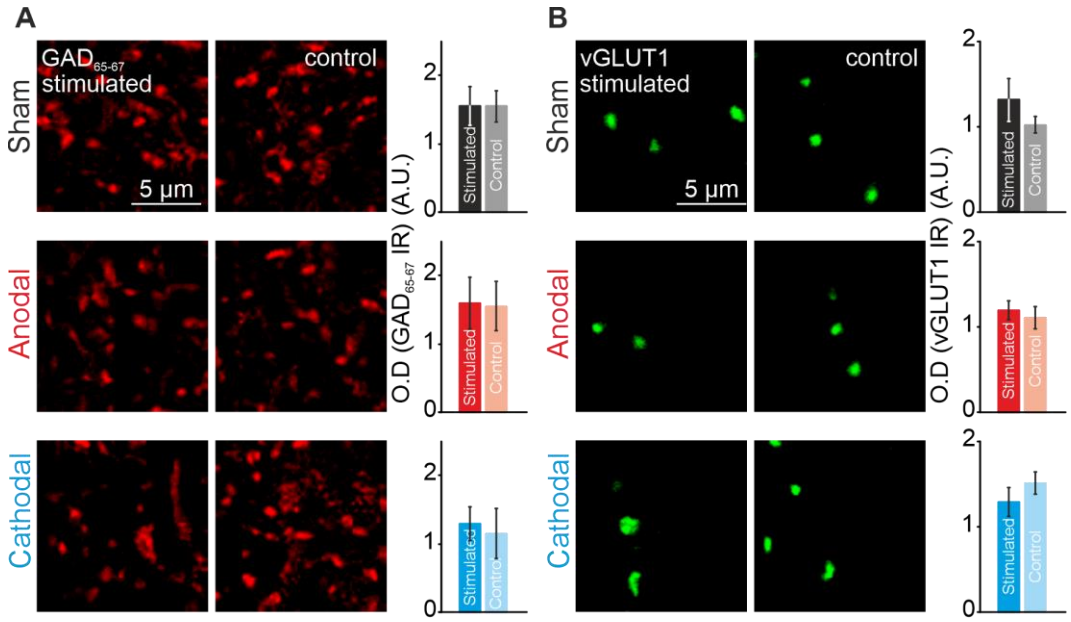

Figure 4.10. Immunohistochemical changes after 20 minutes of Cb-tDCS over lateral cerebellum. *A* and *B*) Confocal photomicrographs (images), quantification and statistics (bars charts) of GAD65-67 expression (*A*) or vGlut-1 expression (*B*) in CrusI-II after 20 min of Sham condition (upper row, n = 7 mice), after 20 min of Anodal Cb-tDCS (middle row, n = 7 mice) and after 20 min of Cathodal Cb-tDCS (lower row, n = 7 mice). Error bars represent SEM. GAD65-67: Glutamic acid decarboxylase isoforms 65 and 67; vGLUT1: vesicular glutamate transporter 1; OD: optical density; IR: immunoreactivity; A.U: arbitrary units.

4.2.6 Neuronal recordings in awake mice.

To understand how Cb-tDCS modulates neuronal firing behavior at a single-cell level, extracellular unitary recordings were performed in CrusI-II region in awake mice. As a first approach, short pulses of Cb-tDCS were applied to avoid the expression of long-term effects, consisting on trials of 15 s (including 5 s ramp-up and 5 s ramp-down) anodal or cathodal Cb-tDCS at 200 µA, with a 10 s pause (no tDCS) between trials.

Figure 4.11 and 4.12 show two examples of isolated cerebellar neurons and their behavior under Cb-tDCS. Spike waveforms under control (black), anodal (red) and cathodal (blue) Cb-tDCS (Fig. 4.11*B* and Fig. 4.12*B*) did not show a significant change, but in 43 out of 78 recorded neurons (n = 29 mice) there was a significant modulation of their firing rate during Cb-tDCS (Fig. 4.11*C*, *D* and Fig. 4.12*C, D*). The observed change in firing rate during the application of Cb-tDCS showed a heterogeneous effect, with some

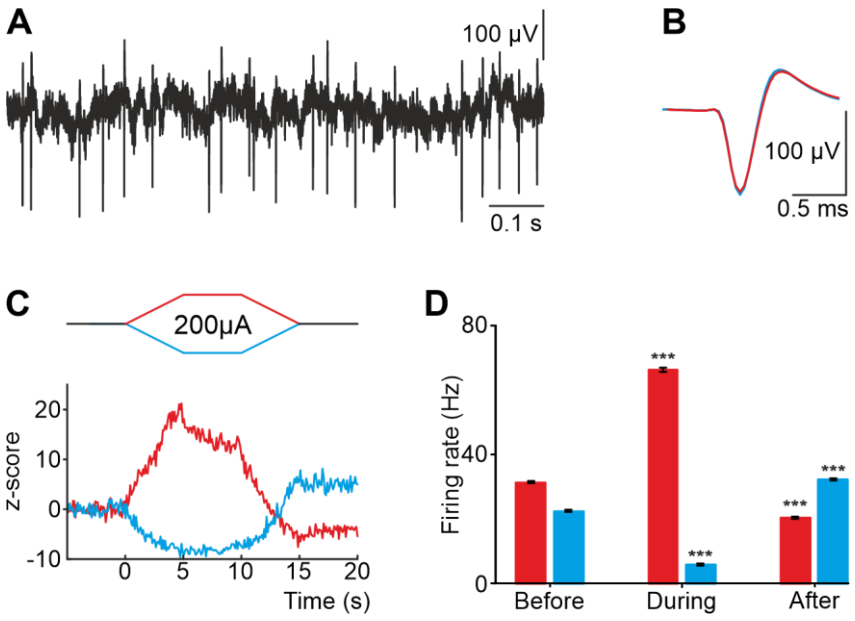

Figure 4.11. Exemplary non-PC showing the increase/decrease in firing rate during anodal/cathodal Cb-tDCS. *A*) Recording of spontaneous firing activity showing the presence of action potentials. *B*) Superimposed averaged action potentials under control (black), anodal (red) and cathodal (blue) Cb-tDCS over lateral cerebellum. *C*) Cb-tDCS current (up) and Z-score-transformed average PSTH (bin size: 0.1 s, bottom) of the spontaneous activity before, during and after anodal (red trace) or cathodal (blue trace) Cb-tDCS. *D*) Statistical comparison of the firing rate (bin size: 0.1 s) between 5 s windows before, during and after Cb-tDCS over lateral cerebellum. Paired Student's t-test, ***p < 0.001. Error bars represent SEM.

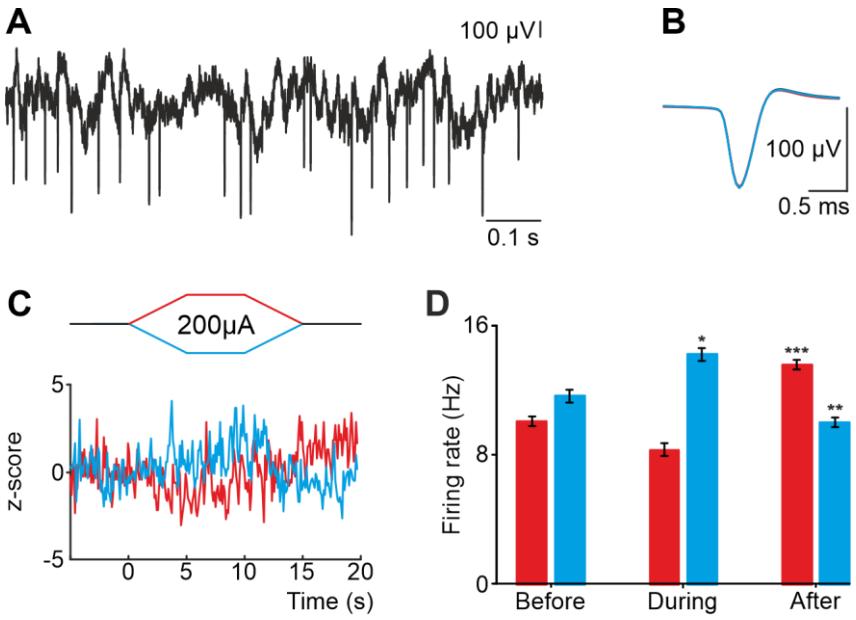

Figure 4.12. Exemplary non-PC showing the decrease/increase in firing rate during anodal/cathodal Cb-tDCS. *A*) Recording of spontaneous firing activity showing the presence of action potentials. *B*) Superimposed averaged action potentials under control (black), anodal (red) and cathodal (blue) Cb-tDCS over lateral cerebellum. *C*) Cb-tDCS current (up) and Z-score-transformed average PSTH (bin size: 0.1 s, bottom) of the spontaneous activity before, during and after anodal (red trace) or cathodal (blue trace) Cb-tDCS. *D*) Statistical comparison of the firing rate (bin size: 0.1 s) between 5 s windows before, during and after Cb-tDCS over lateral cerebellum. Paired Student's t-test, *p < 0.05; **p < 0.01; ***p < 0.001. Error bars represent SEM.

neurons increasing the activity with anodal Cb-tDCS (Fig. 4.11) but others with cathodal Cb-tDCS (Fig. 4.12), and vice versa.

Some of these neurons could be identified as PC based on the presence of CS together with a silence of at least 30 ms in SS after a CS (Fig. 4.13 and Fig. 4.14). These recordings are especially informative since PC are the solely output from cerebellar cortex, so the overall modulation of these neurons likely represents the overall information that cerebellar cortex would convey to downstream regions. As seen in figure 4.13 and figure 4.14, similar results as for non-Purkinje cell (non-PC) neurons were observed in PC, with no modulation of waveform for SS nor CS, but with a reliable effect on firing rate. No statistical differences were found for CS firing rate, probably due to the low firing rate of these spikes (0.5-2 Hz), but as in non-PC the same heterogeneity in modulation was observed for SS in PCs, with anodal increasing and cathodal decreasing

firing rate in some neurons (Fig. 4.13) or vice versa (Fig. 4.14). Noteworthy, some of the neurons showed a significant effect on SS after Cb-tDCS (51.28 % of the recorded neurons, figure 4.11, figure 4.12 and figure 4.14).

If we just consider the PC, 18 out of 31 recorded PC showed a significant modulation of their firing rate during Cb-tDCS, and the heterogeneous behavior of modulation was proportional to that of all neurons together.

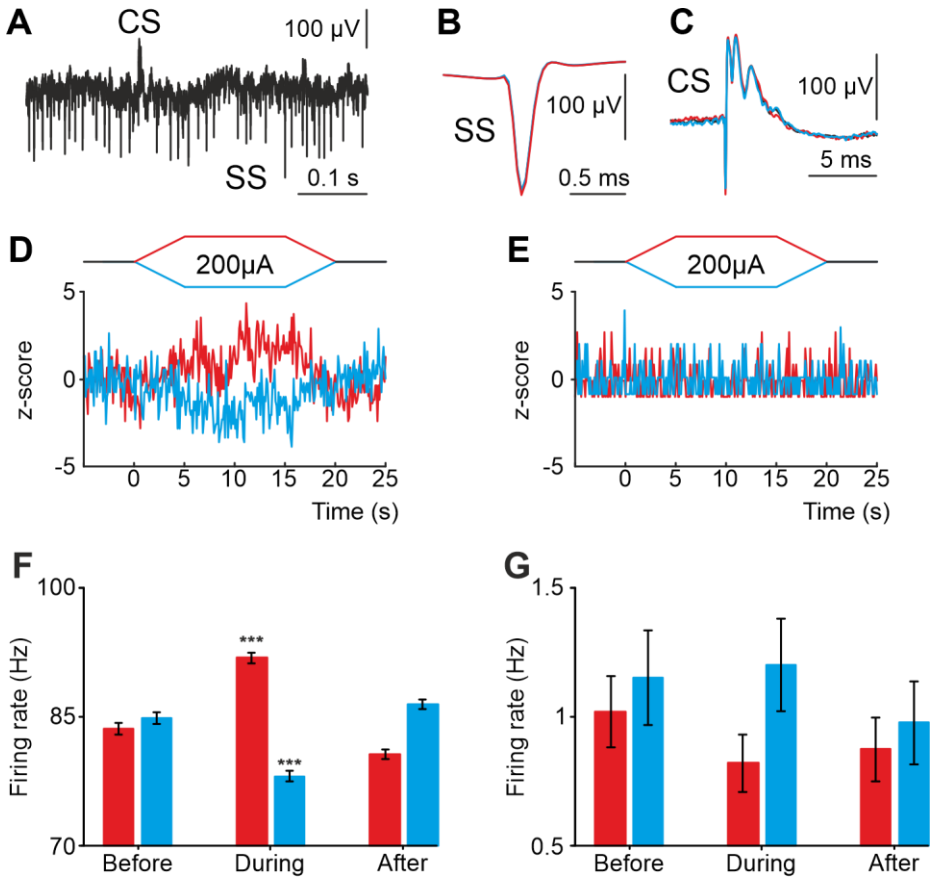

Figure 4.13. Exemplary PC cell showing the increase/decrease in SS firing rate during anodal/cathodal Cb-tDCS. *A*) Recording of spontaneous firing activity of a PC showing the presence of SS and CS. *B* and *C*) Superimposed averaged SS and CS waveforms under control (black), anodal (red) and cathodal (blue) Cb-tDCS over lateral cerebellum. *D*, *E*) Cb-tDCS current (up) and Z-score-transformed average PSTH (bin size: 0.1 s) of the spontaneous activity before, during and after anodal (red trace) or cathodal (blue trace) Cb-tDCS. *F*, *G*) Statistical comparison of the firing rate (bin size: 0.1 s) between 5 s windows before, during and after Cb-tDCS over lateral cerebellum. Paired Student's t-test, ***p < 0.001. Error bars represent SEM.

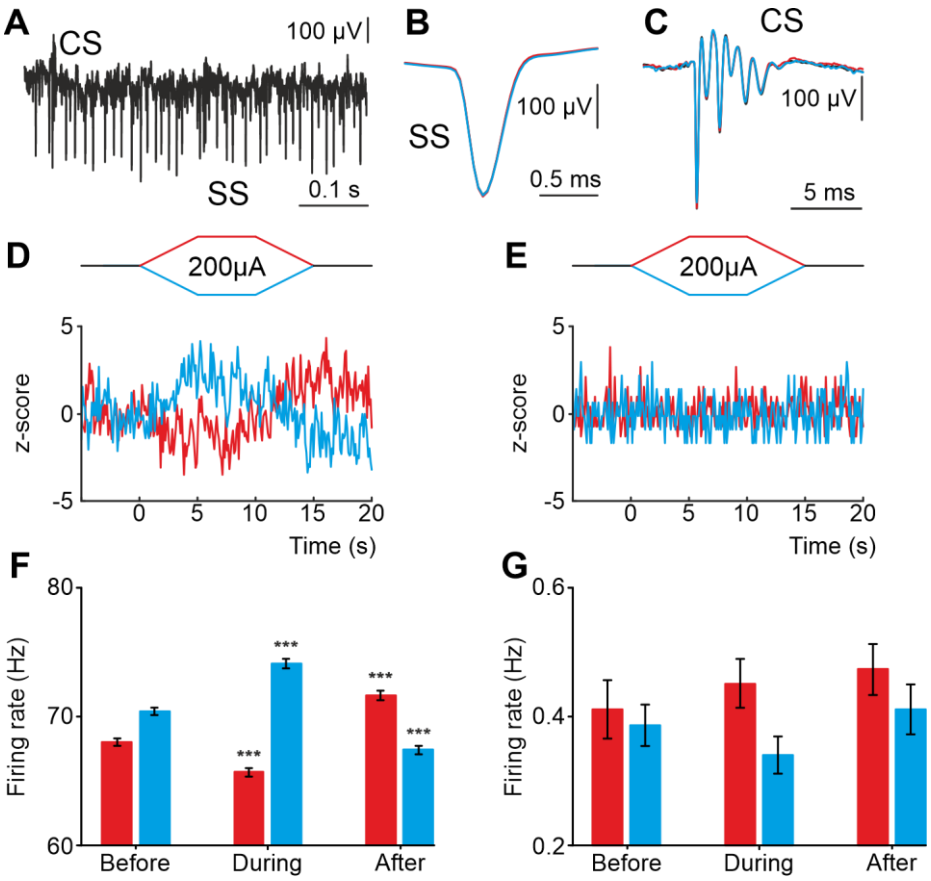

Figure 4.14. Exemplary PC cell showing the decrease/increase in firing rate during anodal/cathodal Cb-tDCS. *A*) Recording of spontaneous firing activity of a PC showing the presence of SS and CS. *B* and *C*) Superimposed averaged SS and CS waveforms under control (black), anodal (red) and cathodal (blue) Cb-tDCS over lateral cerebellum. *D*, *E*) Cb-tDCS current (up) and Z-score-transformed average PSTH (bin size: 0.1 s) of the spontaneous activity before, during and after anodal (red trace) or cathodal (blue trace) Cb-tDCS. *F*, *G*) Statistical comparison of the firing rate (bin size: 0.1 s) between 5 s windows before, during and after Cb-tDCS over lateral cerebellum. Paired Student's t-test, ***p < 0.001. Error bars represent SEM.

Taken together all the different recorded PC and non-PC neurons (n = 78), the most usual modulation during Cb-tDCS was an opposite effect for anodal and cathodal (56.82 % of modulated neurons), thus, the majority of the neurons (43.18 %) increased and decreased its firing activity with anodal and cathodal Cb-tDCS, respectively (Fig. 4.11 and Fig. 4.13), or vice versa (13.64 %) for some others (Fig. 4.14). Several neurons just increase or decrease its firing rate with anodal or cathodal Cb-tDCS but showed no modulation with the opposite polarity (25 %) (Fig. 4.13), and there were even a few neurons that modulated in the same direction for both Cb-tDCS polarities (18.18 %). Furthermore, the modulation used to follow the tDCS dynamics (Fig. 4.15), gradually increasing/decreasing the firing rate according to the ramp-up intensity increase,

holding the modulation during tDCS at its maximum amplitude, and decreasing/increasing the firing rate according to the ramp-down intensity decrease. The modulation of the firing rate followed the dynamics of tDCS even with 5 s more of tDCS at its maximum intensity (5 s in Fig. 4.15*A, B*; 10 s in Fig. 4.15*C, D*), suggesting a direct effect of the applied currents over neuronal activity.

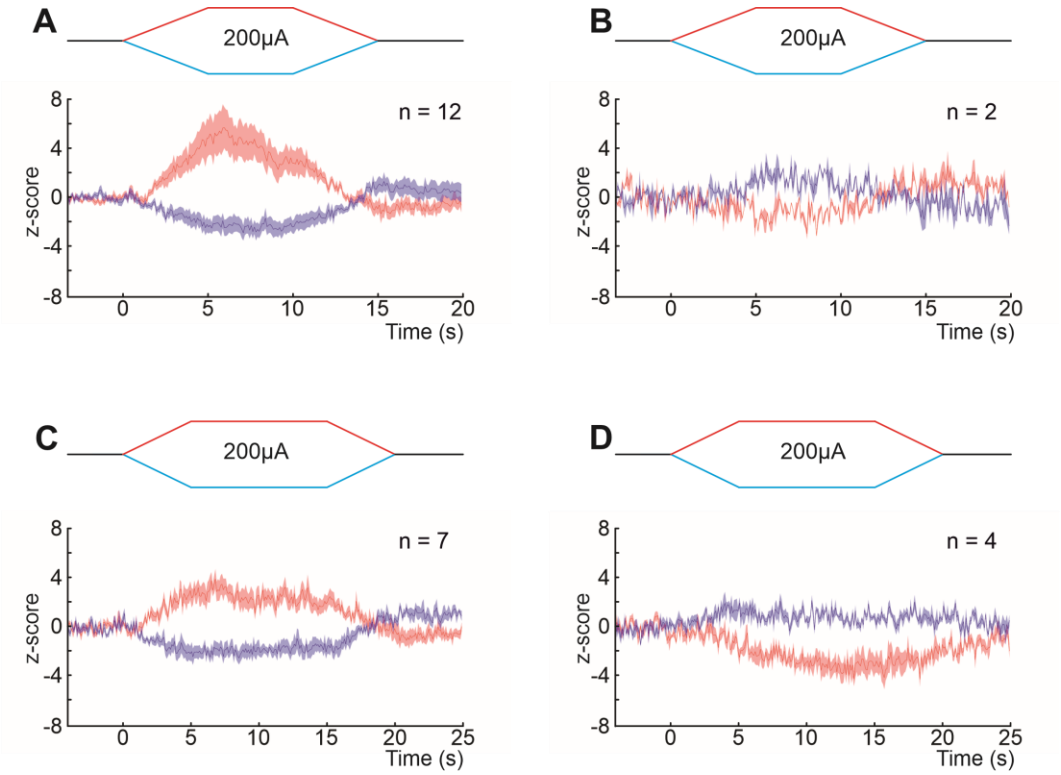

Figure 4.15. Z-score-transformed grand average PSTH (bin size: 0.1 s) of the spontaneous activity before, during and after anodal (red trace) or cathodal (blue trace) Cb-tDCS. Neurons are grouped according to its behavior under Cb-tDCS, with anodal/cathodal increasing/decreasing, respectively (*A* and *C*), the firing rate, and the opposite effect (*B* and *D*) for 5 (*A* and *B*) or 10 (*C* and *D*) seconds of tDCS. n = number of neurons.

These data showed Cb-tDCS capability to modulate firing rate of individual neurons, either PC or non-PC, with a mixed direction of modulation (increase or decrease) for anodal or cathodal polarity depending on the neuron.

In addition, to test the effect of different current intensities on firing rate modulation, trials of 20 s (including 5 s ramp-up and 5 s ramp-down) anodal or cathodal Cb-tDCS at different randomly distributed intensities (100, 200 and 300 μA) were tested. The three intensities were able to consistently modulate the firing rate, with some neurons

responding to the three intensities (Fig. 4.16*A-C*) but others just to one or two. Of the neurons responding to the three intensities (Fig. 4.16*D, E*), about 50 % (8 out of 16 for anodal, 6 out of 16 for cathodal) exhibited a good correlation (R > 0.8) between firing rate modulation and Cb-tDCS intensity, with some neurons showing a tendency to increase their firing rate modulation (either an increase or a decrease of firing rate) with increasing anodal (Fig. 4.16*D*) or cathodal (Fig. 4.16*E*) intensity.

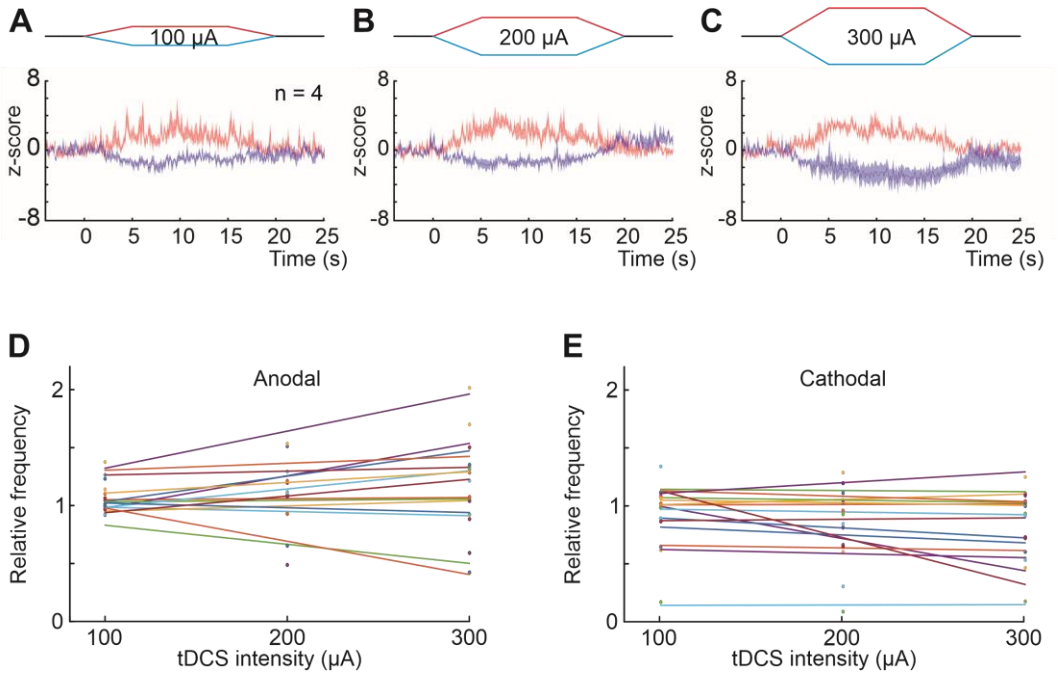

Figure 4.16. Intensity-dependent modulation of neuronal activity. *A-C*) Z-score-transformed grand average PSTH (bin size: 0.1 s) of the neurons (n = 4) that exhibited firing rate modulation during the three intensities tested, with anodal increasing and cathodal decreasing their activity. *D, E*) Firing rate modulation during 10 seconds of Cb-tDCS with respect firing rate during control condition for the three intensities tested under anodal (*D*) and cathodal (*E*) Cb-tDCS. A linear curve was fitted for every neuron. n = number of neurons.

In summary, as shown in figure 4.17 (*A*) for all recorded neurons in awake mice a similar proportion of neurons were modulated with anodal and cathodal Cb-tDCS, and a similar proportion of modulated neurons is observed for each of the three intensities tested (inner circle in right figure). Both anodal and cathodal Cb-tDCS can increase and decrease the firing frequency depending on the neuron, however, a tendency toward increasing firing rate was observed for anodal stimulation, while the opposite effect was observed for cathodal stimulation. If we just take into account the PC (Fig. 4.17*B*), similar proportions of modulation are observed but it seems to be a tendency toward increase

firing activity for both, anodal and cathodal Cb-tDCS, suggesting a net excitatory effect on cerebellar cortex output. These data show that Cb-tDCS can modulate the firing rate of around 50 % of CrusI-II neurons in awake mice in a polarity and intensity-dependent manner.

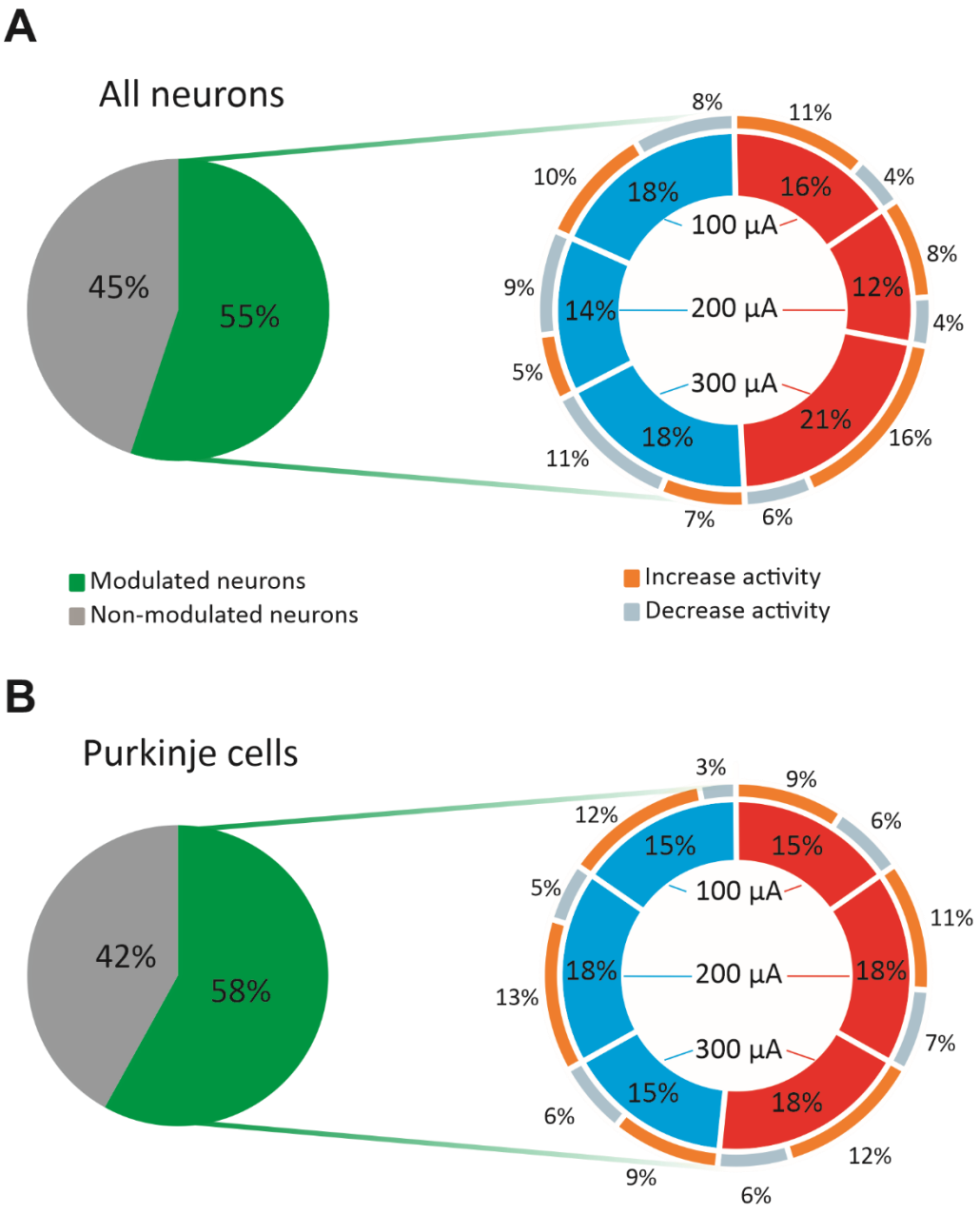

Figure 4.17. Summary of all recorded neurons (*A*) and just PC (*B*) in awake mice. Left circles represent the percentage of neurons modulated (green) or no modulated (grey) during Cb-tDCS. Inner circles in right figures show the proportion of neurons modulated by each Cb-tDCS intensity and polarity (red for anodal, blue for cathodal tDCS). Outer circles in right figures represent the proportion of neurons that exhibit an increase (orange) or decrease (grey) of their firing rate during Cb-tDCS.

4.2.7 Neurobiotin neuronal labeling in anesthetized mice.

To better understand the differences observed in firing rate modulation by Cb-tDCS, neurobiotin labeling of the recorded neurons were performed in CrusI-II (Set 2, n = 20 mice and 39 neurons) and Vermis (Set 3, n = 27 mice and 63 neurons) of anesthetized mice. Juxtacellular labeling (Fig. 4.18*A*) of the recorded neuron was performed after several Cb-tDCS trials to obtain the firing rate modulation and the morphological characterization of the same neuron.

All labeled neurons (n = 7) showed a significant modulation at least with 100, 200 or 300 µA Cb-tDCS and the direction was always to increase with anodal and decrease with cathodal if the somatodendritic axis orientation point towards the active electrode (Fig. 4.18*B*-*D*), and the opposite direction of modulation if the somatodendritic axis orientation point to the opposite direction (Fig. 4.18*C*-*E*). As shown in figure 4.19, Cb-tDCS effects on firing rate highly depends on the somatodendritic axis orientation with respect to the active electrode, with maximum tDCS modulation for orthogonal orientation, and less effect when the axis tilts.

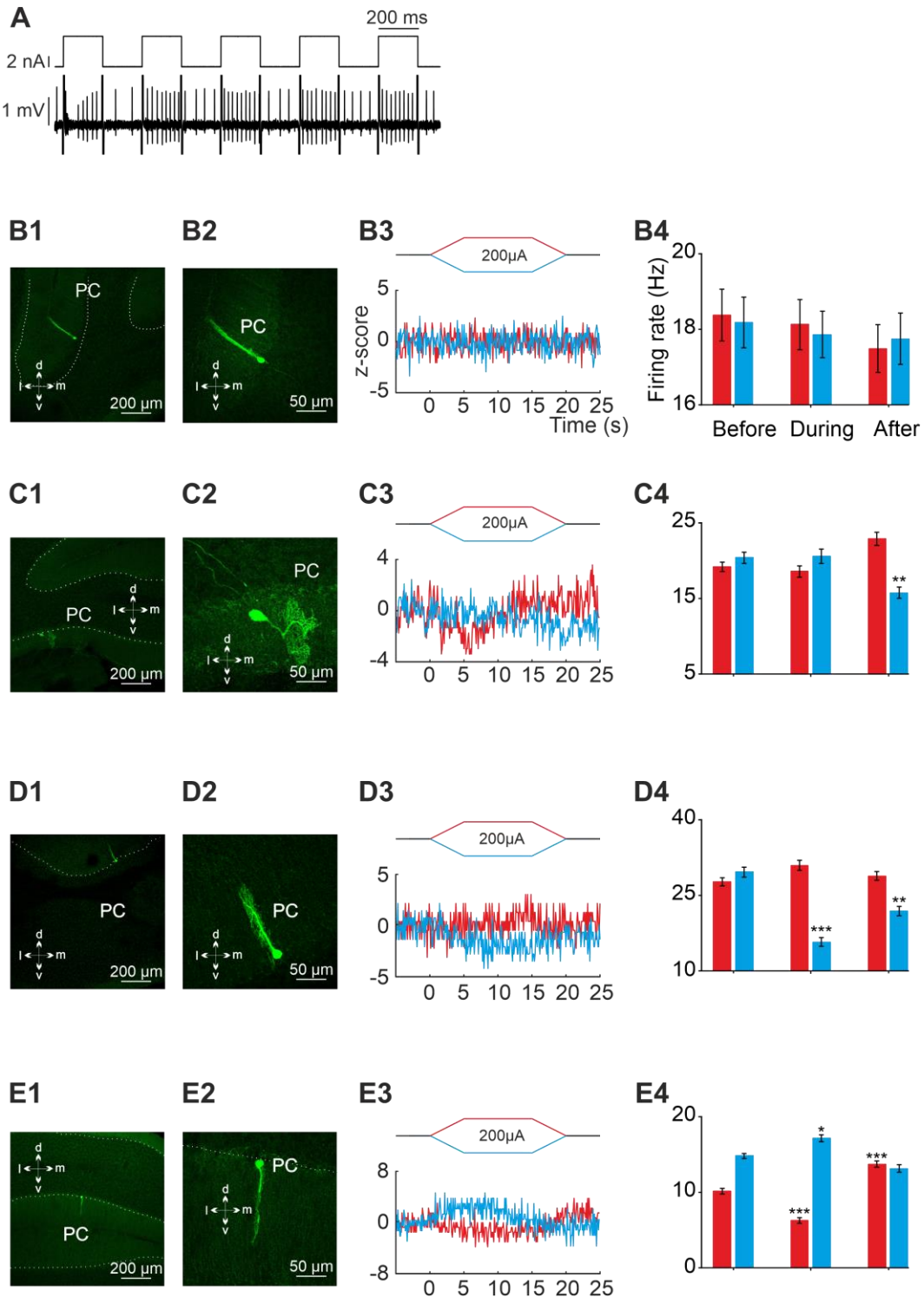

Figure 4.18. Juxtacellular labeling technique and exemplary labeled neurons. *A*) Spontaneous firing rate modulation during 200 ms positive current pulses delivered through the recording pipette. *B–E*) Confocal images of labeled neurons with different somatodendritic angles (*B1* and *B2–E1* and *E2*), z-score of their firing rate modulation during Cb-tDCS (*B3–E3*) and statistical analysis (*B4–E4*).

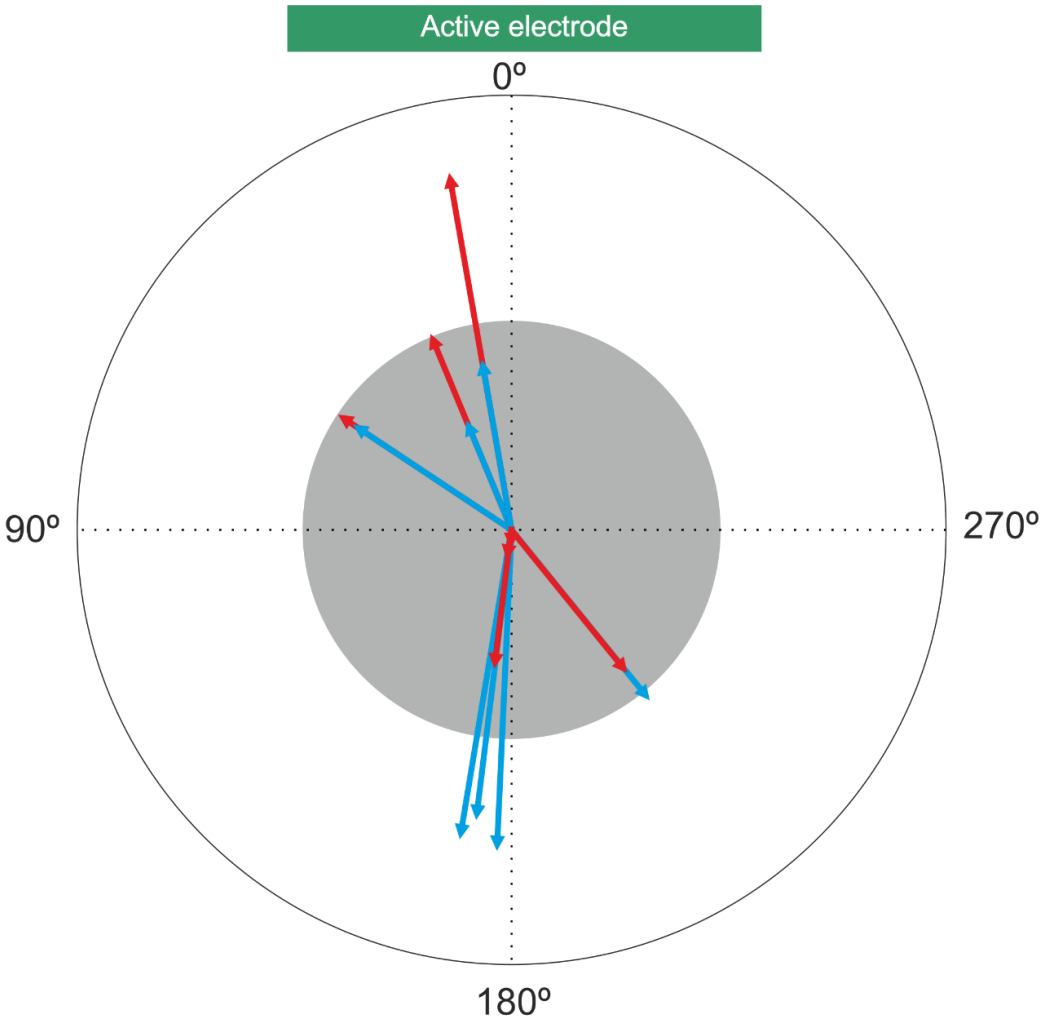

Figure 4.19. Graphical representation relating the firing rate modulation and the somatodendritic axis orientation of recorded and labeled neurons with respect to the generated electric field. Arrows length represent firing rate modulation during 10 s of anodal (red) or cathodal (blue) Cb-tDCS at 200 µA with respect firing rate during control condition (represented by the inner gray disk). Angles of the arrows represent the angle between the neuronal axis and an imaginary line perpendicular to the active electrode (active electrode positioned over skull surface).

In summary, a total of 161 neurons (78 in CrusI-II from awake mice (Fig. 4.20), 20 in CrusI-II from anesthetized mice (Fig. 4.21) and 63 in Vermis from anesthetized mice (Fig. 4.22)) were properly isolated and recorded during time enough for analysis. Based on the individual statistical analysis, the neurons were classified according to their firing rates modulation during Cb-tDCS (increase or decrease during anodal or cathodal) observing the same variety in modulation for CrusI-II anesthetized (Fig. 4.21) as for CrusI-II awake mice recordings (Fig. 4.20). Noteworthy, there are some differences between Vermis and CrusI-II recordings: the proportion of modulated neurons was higher in Vermis; it seems that more neurons modulate in Vermis with anodal than cathodal Cb-

tDCS; it does not seem to be a tendency toward increasing nor decreasing its activity with a specific polarity in the Vermis (Fig. 4.22*C*).

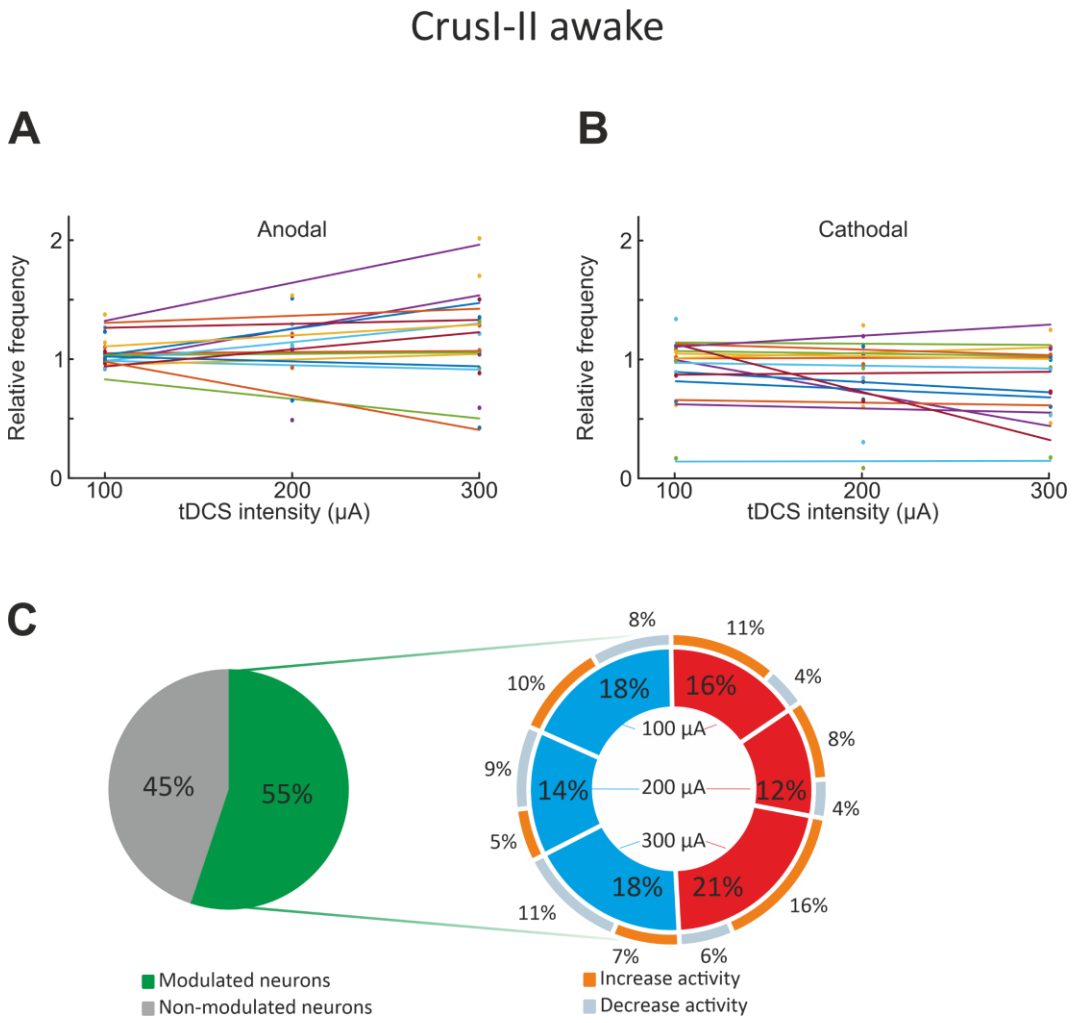

Figure 4.20. Summary of all recorded neurons in CrusI-II in awake mice. *A, B*) Neuronal firing rate modulation during 10 seconds of Cb-tDCS with respect firing rate during control condition for the three intensities tested under anodal (*A*) and cathodal (*B*) Cb-tDCS. A linear curve was fitted for every neuron. *C*) Left circles represent the percentage of neurons modulated (green) or non-modulated (grey) during Cb-tDCS. Inner circles in right figures show the proportion of neurons modulated by each tDCS intensity and polarity (red for anodal, blue for cathodal tDCS). Outer circles in right figures represent the proportion of neurons that exhibit an increase (orange) or decrease (grey) of their firing rate during Cb-tDCS.

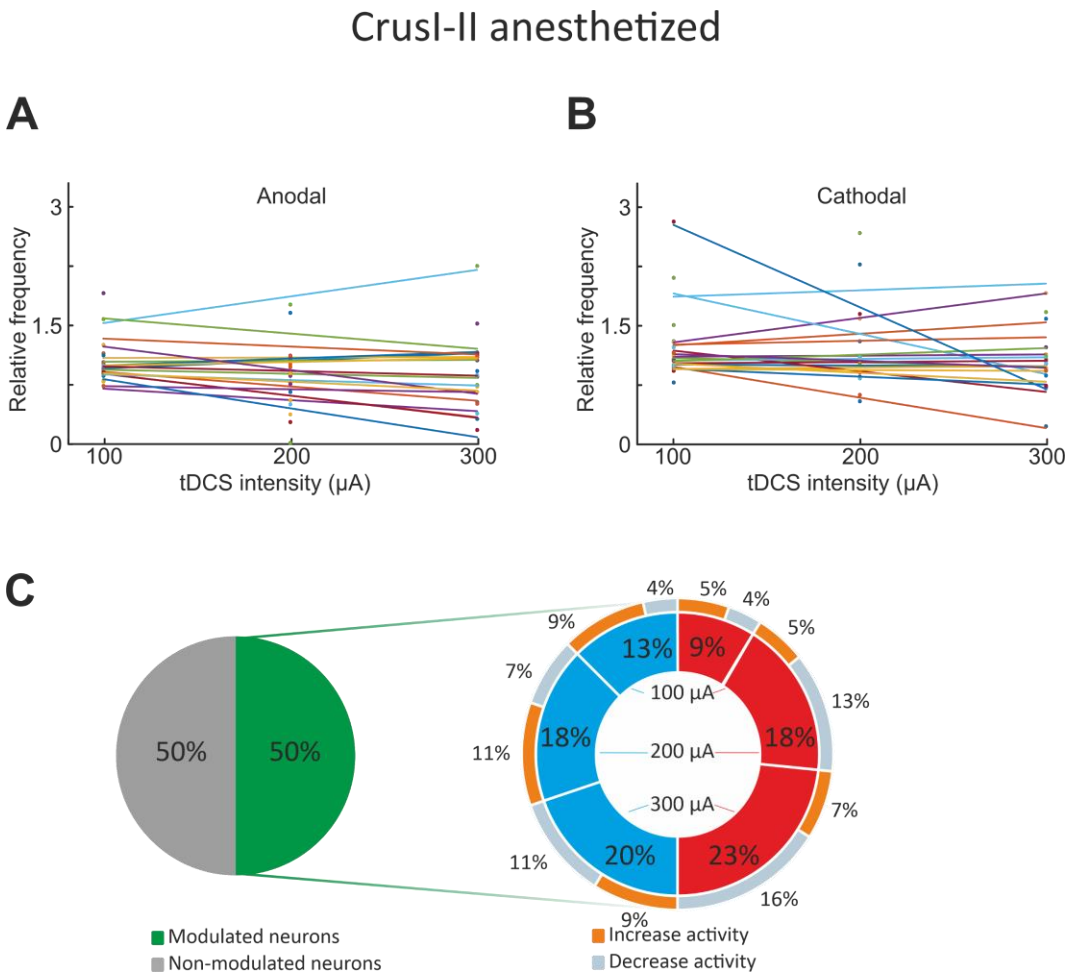

Figure 4.21. Summary of all recorded neurons in CrusI-II in anesthetized mice. *A, B*) Neuronal firing rate modulation during 10 seconds of Cb-tDCS with respect firing rate during control condition for the three intensities tested under anodal (*A*) and cathodal (*B*) Cb-tDCS. A linear curve was fitted for every neuron. *C*) Left circles represent the percentage of neurons modulated (green) or non-modulated (grey) during Cb-tDCS. Inner circles in right figures show the proportion of neurons modulated by each tDCS intensity and polarity (red for anodal, blue for cathodal tDCS). Outer circles in right figures represent the proportion of neurons that exhibit an increase (orange) or decrease (grey) of their firing rate during Cb-tDCS.

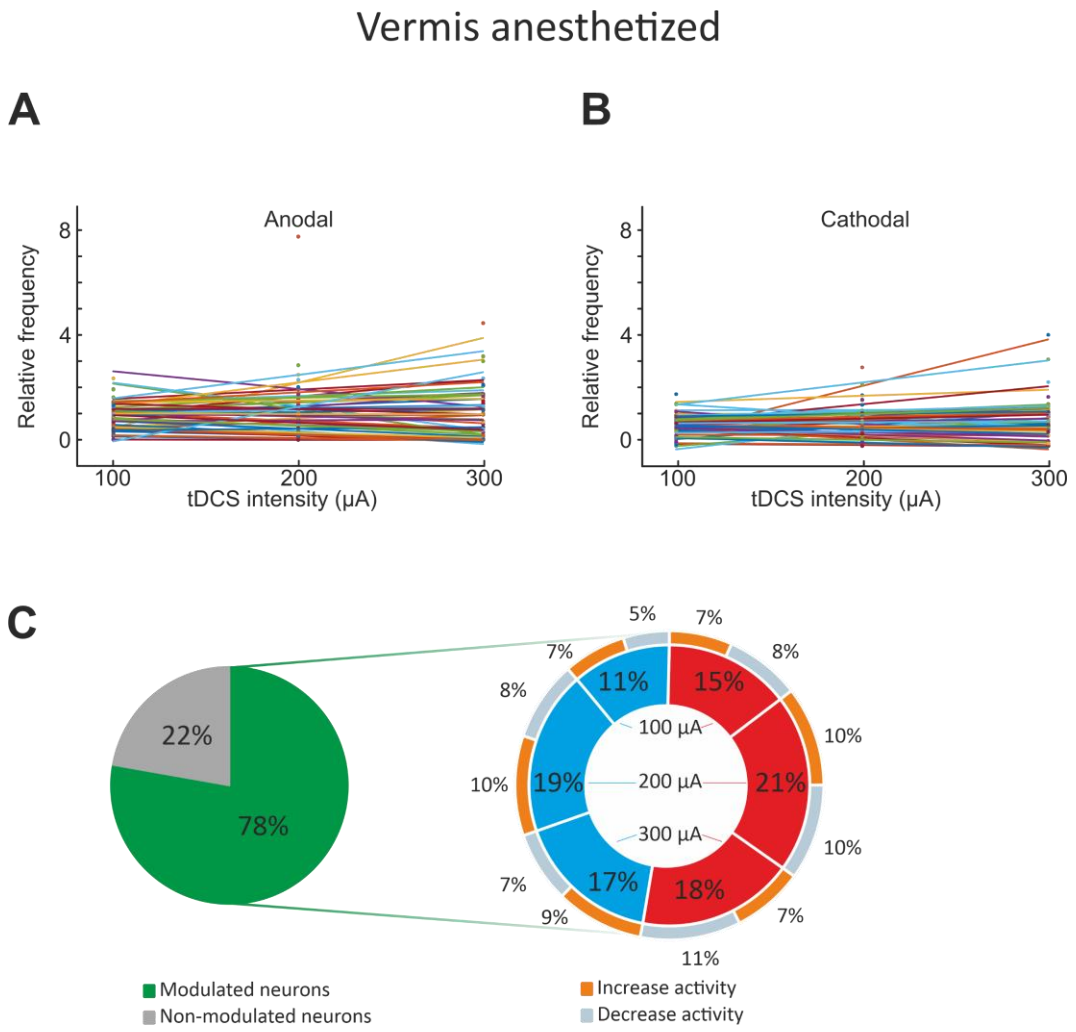

Figure 4.22. Summary of all recorded neurons in Vermis in anesthetized mice. *A, B*) Neuronal firing rate modulation during 10 seconds of Cb-tDCS with respect firing rate during control condition for the three intensities tested under anodal (*A*) and cathodal (*B*) Cb-tDCS. A linear curve was fitted for every neuron. *C*) Left circles represent the percentage of neurons modulated (green) or non-modulated (grey) during Cb-tDCS. Inner circles in right figures show the proportion of neurons modulated by each tDCS intensity and polarity (red for anodal, blue for cathodal tDCS). Outer circles in right figures represent the proportion of neurons that exhibit an increase (orange) or decrease (grey) of their firing rate during Cb-tDCS.

In conclusion, regarding Set 2 experiments, Cb-tDCS demonstrate its ability to modulate cerebellar cortex activity. The validation of SEPs as a measure of cortical excitability allows us to ascertain that anodal and cathodal Cb-tDCS can increase and decrease, respectively, cortical excitability immediately and for 20 minutes of continuous electrical stimulation, but this effects are restricted to the stimulation period since no long-term effects were observed after anodal nor cathodal cessation for SEP amplitude or GAD65-67 and vGlut1 levels. Furthermore, single-cell recordings showed a mixed modulatory effect, with both anodal and cathodal being able to increase and

decrease the firing rate of different neurons. Finally, putting together the neurobiotin-labeled neurons from Set 2 (CrusI-II) and Set 3 (Vermis) experiments, it is clear that the orientation of the somatodendritic axis with respect to the electric field is crucial for the understanding of the tDCS heterogeneous results.

4.3 S1 modulation by Cb-tDCS.

Lastly, once characterized the effects of tDCS on S1 and CrusI-II region, we explored the effects of Cb-tDCS on distant regions. In the last set of experiments (Set 4), tDCS was applied over cerebellar cortex but the modulatory effects were assessed on S1:

- Firstly, the electric field reaching S1 when tDCS is applied in cerebellar cortex was determined, and the electric field strength in the recording area was extrapolated.
- After that, the modulation produced by Cb-tDCS on S1-SEPs was evaluated to test the immediate effects (15 s of Cb-tDCS, including 5 s ramp-up and 5 s ramp-down) and the long-term effects (during 20 minutes of Cb-tDCS and 1 hour after).
- Finally, the long-term impact of Cb-tDCS on excitation/inhibition balance was assessed by immunohistochemical methods, measuring GAD65-67 and vGlut1 levels.

4.3.1 Intracranial electric fields induced in S1 by Cb-tDCS.

The electric field gradient generated by Cb-tDCS over cerebellar cortex is supposed to reach S1 with very low strength. Animals (n = 7) were prepared for chronic recording of S1-LFPs in alert condition during simultaneous application over lateral cerebellum of low-frequency tACS (1 Hz) at different intensities (± 2, ± 20 and ± 200 μA) (Fig. 4.23*A, B*). Differential recordings were obtained between the glass micropipette and a silver reference electrode placed over the contralateral dura and were sequentially performed every 1 mm from cortical surface to 4 mm depth with a 20° lateral angle. The figure 4.23 (*C*) shows the grand average obtained from recordings (unprocessed data) at different depths including data from all the animals in the study. As expected, electric fields induced by Cb-tDCS were very weak in S1, observing very

small voltage differences between depths. The recorded electric field for all the animals is represented in figure 4.23 (*D*).

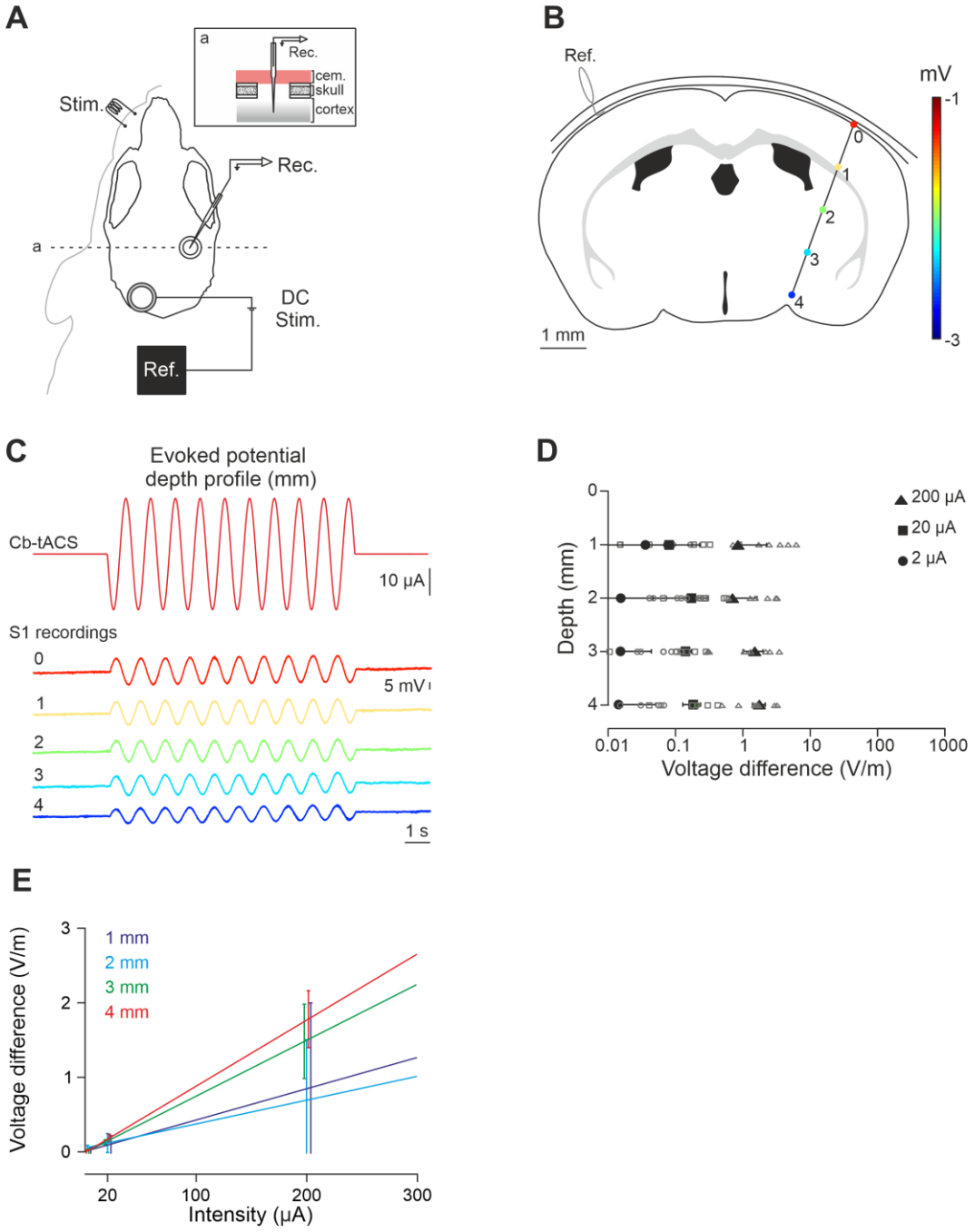

Figure 4.23. S1 intracranial electric fields induced by Cb-tDCS. *A*) Experimental design of Set 4 with Cb-tDCS applied over lateral cerebellum and recordings in S1 cortex. *B*) Schematic representation of electric potentials recorded in S1 at different depths. *C*) tACS (top trace) applied over the cerebellar scalp and grand average (n = 7, unprocessed data) of the actual potentials generated in S1 at different depths (from 0 to 4 mm). *D*) Average (filled symbols) and individual (empty symbols) electric fields recorded at different depths for ± 2 (circles), ± 20 (squares) and ± 200 µA (triangles) tACS. *E*) Linear regression applied to the relation between tACS-intensity and voltage difference for each depth.

To calculate the electric field imposed by tES at different intensities (200 and 300 μA) in the recording site (S1 layer V-VI, 1 mm) we used a linear regression equation extracted from the relation between Cb-tDCS-intensity and voltage difference (y = 0.0042 X + 0.0115; R^2 = 0.9995) for each depth (Fig. 4.23*E*). The calculated electric field strength induced by 200 and 300 μA at the recording site was 0.85 and 1.27 V/m, respectively.

4.3.2 Cb-tDCS immediate effects on S1-SEPs.

For S1-SEPs during Cb-tDCS, figure 4.24 (*A*) shows the averaged SEPs (n = 15) during control before anodal (light-red trace), anodal (red trace), control before cathodal (light-blue trace) and cathodal (blue trace) Cb-tDCS applied at 200 and 300 μA (density currents = 2.86 mA/cm^2 and 4.29 mA/cm^2, respectively) for a representative animal on each intensity. Mean data obtained from the group of animals participating in the experiment (n = 11 for 200 μA and n = 9 for 300 μA) are represented in figure 4.24 (*B*, amplitude; *C*, latency). During 5 seconds of stimulation the amplitude of N1 was significantly decreased and increased in response to anodal and cathodal Cb-tDCS, respectively. Thus, anodal Cb-tDCS progressively decreased the N1 amplitude of simultaneously recorded SEPs with increasing current intensity to a maximum of 17.31 ± 5.27 % at 300 μA whereas cathodal Cb-tDCS increased the N1 amplitude to a maximum of 18.53 ± 6.61 % at 300 μA. The average SEP amplitude change for 200 μA (n = 11; paired t-Test, p = 0.044) and 300 μA (n = 9; paired t-Test, p = 0.011) was a decrease for anodal of 7.49 ± 3.36 % and 17.31 ± 5.27 %, respectively, and an increase for cathodal stimulation of 7.41 ± 3.75 % and 18.53 ± 6.61 %.

Latency values were entered into a paired Student's t-test but no differences were found on N1 latency for anodal nor cathodal Cb-tDCS at any intensity (n = 11; 200 μA: Signed Rank Test, p = 0.765; n = 9; 300 μA: paired t-Test, p = 0.153).

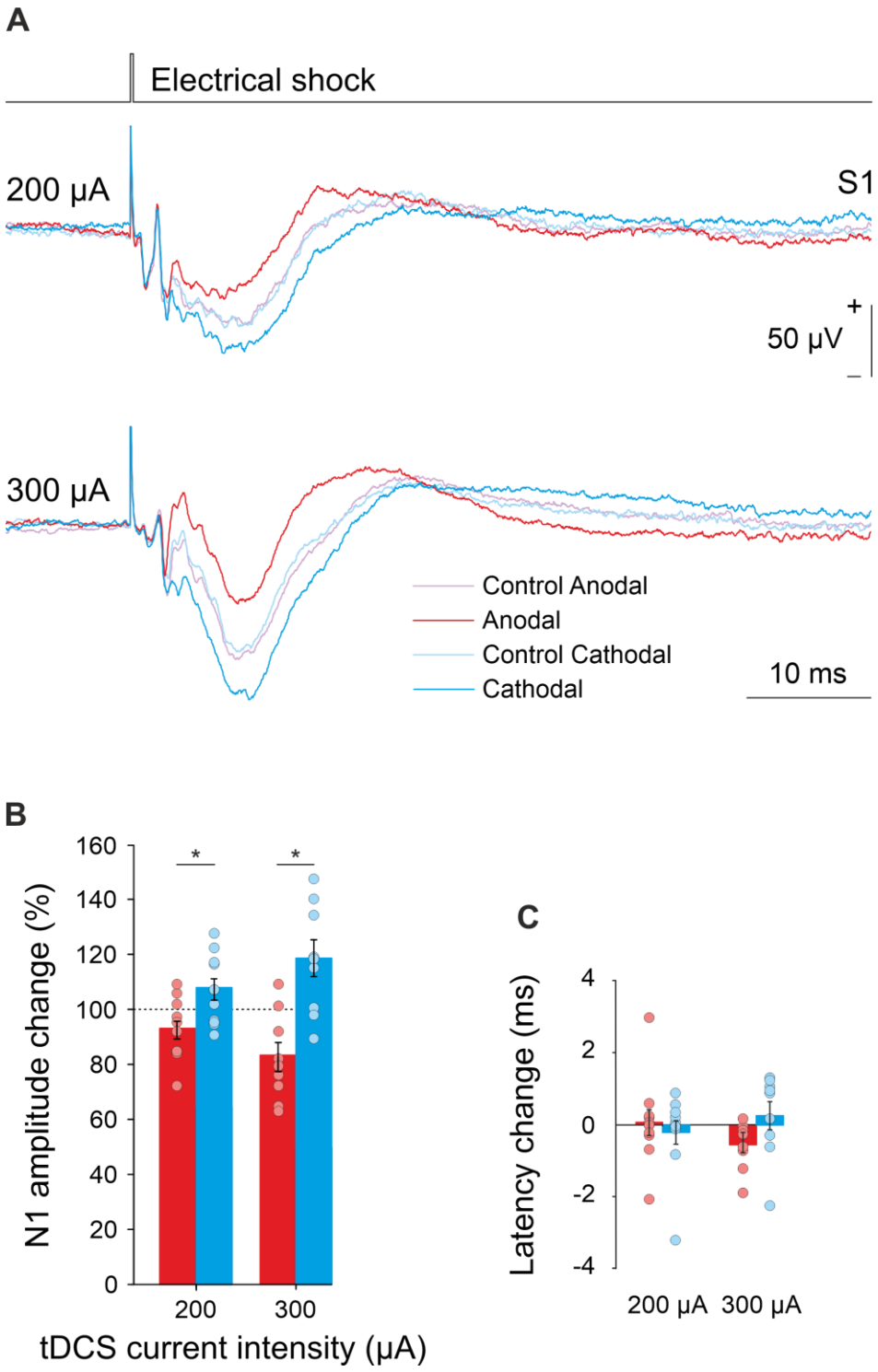

Figure 4.24. Cb-tDCS immediate effects over SEPs in S1 cortex. *A*) SEPs (n = 15) from two representative animals during control before anodal (light-red trace), anodal (red trace), control before cathodal (light-blue trace) and cathodal (blue trace) Cb-tDCS applied at 200 and 300 µA. *B*) Quantification and statistical results of Cb-tDCS effects on SEPs amplitude. Mean (bars) and individual amplitude data (circles) for all the animals are represented as percentage of change with respect to control values (200 µA, n = 11 animals; paired t-Test, p = 0,044; 300 µA, n = 9 animals; paired t-Test, p = 0,011), *p < 0.05. *C*) Quantification and statistical results of Cb-tDCS effects on SEPs latency. Mean for all the animals are represented as the difference with respect to control values. Error bars represent SEM.

4.3.3 Cb-tDCS long-term effects on S1-SEPs.

To test the potential long-term effects in S1 excitability of Cb-tDCS over lateral cerebellum we recorded S1-SEPs induced by whisker pad stimulation (every 10 ± 2 s) and simultaneous Cb-tDCS (n = 5 for anodal, n = 5 for cathodal, n = 8 for sham). During experimental sessions SEPs were recorded along 20 min before Cb-tDCS, during simultaneous Cb-tDCS (300 μA, 20 minutes) and for 1 hour after Cb-tDCS.

As observed in figure 4.25 (*B*) 300 μA Cb-tDCS for 20 minutes has a significant effect on the normalized amplitude of N1 component of SEPs for both cathodal ($p = 0.011$, Friedman Repeated Measures Analysis of Variance on Ranks) and anodal Cb-tDCS ($F_{19,76} = 8.840$, $p < 0.001$, repeated-measures ANOVA). The post hoc analysis showed a significant increase in amplitude after anodal Cb-tDCS application when comparing with control data or during the 20 minutes of stimulation (n = 5 animals, $p < 0.05$, Holm-Sidak post hoc test) (red filled diamonds in Fig. 4.25*B*) but no differences for multiple comparisons within cathodal group were found (blue squares in Fig. 4.25*B*).

Comparing with sham group, we found a significant increase in amplitude during the 20 minutes of cathodal Cb-tDCS ($p < 0.01$, unpaired t-test) whereas a significant decrease in amplitude was observed during the first 10 minutes of anodal Cb-tDCS ($p < 0.05$, unpaired t-test and Mann-Whitney Rank Sum Test) and, according to ANOVA results, a significant increase in amplitude was observed after anodal Cb-tDCS for some temporal periods ($p < 0.05$, unpaired t-test). Thus, cathodal Cb-tDCS significantly increased the amplitude of SEPs (up to a maximum of 45.22 ± 6.96 %, n = 5) with respect to sham values during simultaneous transcranial stimulation, and anodal Cb-tDCS significantly decreased the amplitude of SEPs (up to a maximum of 12.55 ± 7.22 %, n = 5) with respect to sham values during the first 10 minutes of transcranial stimulation. Intriguingly, SEP amplitude during anodal Cb-tDCS returned to control values after the first 10 minutes of stimulation, and a shift toward an increase in amplitude appeared after anodal Cb-tDCS cessation. Finally, the effect during Cb-tDCS for anodal as for cathodal stimulation, seems to be maximum at the beginning of the stimulation but decay over time, being most notorious for anodal Cb-tDCS where after removal of

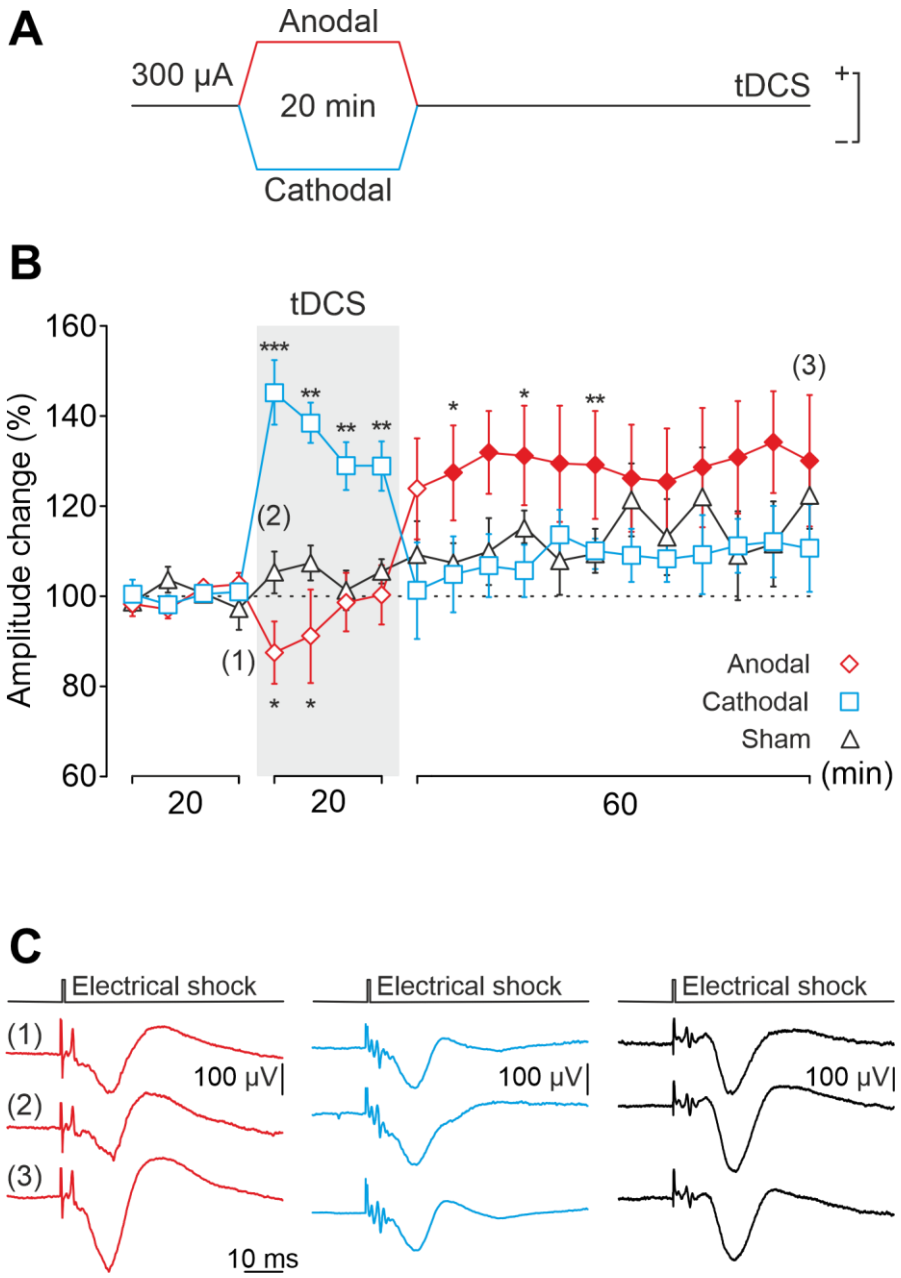

Figure 4.25. Cb-tDCS long-term effects over SEPs in S1 cortex. *A*) Cb-tDCS protocol applied in the long-term experiments. *B*) Normalized amplitude change of N1 averaged every 5 min for 300 µA - 20 min of anodal (red diamonds), cathodal (blue squares) or sham (black triangles) Cb-tDCS. Filled symbols represent statistical differences with the last control period ($p < 0.05$, Holm-Sidak post hoc test). Asterisks mark statistical differences between the same temporal period for anodal or cathodal with sham Cb-tDCS (n = 5 animals for anodal and cathodal, n = 8 for sham, unpaired t-test). *C*) Averaged SEPs from a representative mouse taken 5 minutes before (1) and after Cb-tDCS ramp-up (2), and 1 hour after Cb-tDCS ramp-down (3). *$p < 0.05$; **$p < 0.01$; ***$p < 0.001$. Error bars represent SEM.

stimulation even a strong rebound effect (increase in excitability) can be observed. As expected, no significant effects were observed in the amplitude of N1 component of SEPs within the sham group ($p = 0.119$, Friedman Repeated Measures Analysis of Variance on Ranks).

N1 latency values were entered into a one-way repeated-measures ANOVA but no differences were found for any temporal period for anodal, cathodal nor sham Cb-tDCS.

4.3.4 GAD65-67 and vGLUT1 levels in S1 after 20 minutes of Cb-tDCS.

To elucidate the molecular changes underlying the long-term effects observed after Cb-tDCS in S1, vGlut1 and GAD65-67 levels were used to assess possible modifications of the excitation/inhibition balance. For that, we prepared a group of animals for Cb-tDCS application during whisker stimulation (no electrophysiological recordings were carried out in these experiments) and randomly assigned to anodal (n = 7), cathodal (n = 7) or sham (n = 7) condition.

The number of GAD65-67 (Fig. 4.26*A*) and vGLUT1 (Fig. 4.26*B*) positive clusters of puncta in the stimulated and non-stimulated S1 were analyzed in the sham, anodal and cathodal groups. For that, BRAIN HEMISPHERE (non-stimulated vs stimulated hemisphere) and tDCS POLARITY (anodal, cathodal or sham) conditions were included in a two-way repeated-measures ANOVA. There were no differences for GAD65-67 nor vGLUT1 levels in S1 region after 1 session of 20 minutes cathodal or anodal Cb-tDCS at 200 µA, (Fig. 4.26).

Taken together, the results from experiments in Set 4 provide evidence of the effects that Cb-tDCS can have on distant regions. Anodal and cathodal Cb-tDCS was able to decrease and increase, respectively, S1 excitability immediately. Interestingly, although more data are needed, 20 minutes of cathodal Cb-tDCS seems to increase S1 excitability, with no long-term effects, but 20 minutes of anodal polarity seems to start decreasing cortical excitability in the first minutes but then the effect disappear and after Cb-tDCS cessation a rebound effect is observed in SEPs amplitude. Finally, immunohistochemical analysis in S1 performed after 20 min of Cb-tDCS at 200 µA did not show any significant change in GAD65-67 nor vGlut1 levels.

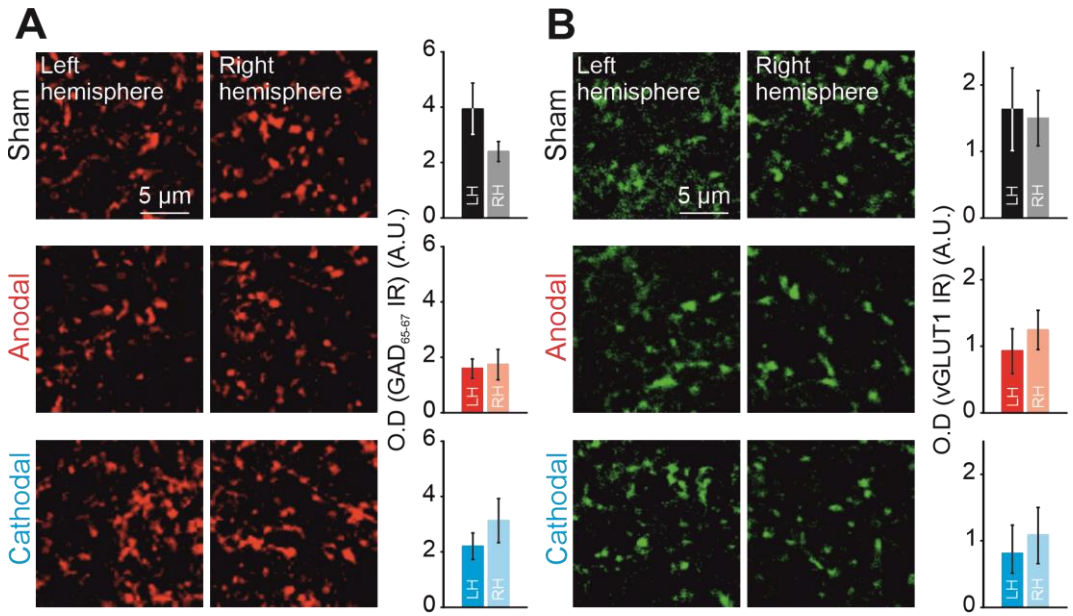

Figure 4.26. Immunohistochemical changes in S1 after 20 minutes of Cb-tDCS over lateral cerebellum. *A,B*) Confocal photomicrographs (images), quantification and statistics (bars charts) of GAD65-67 expression (*A*) or vGlut-1 expression (*B*) in S1 after 20 min of Sham condition (upper row, n = 7 animals), after 20 min of Anodal Cb-tDCS (middle row, n = 7 animals) and after 20 min of Cathodal Cb-tDCS (lower row, n = 7 animals). Error bars represent SEM. GAD65-67: Glutamic acid decarboxylase isoforms 65 and 67; vGLUT1: vesicular glutamate transporter 1; OD: optical density; IR: immunoreactivity; A.U: arbitrary units.

5 Discussion

Present results increase our understanding on the effects that transcranially applied electric currents have on neural activity and highlight the relevance of animal models as a scientific instrument to understand and control these non-invasive neuromodulatory techniques.

5.1 tDCS modulation of S1.

5.1.1 SEP characterization in S1.

The first set of experiments (Set 1) carried out for the present Doctoral Thesis focus in the intracortical recording of SEPs in response to whisker electrical stimulation in the alert mice. This approach has been successfully used in the past for concurrent tDCS application and SEPs recording elicited by whisker electrical stimulation in alert rabbits (Márquez-Ruiz et al., 2012; Márquez-Ruiz et al., 2016). N1 component of S1-SEPs is supposed to represents postsynaptic activity from layers IV, V and VI (Castro-Alamancos and Oldford, 2002; De Kock et al., 2007), which explains our observation of a polarity inversion when going deeper than layer V-VI (Fig. 4.1*C*).

As showed in the present study, the amplitude of N1 was linearly related to the intensity of the electrical shock applied to the whisker pad (Fig. 4.1*D*, *E*) allowing the characterization of the maximum N1 response to posteriorly determine the whisker stimulation necessary to reduce this maximum to 50% (submaximal response). Remarkably, SEPs are a consistent marker for indexing cortical excitability and are easy to electrophysiologically identify based on the waveform (Fig. 4.1*C*), allowing for reliable measurements over long periods of time. In addition, SEPs are usually recorded in human experiments (Dieckhöfer et al., 2006; Woodman, 2010; Sugawara et al., 2015; Vaseghi et al., 2015) providing a link with animal model's results.

S1 neurons represent complex and behaviorally relevant information in the alert animal (Castro-Alamancos, 2004; Le Merre et al., 2018) thus showing some variability regarding mice behavior. Particularly, a strong decrease of N1 amplitude was recorded in the experimental sessions when the animal was running on the treadmill. We

eliminated these running-SEPs, probably related with sensory gating of information, a phenomenon by which predictable-movements activity (i.e. locomotion) suppress S1 activity (Chapin and Woodward, 1982; Chapman et al., 1988; London and Miller, 2013; Favorov et al., 2015), to avoid masking potential plastic changes.

5.1.2 Intracranial electric fields induced by tDCS in S1.

Measuring the real electric field reaching different brain regions during tDCS in humans is one of the most important challenges in the field. Currently, there are many computational models using realistic head models to predict how current diffuse across the brain in different tDCS montages (Ruffini et al., 2014; Huang et al., 2019). Animal models offer an opportunity to characterize the actual electric field imposed in the region of interest for the experimental design (Lee et al., 2015; Opitz et al., 2016, 2017; Sánchez-León et al., 2018a). In the present study, the actual electric field generated in S1 recording site at different current intensities was measured (Fig. 4.2). As expected, the highest electric field values were observed in the first millimeter of the cortex (90.2, 9.9 and 1.4 V/m for 200, 20 and 2 μA, respectively) decaying with distance in a logarithmic manner. These data support previous studies in humans and nonhumans primates confirming that the electric fields generated during tES do behave in a linear ohmic manner (Opitz et al., 2016). Nevertheless, the electric field imposed in the cortical layer of the mice in the present study (23.1 - 90.2 V/m), turned to be much higher than those estimated in human studies (below 1 V/m (Jackson et al., 2016; Opitz et al., 2017; Chhatbar et al., 2018; Modolo et al., 2018; Vöröslakos et al., 2018)). Interestingly, although some *in vitro* studies using DC stimulation have successfully characterized the impact of low-intensity electric fields similar to those imposed in the human brain (Deans et al., 2007; Reato et al., 2010), most of the *in vitro* studies use electric fields in the range of 20 to 60 V/m (Modolo et al., 2018), similar to the values used in the present work. This discrepancy is more evident in those studies using *in vivo* rodent animal models and specifically in alert rodents where electric field intensities used in humans have failed to show neuronal modulation (Ozen et al., 2010; Modolo et al., 2018; Vöröslakos et al., 2018). Despite this intensity increase, animal studies using electric fields in the range of the present study, have decisively contributed to the knowledge of

the mechanisms that mediate the effects of tDCS in the immediate and long-term (Jackson et al., 2016; Liu et al., 2018).

5.1.3 S1-tDCS immediate effects on S1-SEPs.

Since most of the knowledge we have about tDCS mechanisms comes from human studies where tDCS is applied on the motor cortex (Stagg et al., 2018), it is crucial to know if the implicated neural mechanisms and effects described during last years for M1-tDCS are comparable to those induced in other brain regions.

Immediate effect results from our study indicate that tDCS applied for several seconds over S1 is sufficient to modulate cortical excitability in agreement with previous results in humans-M1 (Nitsche and Paulus, 2000), with an increase in excitability during anodal stimulation and a decrease during cathodal stimulation. Furthermore, the effects showed an intensity-dependent modulation, with greater changes for greater intensities. Similar results were previously obtained in S1 cortex from rabbits (Márquez-Ruiz et al., 2012; Márquez-Ruiz et al., 2016) and in motor (Cambiaghi et al., 2010) and visual (Cambiaghi et al., 2011; Monai et al., 2016) cortices in mice. All these data points toward a similar immediate tDCS effect across different cortices, at least for the simplified cortical geometry of mice and rabbits. These similarities in modulation for different cortical areas could be due to the same dendritic and axonal orientation of the pyramidal cells with respect to the electric field (Bikson et al., 2004; Radman et al., 2009; Kabakov et al., 2012), but there are many differences (network complexity, neurons size) between mice and humans cortices to assume it.

5.1.4 S1-tDCS long-term effects on S1-SEPs.

Different studies have shown that tDCS over S1 can modulate SEPs amplitude and change somatosensory information processing. In humans, after anodal tDCS applied over S1, Sugawara and col. (Sugawara et al., 2015) have shown that there is an increase in amplitude of SEPs, whereas Ragert and col. (Ragert et al., 2008) showed an improve in performance in a complex somatosensory task. Meanwhile, after cathodal S1-tDCS, some studies have shown that there is a decrease in amplitude of SEPs

(Dieckhöfer et al., 2006; Vaseghi et al., 2015), that correlates with increasing sensory and pain thresholds (Vaseghi et al., 2015), while Rogalewski and col. (Rogalewski et al., 2004) showed that cathodal tDCS over S1 decreased tactile perception. In animal models, S1-tDCS has been able to potentiate or depress the SEP and the acquisition of classical eyeblink conditioning during the application of anodal or cathodal stimulation, respectively, suggesting that tDCS modulates the sensory perception process necessary for associative learning (Zucker and Regehr, 2002; Márquez-Ruiz et al., 2012). Moreover, based on paired-pulse test results (a test commonly used to highlight presynaptic effects on neurotransmitter release), this study proposes that tDCS modifies thalamocortical synapses at presynaptic sites, a detailed insight that is not possible to get from human experiments.

In the present study, cortical excitability changes were maintained as long as the tDCS was applied (20 minutes), but only cathodal tDCS was able to induce significant long-term effects (i.e., decreased amplitude of the N1 component) in the recorded SEPs, which persisted for up to 60 min. In contrast, no changes were observed after anodal tDCS. The asymmetry in the long-term effects is a crucial issue since long-lasting excitability changes are a key point for clinical treatments (Stagg et al., 2018). Furthermore, it could explain some of the mixed results obtained in human's experiments in which no effects are observed after anodal tDCS (Rogalewski et al., 2004; Dieckhöfer et al., 2006). Also, the lack of long-term effects for anodal stimulation reinforce the idea of performing the testing task, thus recruiting the task-related neuronal network (Ammann et al., 2016; Stagg et al., 2018), during the administration of tDCS rather than after it. A possible explanation for the asymmetrical results comes from the hypothesis that tDCS long-term effects could be caused by alterations in other structures functionally connected to the region of stimulation (Polanía et al., 2012; Holland et al., 2016; Baxter et al., 2017). Thus, the long-term impact of tDCS might differ depending on the interaction of the cortex with these regions (Bikson et al., 2019b).

5.1.5 GAD65-67 and vGlut1 levels in S1 after 20 minutes of S1-tDCS.

Since no external electric fields are present in the tissue after tDCS, the observed long lasting excitability changes must be explained in terms of molecular and connectivity changes. In this regard, our study shows an increase in GAD65-67 levels after cathodal stimulation but no changes for anodal stimulation. The results are in agreement with our electrophysiological measures, suggesting an overall decrease in the excitability of the stimulated cortex after cathodal tDCS, but no long-term changes after anodal tDCS.

The *in vivo* measure of neurotransmitter levels in human experiments show mixed results. Using MRS some studies have repeatedly shown a decrease in GABA after anodal M1-tDCS (Stagg et al., 2009; Bachtiar et al., 2018; Patel et al., 2019), but just one work found polarity-dependent effects on GABA and glutamatergic levels (Stagg et al., 2009). Interestingly, a recent paper showed a decrease in GABA in both the stimulated and non-stimulated M1 after anodal tDCS, whereas a decrease in GABA was only observed in non-stimulated M1 after cathodal stimulation (Bachtiar et al., 2018). Since we analyse our data by comparing the stimulated vs non-stimulated hemisphere, we can be neglecting some of these hemispherical effects. For instance, when comparing values after cathodal tDCS with values after sham tDCS (Fig. 4.5, upper rows) it could be possible that the non-stimulated hemisphere had a decrease in GAD65-67.

There is also a study showing no changes in GABA nor glutamatergic levels for anodal stimulation in the posterior superior temporal gyrus (Dwyer et al., 2019), so it is possible that depending on the stimulated region the long-term effects can be supported by distinct mechanisms, or do not exist at all. Furthermore, others animal-based experiments have demonstrated the implication of different receptors, such as NMDA (Fritsch et al., 2010), mGluR5 (Sun et al., 2016), AMPA (Stafford et al., 2018; Martins et al., 2019), and adenosine receptors (Hattori et al., 1990; Islam et al., 1994, 1995b; Márquez-Ruiz et al., 2012), together with the involvement of neurotrophic BDNF (Fritsch et al., 2010; Ranieri et al., 2012), the activation of early genes participating in protein synthesis (Ranieri et al., 2012; Holmes et al., 2016), and even glial cells (Monai

et al., 2016). In summary, the full machinery behind long-term effects seems to be very complex, so the variability in stimulation parameters should be minimized in order to compare between studies.

5.2 tDCS modulation of cerebellar cortex.

5.2.1 SEP characterization in CrusI-II.

The cerebellum receives sensory information from all body parts (Garwicz et al., 1998; Apps and Garwicz, 2005) conveyed through mossy (Odeh et al., 2005; Jörntell and Ekerot, 2006) and climbing fibers (Ekerot and Jörntell, 2001). Specifically, peripheral stimulation of the whisker pad evokes a sensory potential in CrusI-II lobules of the cerebellar cortex (Brown and Bower, 2002; Lu, 2005; Roggeri et al., 2008) characterized by two main components (Fig. 4.6), corresponding to trigeminal (T) (Armstrong and Drew, 1980; Bower and Woolston, 1983; Morissette and Bower, 1996; Lu, 2005; Roggeri et al., 2008) and cortical (C) (Sasaki et al., 1969; Brown and Bower, 2002; Mostofi et al., 2010; Diwakar et al., 2011; Parasuram et al., 2018) inputs. Furthermore, the N2-N3 wave in the T component is supposed to reflect the activity between parallel fibers and PC (Bengtsson and Jorntell, 2007; Márquez-Ruiz and Cheron, 2012), and since the PC are the solely output of the cerebellar cortex, N2-N3 amplitude can be used as an index of cerebellar cortex excitability. In our experiments, the whisker stimulation intensity was adjusted as to produce an N2-N3 component with half of the maximum amplitude (Fig. 4.6*C*) to ensure the observation of potential increases as well as decreases in the evoked potentials during and/or after Cb-tDCS. Interestingly, as in S1-SEPs recordings, a similar decrease during animal running was observed on the C component amplitude. These amplitude decrease was probably related with sensory gating of information (Apps, 1999; Geborek et al., 2013; Brooks et al., 2015; Lawrenson et al., 2016). In order to avoid masking potential plastic changes we eliminated these SEPs from the analysis.

5.2.2 Intracranial electric fields induced by Cb-tDCS.

Regarding Cb-tDCS, there are just a few studies that specifically address the electric current diffusion along cerebellar tissue (Parazzini et al., 2014; Fiocchi et al.,

2016; Batsikadze et al., 2019; Rezaee and Dutta, 2019), all of them using computational models without *in vivo* data. For this reason, the recordings made for the present Doctoral Thesis provide relevant information to characterize the actual electric field imposed in the cerebellum.

As expected from modelling studies showing that current flow in the cerebellum is largely uniform in direction (Parazzini et al., 2014; Rahman et al., 2014), the highest electric field values were observed in the first millimeter of the cortex (129.5, 13.8 and 1.9 V/m for 200, 20 and 2 µV, respectively) decaying with distance in a logarithmic manner, a similar effect than the observed in S1 recordings. Likewise, the electric field imposed in the recording area of the present study (129.5 V/m) turned to be much higher than those estimated in human studies (below 1 V/m (Parazzini et al., 2014; Fiocchi et al., 2016; Rezaee and Dutta, 2019)). Nonetheless, there is some evidence indicating that higher electric fields have to be applied in alert mice to obtain similar results than in humans, as we will see in the last part of the current discussion.

5.2.3 Cb-tDCS functional effects on CrusI-II-SEPs.

In 2009, Galea and colleagues (Galea et al., 2009) demonstrated that it is possible to increase or decrease the connectivity between the cerebellum and M1, depending on the polarity of tDCS applied to human cerebellum. Since then, Cb-tDCS has been used to modulate motor and non-motor behaviors (Grimaldi et al., 2014a, 2016; Oldrati and Schutter, 2018), as well as to understand cerebellar functions (Galea et al., 2011; Ferrucci et al., 2012; Boehringer et al., 2013; Miall et al., 2016) and learning mechanisms (Spampinato and Celnik, 2017). To properly understand the basics of this neuromodulation, we have to dissociate immediate from long-term effects. As far as we know, there is no single study combining cerebellar *in vivo* recordings with non-invasive neuromodulation techniques, so comparisons made in this discussion section have to be performed with *in vitro* studies or with indirect measurements from human studies.

Regarding immediate effects, we observed that the amplitude of the T components (N1 and N2-N3) of the SEP was increased during anodal and decreased

during cathodal Cb-tDCS. These results are supported from previous *in vitro* experiments performed in isolated turtle cerebellum (Chan and Nicholson, 1986; Chan et al., 1988) where anodal stimulation predominantly excites the cell bodies of PC when applying similar electric fields than us (15 to 20 V/m). Despite that, the majority of Cb-tDCS results come from human experiments, where the evaluation of cerebellar excitability has to be made by indirect measurements. fMRI studies have found mixed results, D'Mello (D'Mello et al., 2017) found that anodal Cb-tDCS increased activation in right Crus I/II during a complex task (semantic prediction) and enhanced resting-state functional connectivity between hubs related to the task (reading/language networks). On the contrary, no differences are reported in cerebellar cortex activity when Cb-tDCS is applied during a simple motor task (finger tapping) (Küper et al., 2019). Interestingly, the same study found the opposite modulation in the dentate nuclei, an increase in activation during cathodal stimulation, and a trend toward decreased activation during anodal stimulation. This result is in accordance with an inhibitory effect of cathodal Cb-tDCS on the cerebellar cortex resulting in less inhibition of the cerebellar nuclei by the PC and vice versa. Furthermore, in the cerebellum 20-50 PC project to a single DCN neuron (Person and Raman, 2012), so sparse modulation of cortical activity could be reinforced at the level of DCN activity. Nonetheless, lower electric fields are thought to be produced in humans by Cb-tDCS (below 1 V/m (Parazzini et al., 2014; Fiocchi et al., 2016; Rezaee and Dutta, 2019)) suggesting that the modulation of cerebellar activity could be inferior that in our mice model.

As observed in the cerebellar immediate-effect results (Fig. 4.8), the C component of the SEP recorded in Crus I-II showed a trend in the opposite modulation direction of the T components, with anodal decreasing and cathodal increasing the amplitude. This tendency seems ambiguous but were somehow expected since it is known that the cerebellum exerts an inhibitory tone over M1 (Batsikadze et al., 2019) (and over S1, as shown in Set 4 experiments), and the C component is supposed to reflect an input from S1 (Morissette and Bower, 1996; Brown and Bower, 2002). The hypothesis states that increasing cerebellar cortex excitability with anodal Cb-tDCS decreases DCN activity, which project to S1 through the thalamus (Proville et al., 2014), thus resulting in a decrease of S1 excitability which in turn projects back to cerebellar

cortex through the pontine nuclei (Shinoda et al., 1987; Odeh et al., 2005) causing the decrease of C component amplitude (Morissette and Bower, 1996; Brown and Bower, 2002), and an increase in C amplitude when cathodal Cb-tDCS is applied.

Regarding long-term effects, after 20 minutes of Cb-tDCS no modulation was observed for any of the SEP components. During the 20 minutes of stimulation, the immediate modulation was maintained, with a robust effect in the T components amplitude, especially in N2-N3 complex, increasing and decreasing with anodal and cathodal, respectively, and a trend for C component towards the opposite modulation direction. However, once the Cb-tDCS is switched off, all amplitude values returned to control values. Similar effects have been shown in fMRI human studies (Küper et al., 2019) with no significant difference of cerebellar cortical activation after Cb-tDCS. No differences were found during Cb-tDCS in this study possibly due to the low spatial and temporal resolutions of fMRI (in comparison with invasive recordings) where the short-latency T and C opposite modulations may hind the detection of stimulation-related fMRI activity changes. Another study where a complex cerebellar-dependent task is being performed during Cb-tDCS, have reported that anodal stimulation shows an increase in CrusI-II activity together with an increase of functional connectivity between the hubs related to the task (D'Mello et al., 2017). Nonetheless, human studies applying Cb-tDCS usually rely on indirect measurements of cerebellar excitability, as behavioral outcome or excitability of connected regions. In these cases, contradictory results are common (Pope and Miall, 2012; Zuchowski et al., 2014; Miall et al., 2016; Beyer et al., 2017; Batsikadze et al., 2019). There could be several causes for this disparity as the fact that the orientation of neurons in different cerebellar areas varies in relation to the applied electric field (Grimaldi et al., 2016), or the fact that cerebellar modulation could distinctly affects distant interconnected regions (Stagg et al., 2018; Miterko et al., 2019). In addition to that, present results reinforce the importance of performing the experimental measurements and potential behavioral tasks during the administration of Cb-tDCS and not after stimulation, since even with much higher electric fields as used in our experiments, no long-term effects were observed in cerebellar cortex. There is currently some evidence on the relevance of this assumption, with several studies showing that anodal tDCS applied over the cerebellum increases skill learning relative to

sham specifically by increasing on-line (during Cb-tDCS) rather than off-line (after Cb-tDCS) learning (Cantarero et al., 2015), and also showing the relevance of the cerebellum during the early phases of a motor skill learning (Spampinato and Celnik, 2017) or during a visuomotor adaptation task (Galea et al., 2011).

Unlike the observation of an LTD-like effect after cathodal tDCS over S1, our immunohistochemical analysis of the GAD65-67 and vGlut1 levels in CrusI-II showed no changes after 20 minutes of Cb-tDCS, pointing in the same direction of no long-term effects as the electrophysiological recordings. This absence of change in neurotransmitters levels after Cb-tDCS has also been observed for GABA and glutamate levels in human experiments using MRS (Jalali et al., 2018). Nevertheless, they did not find differences during Cb-tDCS neither, suggesting that tDCS immediate effects over cerebellar cortex could be limited to the polarization imposed by the electric field and not correlated with changes in neurotransmitters levels.

5.2.4 Cerebellar single-cell activity modulation by Cb-tDCS in awake mice.

In order to understand basic mechanisms by which tDCS modulates neuronal activity, the most direct read-out we can have is the modulation of single-cell activity. The majority of neuronal recordings obtained during externally applied electric fields have been performed in brain slices and have laid the basis mechanisms explaining the relationship between the magnitude of voltage gradients and spiking activity (Bikson et al., 2004), as well as the importance of different neuronal features, such as the orientation of somatodendritic axes with respect to the electrical field (Rahman et al., 2013), the neuronal morphology (Radman et al., 2009), or the axonal orientation (Kabakov et al., 2012). Nonetheless, in these studies all synaptic signalling use to be blocked, the slices lack the connections with other parts of the brain, and the electric field is not applied transcranially, for this reason, many of these results should be confirmed on *in vivo* preparations too.

Despite the increasing interest in the tDCS technique, there are very few studies specifically addressing the spiking modulation *in vivo* under tES (Ozen et al., 2010;

Grossman et al., 2017; Vöröslakos et al., 2018). In these reported experiments, anodal and cathodal tDCS affect spiking activity and transmembrane potential in a linear manner, with a preference toward increase excitability for anodal and decrease it for cathodal stimulation. In the present study, we found no clear directionality in the modulation, with some neurons increasing their spiking for anodal stimulation, others for cathodal stimulation, and vice versa. However, Ozen and Vöröslakos experiments were carried out in rat neocortex, where there are no circumvolutions, whereas our experiments were performed in mice cerebellar cortex, which is highly convoluted. Also, they found that the minimum voltage gradient necessary to affect neuronal spiking was at least ~1 V/m and that strength of the modulation increased as the stimulation intensity increased. Considering that we use higher intensities (129,52 V/m), our results on neuronal modulation were expected.

Of high interest for this issue, during last years some studies have started to measure spiking modulation *in vivo* under tDCS in alert non-human primates (Krause et al., 2017, 2019), an ideal animal model because, like humans—and unlike other animal models— they have a thick, dense skull and gyrencephalic cortex. Interestingly, weak electric fields induced by tDCS as those typically used in humans (below 1 V/m) were not able to change firing rates within the targeted area (Krause et al., 2017) but induced large low-frequency oscillations in the underlying tissue. Meanwhile, for tACS a frequency- and location-specific modulation of the firing timing, but not firing rate value, was observed in the recorded neurons (Krause et al., 2019).

5.2.5 Importance of the somatodendritic axis orientation.

In vitro studies have already established that the orientation of the soma, the dendrites and the axon with respect to the electrical field determine the modulation of neuronal excitability, at least for neocortical (Rahman et al., 2013) and hippocampal neurons (Bikson et al., 2004). Nevertheless, no *in vivo* study has been published experimentally supporting this critical issue. Present results provide a direct measurement of the relation between Cb-tDCS modulation and neuronal orientation. Moreover, they represent the first evidence of cerebellar neurons modulation with DC

since the 80's (Chan and Nicholson, 1986; Chan et al., 1988), where it was demonstrated that current flows that depolarizes the soma leads to excitation while current flows that hyperpolarizes the soma leads to inhibition of firing. In addition, PC were polarized by 0.2 mV per 1 V/m applied electric field, which is in the range reported for layer V/VI pyramidal cells (Radman et al., 2009).

Accordingly, our present results show strong evidence supporting the key role of somatic polarization. Thus, we found an almost perfect correspondence between current flows depolarizing the soma leading to an increase in firing activity of PC (either anodal for a PC with the dendrites pointing toward the active electrode, or cathodal for a PC with the opposite orientation) and current flows hyperpolarizing the soma leading to a decrease in firing activity. These effects, clearly observed in the different neurons recorded in the cerebellar Vermis, were smaller, but in the same direction, for neurons with intermediate somatodendritic angles in the case of neurons located in CrusI-II. These data strongly support modelling studies showing that current flow in the cerebellum is largely uniform in direction, thereby producing an alternating direction of polarization across the alternating direction of cerebellar cortex layers (Parazzini et al., 2014; Rahman et al., 2014). Nonetheless, the influence of the different cellular compartments (somas, dendrites, axons) being differentially polarized should not be discarded, although we cannot give insights into this topic with our data.

This result highlight the relevance of focalize tDCS targets since the orientation of different neurons in different cerebellar and cerebral (in primates) areas varies in relation to the applied electric field (Grimaldi et al., 2016).

5.3 S1 modulation by cerebellar cortex tDCS.

5.3.1 Intracranial electric fields induced in S1 by tDCS in cerebellar cortex.

In the present study, the actual electric field reaching S1 when tDCS was applied over cerebellar cortex was measured (Fig. 4.19). As opposed to the recordings made in Set 1 and Set 2 experiments where the electric field was measured just below the active

electrode, in this case the electric field reaching the recording site was similar across the different depths, with a value of ~1 V/m for 200 μA. Even when we fail to induce significant tDCS effects with such a low electric fields, this magnitude is just in the threshold suggested to have a direct neuromodulatory effect (Vöröslakos et al., 2018), so we cannot rule out the possibility of some interference by a direct neuromodulation from the applied current by itself.

5.3.2 Cb-tDCS functional effects on S1-SEPs.

S1 is highly interconnected with the cerebellum (Schmahmann, 2001; Ramnani, 2006; Buckner et al., 2011). The broad characterization of these projections was made at an anatomical (Leergaard et al., 2000) and functional (Allen et al., 1979; Shinoda et al., 1987; Swenson et al., 1989; Morissette and Bower, 1996; Brown and Bower, 2002; Nagao, 2004; Odeh et al., 2005; Watson, 2009) level, but it was not until very recently that the details and relevance of this connection has started to be clarified (Proville et al., 2014; Caligiore et al., 2017; Bostan and Strick, 2018).

By means of chemogenetics tools, a recent animal study have shown that increasing or decreasing the PC activity of CrusI induce a decrease or an increase, respectively, of the firing rate of contralateral parietal association cortex neurons (Stoodley et al., 2017). Accordingly, our results showed an increase or a decrease in S1-SEPs amplitude during cathodal or anodal Cb-tDCS, respectively, in an intensity-dependent manner. On the other hand, human studies using indirect measurements have shown that cathodal tDCS over the cerebellum resulted in a decrease of the inhibition exerted by the cerebellum over M1, whereas anodal Cb-tDCS increased it (Galea et al., 2009; Batsikadze et al., 2019).

For long-term Cb-tDCS effects experiments, density current applied to the epicranial tube (4.29 mA/cm^2) was equivalent to those obtained by applying 200 μA to the silver-ring (4.26 mA/cm^2) (Set 2 experiments). Thus, cathodal Cb-tDCS (20 min, 300 μA) showed an increase in the amplitude of S1-SEPs during the application of Cb-tDCS, with no long-term effects after Cb-tDCS cessation, whereas anodal Cb-tDCS started by

decreasing the excitability of S1 but after several minutes this effect was abolished (Fig. 4.25). Interestingly, when Cb-tDCS was switched off the amplitude of S1-SEPs displayed a rebound effect, meaning a rapid increase in excitability that was maintained at least for 1 hour. This amplitude increase rebound could be caused by some homeostatic mechanisms balancing the overall excitability so when anodal start to decrease the S1-SEPs amplitude (by increasing CrusI-II excitability) the mechanism tries to compensate increasing it, thus cancelling the Cb-tDCS effect, but when anodal stimulation is removed, this mechanism still tries to compensate the effect maintaining S1 excitability increased. Supporting these results, other animal study have shown that, by means of optogenetic stimulation and for a brief period (100 ms), stimulation of the Crus I area produced an inhibition and a post-inhibitory activation (rebound) of the cerebello-thalamo-cortical pathway, yielding M1 activation (Proville et al., 2014). Given the absence of this rebound long-lasting effect in our recordings from CrusI-II during Cb-tDCS (Fig. 4.9), it seems feasible that the mechanism of the rebound should reside in another region, probably thalamus or S1.

Regarding the immunohistochemical analysis, no changes were observed in the levels of GAD65-67 nor vGlut1 in S1 after 20 minutes of 200 µA Cb-tDCS. Given the correlation between electrophysiological and immunohistochemical analysis in experiments from Set 1 (LTD-like effect after cathodal, increase in GAD65-67 levels) and Set 2 (No long-term effect for SEP amplitude nor GAD65-67 or vGlut1 levels), we expected to see some correlation with the observed increase in amplitude after anodal Cb-tDCS. The absence of change could be due to the lower intensity used for the immunohistochemical experiments (200 µA, resulting in a current density of 2.86 mA/cm^2), or to a change of neurotransmitters levels in other parts of the circuit (thalamus, DCN), but further experiments are needed to prove them.

Taken together, these results provide direct evidence regarding the distant effects of tDCS applied over the cerebellum, suggesting that non-invasive neuromodulation effects are not limited to the stimulated region, rather, they may be seen across the whole network (Stagg et al., 2018) and they could be useful for current

(Pope and Miall, 2012; Marron et al., 2018; Yosephi et al., 2018) and future (Stoodley et al., 2017; Menardy et al., 2019) therapies trying to modulate cerebellar networks.

5.4 Limitations of the mice model.

Finally, the limitations of this study must be taken into account, since *in vivo* animal experiments present important differences with respect to human interventions. Some of these limitations are inherent to the anatomy and complexity of the rodent's brain, which lacks cortical circumvolutions, are smaller in size and contain fewer neurons. A closer approach to human studies can be achieved by cerebellar experiments, which is highly convoluted in rodents too, and as we show in our single-cell experiments the entrainment efficacy of neurons depends on how the neuron align with the direction of the electrical field, as expected in human cerebellar and cerebral cortices. However, the cytoarchitecture of cerebral and cerebellar cortices is very different, so the translation to human cortex is still questionable. Additionally, more limitations arise from the restrictions that mice behavior imposes, specifically when trying to compare complex behaviors or cognitive processes. To overcome these problems, the use of learning paradigms that can be performed in humans as well as in mice (i.e., eyeblink conditioning (Márquez-Ruiz et al., 2012; Zuchowski et al., 2014)) provide a valuable tool for the translation of the results. Moreover, brain activity can be compared between human and mice experiments by measuring different oscillations and ERPs, not just sensory-related potentials but even cognitive-related ones (Buzsáki et al., 2013; Modi and Sahin, 2017; Pinault, 2017).

Nonetheless, the main limitation of the present study is related to the specific details of the stimulation protocols, particularly the application of higher density currents (Márquez-Ruiz et al., 2014). Animal studies usually apply around ten-fold stronger current intensities compared to human experiments (Jackson et al., 2016; Liu et al., 2018), and based in our data we typically generate an electric field between 20-120 V/m in the recording area, values much higher than typically generated in humans (below 1 V/m) (Opitz et al., 2016; Chhatbar et al., 2018; Vöröslakos et al., 2018). However, it seems that higher electric fields are needed in mice to obtain similar results

as in humans. In our experiments from Set 1, a current density of ± 4.26 mA/cm^2 during 15 s of tDCS resulted in a SEP amplitude change of ~40 % for anodal and ~-30 % por cathodal tDCS (Fig. 3*B*), and for 20 min of tDCS, cathodal elicited a decrease up to ~64 %, and a current density of 3.19 mA/cm^2 for anodal tDCS reached a maximum change of ~50 % (Fig. 4). Meanwhile, for human experiments, in Matsunaga and col. (Matsunaga et al., 2004) for a density current of 0.03 mA/cm^2 during 10 minutes of anodal tDCS, the observed amplitude change was an increase of up to ~60 %, and Vaseghi and col. (Vaseghi et al., 2015) observed a reduction of ~25 % for 20 minutes of cathodal tDCS at 0.1 mA/cm^2. These results are more striking since we applied tDCS directly over the scalp, avoiding the loss of around 75 % of the applied current due to the shunting effect of the skin (Liu et al., 2018; Vöröslakos et al., 2018), that is present in human studies.

Also, macaque experiments, an animal model closer to human experiments since they have a large head with a gyrated cortical surface, determined an electric field of ~35–55 V/m in the motor cortex to elicit a suprathreshold stimulus (triggering a visible twitch) (Lee et al., 2015). We usually apply electric fields in this range and above, but, to our knowledge, we did not observe any evidence of suprathreshold stimulus. Besides, our single-cell experiments reveal a clear modulation of the firing rate for some neurons but no modulation at all for some nearby neurons, suggesting a subthreshold modulatory effect.

A possible explanation for the divergence between rodent and primates (human and non-human) results could be related with larger neuronal densities found in primates with respect to rodents (Herculano-Houzel, 2009). For instance, the human brain has about sevenfold more neurons than the 12 billion neurons that a hypothetical rodent brain of 1.5 kg would be expected to have (Herculano-Houzel, 2012). Also, much bigger electrodes are used in human experiments, thus entraining immensely much more neurons than mice experiments. On the contrary, total brain size in mice constrains the size of the electrodes and difficult the stimulation of specific circuits. In spite of the later, mice models promise to play a relevant role in the tES field since they take advantage of powerful invasive neuroscientific tools that cannot be readily

implemented in human studies such as electrophysiological recordings of neural activity, fluorescent and two-photon imaging, or optogenetic manipulation of the circuits.

In summary, animal models provide a powerful scientific tool that can facilitate the successful utilization of tES in human subjects, but they should be carefully designed to maximize translation of the results for human application.

6 Conclusions

The present Doctoral Thesis tries to shed some light on tDCS mechanisms, specifically in somatosensory and cerebellar neuromodulation, and the relation between them. To accomplish this, electrophysiological and immunohistochemical techniques have been used in awake and anesthetized mice. The main conclusions of this study are the following:

1) The actual electric field generated by tDCS applied over S1 or lateral cerebellum decay with distance from the electrode in a logarithmic manner. The field generated in S1 by Cb-tDCS is two orders of magnitude lower than the electric field generated by tDCS directly applied over S1.

2) tDCS applied over S1 immediately modulates cortical excitability during anodal and cathodal stimulation in an intensity-dependent manner. Cathodal but not anodal S1-tDCS induces long-term changes in S1 and this effect is consistent with observed changes in GAD65-67 levels in the stimulated S1.

3) Cb-tDCS applied over lateral cerebellum immediately modulates cerebellar cortex excitability during anodal and cathodal stimulation, but no long-term effects were observed in SEPs nor GAD65-67 or vGlut1 levels in the cerebellar cortex after Cb-tDCS.

4) Cb-tDCS applied for several seconds is able to modulate ongoing firing activity of PC and non-PC in a heterogeneous and intensity-dependent manner. The heterogeneous modulation observed is highly dependent on the somatodendritic axis orientation with respect to the generated electric field.

5) Cb-tDCS applied over lateral cerebellum modulates S1 excitability during cathodal and anodal stimulation in an intensity-dependent manner. Anodal but not cathodal Cb-tDCS induces a long-term increase in S1 excitability.

7 References

Adams, G. (1799) An Essay on Electricity, 5th ed. London: W. and S. Jones.

Aldini, G. (1794) De animali electricitate dissertationes duae. Bologna.

Aldini, G. (1804) Essai theorique et experimental sur le galvanisme. 2 Vols. Paris: Fournier.

Allen GI, Azzena GB, Ohno T (1979) Pontine and non-pontine pathways mediating early mossy fiber responses from sensorimotor cortex to cerebellum in the cat. Exp Brain Res 36:359–374.

Ammann C, Spampinato D, Márquez-Ruiz J (2016) Modulating motor learning through transcranial direct-current stimulation: An integrative view. Front Psychol 7.

Andrade C (2013) Once- to twice-daily, 3-year domiciliary maintenance transcranial direct current stimulation for severe, disabling, clozapine-refractory continuous auditory hallucinations in schizophrenia. J ECT 29:239–242.

Apps R (1999) Movement-related gating of climbing fibre input to cerebellar cortical zones. Prog Neurobiol 57:537–562.

Apps R, Garwicz M (2005) Anatomical and physiological foundations of cerebellar information processing. Nat Rev Neurosci 6:297–311.

Armstrong BYDM, Drew T (1980) Responses in the posterior lobe of the rat cerebellum to electrical stimulation of cutaneous afferents to the snout. J Physiol 309:357–374.

Asamoah B, Khatoun A, Mc Laughlin M (2019) tACS motor system effects can be caused by transcutaneous stimulation of peripheral nerves. Nat Commun 10.

Bachtiar V, Johnstone A, Berrington A, Lemke C, Johansen-Berg H, Emir U, Stagg CJ (2018) Modulating Regional Motor Cortical Excitability with Noninvasive Brain Stimulation Results in Neurochemical Changes in Bilateral Motor Cortices. J Neurosci 38:7327–7336.

Batsikadze G, Rezaee Z, Chang D, Gerwig M, Herlitze S, Dutta A, Nitsche MA, Timmann D (2019) Effects of cerebellar transcranial direct current stimulation on cerebellar-brain inhibition in humans: a systematic evaluation. Brain Stimul 12:1177–1186.

Baxter BS, Edelman BJ, Sohrabpour A, He B (2017) Anodal transcranial direct current stimulation increases bilateral directed brain connectivity during motor-imagery based brain-computer interface control. Front Neurosci 11:1–17.

Bengtsson F, Jörntell H (2007) Ketamine and Xylazine Depress Sensory-Evoked Parallel Fiber and Climbing Fiber Responses. J Neurophysiol 98:1697–1705.

Benussi A, Koch G, Cotelli M, Padovani A, Borroni B (2015) Cerebellar transcranial direct current stimulation in patients with ataxia: A double-blind, randomized, sham-controlled study. Mov Disord 30:1701–1705.

Berenyi A, Belluscio M, Mao D, Buzsaki G (2012) Closed-loop control of epilepsy by transcranial electrical stimulation. Science 337:735–737.

Beyer L, Batsikadze G, Timmann D, Gerwig M (2017) Cerebellar tDCS Effects on Conditioned Eyeblinks using Different Electrode Placements and Stimulation Protocols. Front Hum Neurosci 11:1–12.

Bikson M, Esmaeilpour Z, Adair D, Kronberg G, Tyler WJ, Antal A, Datta A, Sabel BA, Nitsche MA, Loo C, Edwards D, Ekhtiari H, Knotkova H, Woods AJ, Hampstead BM, Badran BW, Peterchev A V. (2019a) Transcranial electrical stimulation nomenclature. Brain Stimulion (In Press).

Bikson M, Grossman P, Thomas C, Zannou AL, Adnan T, Mourdoukoutas AP, Kronberg G, Truong D, Boggio P, Brunoni AR, Charvet L, Fregni F, Fritsch B, Gillick B, Hamilton RH, Hampstead BM, Jankord R (2017) Safety of transcranial Direct Current Stimulation: Evidence Based Update 2016. Brain Stimul 9:641–661.

Bikson M, Inoue M, Akiyama H, Deans JK, Fox JE, Miyakawa H, Jefferys JGR (2004) Effect of uniform extracellular DC electric fields on excitability in rat hippocampal slices in vitro. J Physiol 557:175–190.

Bikson M, Paulus W, Esmaeilpour Z, Kronberg G, Nitsche MA (2019b) Mechanisms of Acute and After Effects of Transcranial Direct Current Stimulation.

Bindman LJ, Lippold OCJ, Redfearn JWT (1964) The action of brief polarizing currents on the cerebral cortex of the rat (1) during current flow and (2) in the production of

long-lasting after-effects. J Physiol 172:369–382.

Boehringer A, Macher K, Dukart J, Villringer A, Pleger B (2013) Cerebellar transcranial direct current stimulation modulates verbal working memory. Brain Stimul 6:649–653.

Bolzoni F, Pettersson LG, Jankowska E (2013) Evidence for long-lasting subcortical facilitation by transcranial direct current stimulation in the cat. J Physiol 591:3381–3399.

Bosman LWJ, Houweling AR, Owens CB, Tanke N, Shevchouk OT, Rahmati N, Teunissen WHT, Ju C, Gong W, Koekkoek SKE, De Zeeuw CI (2011) Anatomical Pathways Involved in Generating and Sensing Rhythmic Whisker Movements. Front Integr Neurosci 5:1–28.

Bostan AC, Strick PL (2018) The basal ganglia and the cerebellum: Nodes in an integrated network. Nat Rev Neurosci 19:338–350.

Bower JM, Woolston DC (1983) Congruence of spatial organization of tactile projections to granule cell and Purkinje cell layers of cerebellar hemispheres of the albino rat: vertical organization of cerebellar cortex. J Neurophysiol 49:745–766.

Braun R, Klein R, Walter HL, Ohren M, Freudenmacher L, Getachew K, Ladwig A, Luelling J, Neumaier B, Endepols H, Graf R, Hoehn M, Fink GR, Schroeter M, Rueger MA (2016) Transcranial direct current stimulation accelerates recovery of function, induces neurogenesis and recruits oligodendrocyte precursors in a rat model of stroke. Exp Neurol 279:127–136.

Brooks JX, Carriot J, Cullen KE (2015) Learning to expect the unexpected: Rapid updating in primate cerebellum during voluntary self-motion. Nat Neurosci 18:1310–1317.

Brown IE, Bower JM (2002) The influence of somatosensory cortex on climbing fiber responses in the lateral hemispheres of the rat cerebellum after peripheral tactile stimulation. J Neurosci 22:6819–6829.

Brunoni A, Nitsche M, Bolognini N, Bikson M, Wagner T, Merabet L, Edwards D, Valero-Cabre A, Rotenberg A, Pascual-Leone A, Ferrucci R, Priori A, Boggio P, Fregni F

(2012) Clinical research with tDCS: Challenges and future directions. Brain Stimul 5:175–195.

Buckner RL, Krienen FM, Castellanos A, Diaz JC, Yeo BTT (2011) The organization of the human cerebellum estimated by intrinsic functional connectivity. J Neurophysiol 106:2322–2345.

Buzsáki G, Logothetis N, Singer W (2013) Scaling brain size, keeping timing: Evolutionary preservation of brain rhythms. Neuron 80:751–764.

Caligiore D, Pezzulo G, Baldassarre G, Bostan AC, Strick PL, Doya K, Helmich RC, Dirkx M, Houk J, Jörntell H, Lago-Rodriguez A, Galea JM, Miall RC, Popa T, Kishore A, Verschure PFMJ, Zucca R, Herreros I (2017) Consensus Paper: Towards a Systems-Level View of Cerebellar Function: the Interplay Between Cerebellum, Basal Ganglia, and Cortex. Cerebellum 16:203–229.

Cambiaghi M, Teneud L, Velikova S, Gonzalez-Rosa JJ, Cursi M, Comi G, Leocani L (2011) Flash visual evoked potentials in mice can be modulated by transcranial direct current stimulation. Neuroscience 185:161–165.

Cambiaghi M, Velikova S, Gonzalez-Rosa JJ, Cursi M, Comi G, Leocani L (2010) Brain transcranial direct current stimulation modulates motor excitability in mice. Eur J Neurosci 31:704–709.

Cantarero G, Spampinato D, Reis J, Ajagbe L, Thompson T, Kulkarni K, Celnik P (2015) Cerebellar Direct Current Stimulation Enhances On-Line Motor Skill Acquisition through an Effect on Accuracy. J Neurosci 35:3285–3290.

Carrasco-López C, Soto-León V, Céspedes V, Profice P, Strange BA, Foffani G, Oliviero A (2017) Static Magnetic Field Stimulation over Parietal Cortex Enhances Somatosensory Detection in Humans. J Neurosci 37:3840–3847.

Castro-Alamancos MA (2004) Dynamics of sensory thalamocortical synaptic networks during information processing states. Prog Neurobiol 74:213–247.

Castro-Alamancos MA, Oldford E (2002) Cortical sensory suppression during arousal is due to the activity-dependent depression of thalamocortical synapses. J Physiol

541:319–331.

Cerminara NL, Lang EJ, Sillitoe RV, Apps R (2015) Re-defining the cerebellar cortex as an assembly of non-uniform Purkinje cell microcircuits. Nat Rev Neurosci 16:79–93.

Chan C, Hounsgaard J, Nicholson C (1988) Effects of electric fuelds on transmembrane potential and excitability of turtle cerebellar purkinje cells in vitro. Physiology:751–771.

Chan CY, Nicholson C (1986) Modulation by applied electric fields of purkinje and stellate cell activity in the in the isolated turtle cerebellum. J Physiol 371:89–114.

Chapin JK, Woodward DJ (1982) Somatic sensory transmission to the cortex during movement: Gating of single cell responses to touch. Exp Neurol 78:654–669.

Chapman CE, Jiang W, Lamarre Y (1988) Modulation of lemniscal input during conditioned arm movements in the monkey. Exp Brain Res 72:316–334.

Chen J-C, Hämmerer D, D'Ostilio K, Casula EP, Marshall L, Tsai C-H, Rothwell JC, Edwards MJ (2014) Bi-directional modulation of somatosensory mismatch negativity with transcranial direct current stimulation: an event related potential study. J Physiol 592:745–757.

Chhatbar PY, Kautz SA, Takacs I, Rowland NC, Revuelta GJ, George MS, Bikson M, Feng W (2018) Evidence of transcranial direct current stimulation-generated electric fields at subthalamic level in human brain in vivo. Brain Stimul 11:727–733.

Creutzfeld OD, Fromm GH, Kapp H (1962) Influence of transcortical dc-currents on cortical neuronal activity. Exp Neurol 5:436–452.

D'Mello AM, Turkeltaub PE, Stoodley CJ (2017) Cerebellar tDCS Modulates Neural Circuits during Semantic Prediction: A Combined tDCS-fMRI Study. J Neurosci 37:1604–1613.

D'Urso G, Ferrucci R, Bruzzese D, Pascotto A, Priori A, Altamura CA, Galderisi S, Bravaccio C (2014) Transcranial direct current stimulation for autistic disorder. Biol Psychiatry 76:1–2.

De Kock CPJ, Bruno RM, Spors H, Sakmann B (2007) Layer- and cell-type-specific suprathreshold stimulus representation in rat primary somatosensory cortex. J Physiol 581:139–154.

Deans JK, Powell AD, Jefferys JGR (2007) Sensitivity of coherent oscillations in rat hippocampus to AC electric fields. J Physiol 583:555–565.

Dieckhöfer A, Waberski TD, Nitsche M, Paulus W, Buchner H, Gobbelé R (2006) Transcranial direct current stimulation applied over the somatosensory cortex - Differential effect on low and high frequency SEPs. Clin Neurophysiol 117:2221–2227.

Diwakar S, Lombardo P, Solinas S, Naldi G, D'Angelo E (2011) Local field potential modeling predicts dense activation in cerebellar granule cells clusters under LTP and LTD control. PLoS One 6:e21928.

Dwyer GE, Craven AR, Hirnstein M, Kompus K, Assmus J, Ersland L, Hugdahl K, Grüner R (2019) No effects of anodal tDCS on local GABA and GLx levels in the left posterior superior temporal gyrus. Front Neurol 10:1–10.

Ekerot C, Jörntell H (2001) Parallel fibre receptive fields of Purkinje cells and interneurons are climbing fibre-specific. Eur J Neurosci 13:1303–1310.

Esse Wilson J, Quinn DK, Wilson JK, Garcia CM, Tesche CD (2018) Transcranial Direct Current Stimulation to the Right Temporoparietal Junction for Social Functioning in Autism Spectrum Disorder: A Case Report. J ECT 34:e10–e13.

Favorov O V., Nilaweera WU, Miasnikov AA, Beloozerova IN (2015) Activity of Somatosensory-Responsive Neurons in High Subdivisions of SI Cortex during Locomotion. J Neurosci 35:7763–7776.

Fernández M, Sierra-Arregui T, Peñagarikano O (2019) The Cerebellum and Autism: More than Motor Control. In: Behavioral Neuroscience.

Ferrucci R, Giannicola G, Rosa M, Fumagalli M, Boggio PS, Hallett M, Zago S, Priori A (2012) Cerebellum and processing of negative facial emotions: Cerebellar transcranial DC stimulation specifically enhances the emotional recognition of

facial anger and sadness. Cogn Emot 26:786–799.

Fiocchi S, Ravazzani P, Priori A, Parazzini M (2016) Cerebellar and spinal direct current stimulation in children: Computational modeling of the induced electric field. Front Hum Neurosci 10:1–13.

Fritsch B, Reis J, Martinowich K, Schambra HM, Ji Y, Cohen LG, Lu B (2010) Direct current stimulation promotes BDNF-dependent synaptic plasticity: Potential implications for motor learning. Neuron 66:198–204.

Fujimoto S, Kon N, Otaka Y, Yamaguchi T, Nakayama T, Kondo K, Ragert P, Tanaka S (2016) Transcranial direct current stimulation over the primary and secondary somatosensory cortices transiently improves tactile spatial discrimination in stroke patients. Front Neurosci 10:1–9.

Galea JM, Jayaram G, Ajagbe L, Celnik P (2009) Modulation of Cerebellar Excitability by Polarity-Specific Noninvasive Direct Current Stimulation. J Neurosci 29:9115–9122.

Galea JM, Vazquez A, Pasricha N, Orban De Xivry JJ, Celnik P (2011) Dissociating the roles of the cerebellum and motor cortex during adaptive learning: The motor cortex retains what the cerebellum learns. Cereb Cortex 21:1761–1770.

Garwicz M, Ekerot C-F, Jörntell H (1998) Organizational Principles of Cerebellar Neuronal Circuitry. News Physiol Sci 13:26–32.

Geborek P, Jörntell H, Bengtsson F (2013) Stimulation within the cuneate nucleus suppresses synaptic activation of climbing fibers. Front Neural Circuits 6:1–9.

Gómez L, Vidal B, Maragoto C, Morales L, Berrillo S, Vera Cuesta H, Baez M, Denis M, Marín T, Cabrera Y, Sánchez A, Alarcón C, Selguera M, Llanez Y, Dieguez L, Robinson M (2017) Non-Invasive Brain Stimulation for Children with Autism Spectrum Disorders: A Short-Term Outcome Study. Behav Sci (Basel) 7:63.

Grimaldi G, Argyropoulos GP, Bastian A, Cortes M, Davis NJ, Edwards DJ, Ferrucci R, Fregni F, Galea JM, Hamada M, Manto M, Miall RC, Morales-Quezada L, Pope PA, Priori A, Rothwell J, Tomlinson SP, Celnik P (2016) Cerebellar Transcranial Direct Current Stimulation (ctDCS): A Novel Approach to Understanding Cerebellar

Function in Health and Disease. Neuroscientist 22:83–97.

Grimaldi G, Argyropoulos GP, Boehringer A, Celnik P, Edwards MJ, Ferrucci R, Galea JM, Groiss SJ, Hiraoka K, Kassavetis P, Lesage E, Manto M, Miall RC, Priori A, Sadnicka A, Ugawa Y, Ziemann U (2014a) Non-invasive cerebellar stimulation - A consensus paper. Cerebellum 13:121–138.

Grimaldi G, Oulad Ben Taib N, Manto M, Bodranghien F (2014b) Marked reduction of cerebellar deficits in upper limbs following transcranial cerebello-cerebral DC stimulation: tremor reduction and re-programming of the timing of antagonist commands. Front Syst Neurosci 8:1–12.

Grossman N, Bono D, Dedic N, Kodandaramaiah SB, Rudenko A, Suk HJ, Cassara AM, Neufeld E, Kuster N, Tsai LH, Pascual-Leone A, Boyden ES (2017) Noninvasive Deep Brain Stimulation via Temporally Interfering Electric Fields. Cell 169:1029-1041.e16.

Gschwind M, Seeck M (2016) Transcranial direct-current stimulation as treatment in epilepsy. Expert Rev Neurother 16:1427–1441.

Guarienti F, Caumo W, Shiozawa P, Cordeiro Q, Boggio PS, Benseñor IM, Lotufo PA, Bikson M, Brunoni AR (2015) Reducing Transcranial Direct Current Stimulation-Induced Erythema With Skin Pretreatment: Considerations for Sham-Controlled Clinical Trials. Neuromodulation 18:261–265.

Hattori Y, Moriwaki A, Hori Y (1990) Biphasic effects of polarizing current on adenosine-sensitive generation of cyclic AMP in rat cerebral cortex. Neurosci Lett 116:320–324.

Herculano-Houzel S (2009) The human brain in numbers: a linearly scaled-up primate brain. Front Hum Neurosci 3:1–11.

Herculano-Houzel S (2012) The remarkable, yet not extraordinary, human brain as a scaled-up primate brain and its associated cost. Proc Natl Acad Sci 109:10661–10668.

Hertenstein E, Waibel E, Frase L, Riemann D, Feige B, Nitsche MA, Kaller CP, Nissen C

(2019) Modulation of creativity by transcranial direct current stimulation. Brain Stimul:1–9.

Hill AT, Rogasch NC, Fitzgerald PB, Hoy KE (2017) Effects of prefrontal bipolar and high-definition transcranial direct current stimulation on cortical reactivity and working memory in healthy adults. Neuroimage 152:142–157.

Holland R, Leff AP, Penny WD, Rothwell JC, Crinion J (2016) Modulation of frontal effective connectivity during speech. Neuroimage 140:126–133 Available at: http://dx.doi.org/10.1016/j.neuroimage.2016.01.037.

Holmes B, Jung SH, Lu J, Wagner JA, Rubbi L, Pellegrini M, Jankord R (2016) Transcriptomic Modification in the Cerebral Cortex following Noninvasive Brain Stimulation: RNA-Sequencing Approach. Neural Plast 2016:5942980.

Horvath JC, Carter O, Forte JD (2016) No significant effect of transcranial direct current stimulation (tDCS) found on simple motor reaction time comparing 15 different simulation protocols. Neuropsychologia 91:544–552.

Horvath JC, Forte JD, Carter O (2015) Evidence that transcranial direct current stimulation (tDCS) generates little-to-no reliable neurophysiologic effect beyond MEP amplitude modulation in healthy human subjects: A systematic review. Neuropsychologia 66:213–236.

Huang Y, Datta A, Bikson M, Parra LC (2019) Realistic volumetric-approach to simulate transcranial electric stimulation—ROAST—a fully automated open-source pipeline. J Neural Eng 16:056006.

Huang YZ, Lu MK, Antal A, Classen J, Nitsche M, Ziemann U, Ridding M, Hamada M, Ugawa Y, Jaberzadeh S, Suppa A, Paulus W, Rothwell J (2017) Plasticity induced by non-invasive transcranial brain stimulation: A position paper. Clin Neurophysiol 128:2318–2329.

Islam N, Aftabuddin M, Moriwaki A, Hattori Y, Hori Y (1995a) Increase in the calcium level following anodal polarization in the rat brain. Brain Res 684:206–208.

Islam N, Moriwaki A, Hattori Y, Hayashi Y, Lu YF, Hori Y (1995b) c-Fos expression

mediated by N-methyl-D-aspartate receptors following anodal polarization in the rat brain. Exp Neurol 133:25–31.

Islam N, Moriwaki A, Hattori Y, Hori Y (1994) Anodal polarization induces protein kinase C γ (PKCγ)-like immunoreactivity in the rat cerebral cortex. Neurosci Res 21:169–172.

Ito M (2002) Historical review of the significance of the cerebellum and the role of purkinje cells in motor learning. Ann N Y Acad Sci 978:273–288.

Jackson MP, Rahman A, Lafon B, Kronberg G, Ling D, Parra LC, Bikson M (2016) Animal models of transcranial direct current stimulation: Methods and mechanisms. Clin Neurophysiol 127:3425–3454.

Jackson MP, Truong D, Brownlow ML, Wagner JA, McKinley RA, Bikson M, Jankord R (2017) Safety parameter considerations of anodal transcranial Direct Current Stimulation in rats. Brain Behav Immun 64:152–161.

Jalali R, Chowdhury A, Wilson M, Miall RC, Galea JM (2018) Neural changes associated with cerebellar tDCS studied using MR spectroscopy. Exp Brain Res 236:997–1006.

Jamil A, Batsikadze G, Kuo HI, Labruna L, Hasan A, Paulus W, Nitsche MA (2017) Systematic evaluation of the impact of stimulation intensity on neuroplastic after-effects induced by transcranial direct current stimulation. J Physiol 595:1273–1288.

Jörntell H, Ekerot C-F (2006) Properties of Somatosensory Synaptic Integration in Cerebellar Granule Cells In Vivo. J Neurosci 26:11786–11797.

Kabakov AY, Muller PA, Pascual-Leone A, Jensen FE, Rotenberg A (2012) Contribution of axonal orientation to pathway-dependent modulation of excitatory transmission by direct current stimulation in isolated rat hippocampus. J Neurophysiol 107:1881–1889.

Kessler SK, Minhas P, Woods AJ, Rosen A, Gorman C, Bikson M (2013) Dosage Considerations for Transcranial Direct Current Stimulation in Children: A Computational Modeling Study. PLoS One 8:1–15.

Krause MR, Vieira PG, Csorba BA, Pilly PK, Pack CC (2019) Transcranial alternating current stimulation entrains single-neuron activity in the primate brain. Proc Natl Acad Sci U S A 116:5747–5755.

Krause MR, Zanos TP, Csorba BA, Pilly PK, Choe J, Phillips ME, Datta A, Pack CC (2017) Transcranial Direct Current Stimulation Facilitates Associative Learning and Alters Functional Connectivity in the Primate Brain. Curr Biol 27:3086-3096.e3.

Kronberg G, Bridi M, Abel T, Bikson M, Parra LC (2017) Direct Current Stimulation Modulates LTP and LTD: Activity Dependence and Dendritic Effects. Brain Stimul 10:51–58.

Küper M, Mallick JS, Ernst T, Kraff O, Thürling M, Stefanescu MR, Göricke S, Nitsche MA, Timmann D (2019) Cerebellar transcranial direct current stimulation modulates the fMRI signal in the cerebellar nuclei in a simple motor task. Brain Stimul 12:1169–1176.

Lawrenson CL, Watson TC, Apps R (2016) Transmission of Predictable Sensory Signals to the Cerebellum via Climbing Fiber Pathways Is Gated during Exploratory Behavior. J Neurosci 36:7841–7851.

Le Merre P, Esmaeili V, Charrière E, Galan K, Salin PA, Petersen CCH, Crochet S (2018) Reward-Based Learning Drives Rapid Sensory Signals in Medial Prefrontal Cortex and Dorsal Hippocampus Necessary for Goal-Directed Behavior. Neuron 97:83-91.e5.

Lee WH, Lisanby SH, Laine AF, Peterchev A V. (2015) Electric Field Model of Transcranial Electric Stimulation in Nonhuman Primates: Correspondence to Individual Motor Threshold. IEEE Trans Biomed Eng 62:2095–2105.

Leergaard TB, Lyngstad KA, Thompson JH, Taeymans S, Vos BP, De Schutter E, Bower JM, Bjaalie JG (2000) Rat somatosensory cerebropontocerebellar pathways: Spatial relationships of the somatotopic map of the primary somatosensory cortex are preserved in a three-dimensional clustered pontine map. J Comp Neurol 422:246–266.

Liebetanz D, Koch R, Mayenfels S, König F, Paulus W, Nitsche MA (2009) Safety limits of cathodal transcranial direct current stimulation in rats. Clin Neurophysiol 120:1161–1167.

Liu A, Vöröslakos M, Kronberg G, Henin S, Krause MR, Huang Y, Opitz A, Mehta A, Pack CC, Krekelberg B, Berényi A, Parra LC, Melloni L, Devinsky O, Buzsáki G (2018) Immediate neurophysiological effects of transcranial electrical stimulation. Nat Commun 9.

London BM, Miller LE (2013) Responses of somatosensory area 2 neurons to actively and passively generated limb movements. J Neurophysiol 109:1505–1513.

Lu H (2005) Correlations Between Purkinje Cell Single-Unit Activity and Simultaneously Recorded Field Potentials in the Immediately Underlying Granule Cell Layer. J Neurophysiol 94:1849–1860.

Mapelli J, D'Angelo E (2007) The Spatial Organization of Long-Term Synaptic Plasticity at the Input Stage of Cerebellum. J Neurosci 27:1285–1296.

Márquez-Ruiz J, Ammann C, Leal-Campanario R, Ruffini G, Gruart A, Delgado-García JM (2016) Synthetic tactile perception induced by transcranial alternating-current stimulation can substitute for natural sensory stimulus in behaving rabbits. Sci Rep 6:1–12.

Márquez-Ruiz J, Cheron G (2012) Sensory Stimulation-Dependent Plasticity in the Cerebellar Cortex of Alert Mice. PLoS One 7:e36184.

Márquez-Ruiz J, Leal-Campanario R, Sanchez-Campusano R, Molaee-Ardekani B, Wendling F, Miranda PC, Ruffini G, Gruart A, Delgado-García JM (2012) Transcranial direct-current stimulation modulates synaptic mechanisms involved in associative learning in behaving rabbits. Proc Natl Acad Sci 109:6710–6715.

Márquez-Ruiz J, Leal-Campanario R, Wendling F, Ruffini G, Gruart A, Delgado-García J (2014) Transcranial electrical-current stimulation in animals Javier. In: The Stimulated Brain.

Marron EM, Viejo-Sobera R, Cuatrecasas G, Redolar-Ripoll D, Lorda PG, Datta A, Bikson

M, Magerowski G, Alonso-Alonso M (2018) Prefronto-cerebellar neuromodulation affects appetite in obesity. Int J Obes:9–14.

Martins CW, de Melo Rodrigues LC, Nitsche MA, Nakamura-Palacios EM (2019) AMPA receptors are involved in prefrontal direct current stimulation effects on long-term working memory and GAP-43 expression. Behav Brain Res 362:208–212.

Matsugi A, Okada Y (2017) Cerebellar transcranial static magnetic field stimulation transiently reduces cerebellar brain inhibition. Funct Neurol 32:77–82.

Matsunaga K, Nitsche MA, Tsuji S, Rothwell JC (2004) Effect of transcranial DC sensorimotor cortex stimulation on somatosensory evoked potentials in humans. Clin Neurophysiol 115:456–460.

Menardy F, Varani AP, Combes A, Léna C, Popa D (2019) Functional Alteration of Cerebello-Cerebral Coupling in an Experimental Mouse Model of Parkinson's Disease. Cereb Cortex 29:1752–1766.

Miall RC, Antony J, Goldsmith-Sumner A, Harding SR, McGovern C, Winter JL (2016) Modulation of linguistic prediction by TDCS of the right lateral cerebellum. Neuropsychologia 86:103–109.

Miranda PC, Lomarev M, Hallett M (2006) Modeling the current distribution during transcranial direct current stimulation. Clin Neurophysiol 117:1623–1629.

Miterko LN et al. (2019) Consensus Paper: Experimental Neurostimulation of the Cerebellum. Cerebellum.

Modi ME, Sahin M (2017) Translational use of event-related potentials to assess circuit integrity in ASD. Nat Rev Neurol 13:160–170.

Modolo J, Denoyer Y, Wendling F, Benquet P (2018) Physiological effects of low-magnitude electric fields on brain activity: advances from in vitro, in vivo and in silico models. Curr Opin Biomed Eng 8:38–44.

Monai H, Ohkura M, Tanaka M, Oe Y, Konno A, Hirai H, Mikoshiba K, Itohara S, Nakai J, Iwai Y, Hirase H (2016) Calcium imaging reveals glial involvement in transcranial

direct current stimulation-induced plasticity in mouse brain. Nat Commun 7:1–10.

Morissette J, Bower JM (1996) Contribution of somatosensory cortex to responses in the rat cerebellar granule cell layer following peripheral tactile stimulation. Exp Brain Res 109:240–250.

Mostofi A, Holtzman T, Grout AS, Yeo CH, Edgley SA (2010) Electrophysiological Localization of Eyeblink-Related Microzones in Rabbit Cerebellar Cortex. J Neurosci 30:8920–8934.

Nagao S (2004) Pontine nuclei-mediated cerebello-cerebral interactions and its functional role. Cerebellum 3:11–15.

Nitsche M, Paulus W (2000) Excitability changes induced in the human motor cortex by weak transcranial direct current stimulation. J Physiol 527:633–639.

Nitsche MA, Cohen LG, Wassermann EM, Priori A, Lang N, Antal A, Paulus W, Hummel F, Boggio PS, Fregni F, Pascual-Leone A (2008) Transcranial direct current stimulation: State of the art 2008. Brain Stimul 1:206–223.

Nitsche MA, Niehaus L, Hoffmann KT, Hengst S, Liebetanz D, Paulus W, Meyer BU (2004) MRI study of human brain exposed to weak direct current stimulation of the frontal cortex. Clin Neurophysiol 115:2419–2423.

Notturno F, Pace M, Zappasodi F, Cam E, Bassetti CL, Uncini A (2014) Neuroprotective effect of cathodal transcranial direct current stimulation in a rat stroke model. J Neurol Sci 342:146–151.

Odeh F, Ackerley R, Bjaalie JG, Apps R (2005) Pontine Maps Linking Somatosensory and Cerebellar Cortices Are in Register with Climbing Fiber Somatotopy. J Neurosci 25:5680–5690.

Oldrati V, Schutter DJLG (2018) Targeting the Human Cerebellum with Transcranial Direct Current Stimulation to Modulate Behavior: a Meta-Analysis. Cerebellum 17:228–236.

Oliviero A, Mordillo-Mateos L, Arias P, Panyavin I, Foffani G, Aguilar J (2011) Transcranial

static magnetic field stimulation of the human motor cortex. J Physiol 589:4949–4958.

Opitz A, Falchier A, Linn GS, Milham MP, Schroeder CE (2017) Limitations of ex vivo measurements for in vivo neuroscience. Proc Natl Acad Sci 114:5243–5246.

Opitz A, Falchier A, Yan CG, Yeagle EM, Linn GS, Megevand P, Thielscher A, Deborah RA, Milham MP, Mehta AD, Schroeder CE (2016) Spatiotemporal structure of intracranial electric fields induced by transcranial electric stimulation in humans and nonhuman primates. Sci Rep 6:1–11.

Ozen S, Sirota A, Belluscio MA, Anastassiou CA, Stark E, Koch C, Buzsaki G (2010) Transcranial Electric Stimulation Entrains Cortical Neuronal Populations in Rats. J Neurosci 30:11476–11485.

Parasuram H, Nair B, Naldi G, D'Angelo E, Diwakar S (2018) Understanding Cerebellum Granular Layer Network Computations through Mathematical Reconstructions of Evoked Local Field Potentials. Ann Neurosci 25:11–24.

Parazzini M, Rossi E, Ferrucci R, Liorni I, Priori A, Ravazzani P (2014) Modelling the electric field and the current density generated by cerebellar transcranial DC stimulation in humans. Clin Neurophysiol 125:577–584.

Parent A (2004) Giovanni Aldini: From Animal Electricity to Human Brain Stimulation. Can J Neurol Sci 31:576–584.

Patel HJ, Romanzetti S, Pellicano A, Nitsche MA, Reetz K, Binkofski F (2019) Proton Magnetic Resonance Spectroscopy of the motor cortex reveals long term GABA change following anodal Transcranial Direct Current Stimulation. Sci Rep 9:1–8.

Paxinos G, Franklin KBJ (2004) The mouse brain in stereotaxic coordinates, Second edition.

Peron SP, Freeman J, Iyer V, Guo C, Svoboda K (2015) A Cellular Resolution Map of Barrel Cortex Activity during Tactile Behavior. Neuron 86:783–799.

Person AL, Raman IM (2012) Purkinje neuron synchrony elicits time-locked spiking in the

cerebellar nuclei. Nature 481:502–505.

Petersen CCH (2007) The functional organization of the barrel cortex. Neuron 56:339–355.

Pikhovych A, Stolberg NP, Jessica Flitsch L, Walter HL, Graf R, Fink GR, Schroeter M, Rueger MA (2016) Transcranial Direct Current Stimulation Modulates Neurogenesis and Microglia Activation in the Mouse Brain. Stem Cells Int 2016:1–9.

Pinault D (1996) A novel single-cell staining procedure performed in vivo under electrophysiological control: Morpho-functional features of juxtacellularly labeled thalamic cells and other central neurons with biocytin or Neurobiotin. J Neurosci Methods 65:113–136.

Pinault D (2017) A neurophysiological perspective on a preventive treatment against schizophrenia using transcranial electric stimulation of the corticothalamic pathway. Brain Sci 7:brainsci7040034.

Pirulli C, Fertonani A, Miniussi C (2014) Is neural hyperpolarization by cathodal stimulation always detrimental at the behavioral level? Front Behav Neurosci 8:1–10.

Polanía R, Paulus W, Nitsche MA (2012) Modulating cortico-striatal and thalamo-cortical functional connectivity with transcranial direct current stimulation. Hum Brain Mapp 33:2499–2508.

Pope PA, Miall RC (2012) Task-specific facilitation of cognition by cathodal transcranial direct current stimulation of the cerebellum. Brain Stimul 5:84–94.

Priori A, Berardelli A, Rona S, Accorneo N, Manfredi M (1998) Polarization of the human motor cortex thourgh the scalp. Neuroreport 9:2257–2260.

Proville RD, Spolidoro M, Guyon N, Dugue GP, Selimi F, Isope P, Popa D, Lena C (2014) Cerebellum involvement in cortical sensorimotor circuits for the control of voluntary movements. Nat Neurosci 17:1233–1239.

Purpura D, McMurtry J (1964) Intracellular Activities and Evoked Potential Changes

During Polarization of Motor Cortex. J Neurophysiol 28:166–185.

Radman T, Ramos R, Brumberg J, Bikson M (2009) Role of Cortical Cell Type and Morphology in Sub- and Suprathreshold Uniform Electric Field Stimulation. Brain Stimul 2:215–228.

Ragert P, Vandermeeren Y, Camus M, Cohen LG (2008) Improvement of spatial tactile acuity by transcranial direct current stimulation. Clin Neurophysiol 119:805–811.

Rahman A, Reato D, Arlotti M, Gasca F, Datta A, Parra LC, Bikson M (2013) Cellular effects of acute direct current stimulation: Somatic and synaptic terminal effects. J Physiol 591:2563–2578.

Rahman A, Toshev PK, Bikson M (2014) Polarizing cerebellar neurons with transcranial Direct Current Stimulation. Clin Neurophysiol J 125:435–438.

Ramnani N (2006) The primate cortico-cerebellar system: Anatomy and function. Nat Rev Neurosci 7:511–522.

Ranieri F, Podda M V., Riccardi E, Frisullo G, Dileone M, Profice P, Pilato F, Di Lazzaro V, Grassi C (2012) Modulation of LTP at rat hippocampal CA3-CA1 synapses by direct current stimulation. J Neurophysiol 107:1868–1880.

Reato D, Rahman A, Bikson M, Parra LC (2010) Low-Intensity Electrical Stimulation Affects Network Dynamics by Modulating Population Rate and Spike Timing. J Neurosci 30:15067–15079.

Reed T, Cohen Kadosh R (2018) Transcranial electrical stimulation (tES) mechanisms and its effects on cortical excitability and connectivity. J Inherit Metab Dis 41:1123–1130.

Regner GG, Pereira P, Leffa DT, de Oliveira C, Vercelino R, Fregni F, Torres ILS (2018) Preclinical to clinical translation of studies of transcranial direct-current stimulation in the treatment of epilepsy: A systematic review. Front Neurosci 12.

Reinhart RMG, Zhu J, Park S, Woodman GF (2015a) Medial-Frontal Stimulation Enhances Learning in Schizophrenia by Restoring Prediction Error Signaling. J Neurosci

35:12232–12240.

Reinhart RMG, Zhu J, Park S, Woodman GF (2015b) Synchronizing theta oscillations with direct-current stimulation strengthens adaptive control in the human brain. Proc Natl Acad Sci 112:9448–9453.

Rezaee Z, Dutta A (2019) Cerebellar lobules optimal stimulation (CLOS): A computational pipeline to optimize cerebellar lobule-specific electric field distribution. Front Neurosci 13:1–16.

Rogalewski A, Breitenstein C, Nitsche M a, Paulus W, Knecht S (2004) SHORT COMMUNICATION Transcranial direct current stimulation disrupts tactile perception. Eur J Neurosci 20:2001–2004.

Roggeri L, Rivieccio B, Rossi P, D'Angelo E (2008) Tactile Stimulation Evokes Long-Term Synaptic Plasticity in the Granular Layer of Cerebellum. J Neurosci 28:6354–6359.

Rossi S, Hallett M, Rossini P, Pascual-Leone A, Consensus TSG of T (2009) Safety, ethical considerations, and application guidelines for the use of transcranial magnetic stimulation in clinical practice and research. Clin Neurophysiol 120:2008–2039.

Rueger MA, Keuters MH, Walberer M, Braun R, Klein R, Sparing R, Fink GR, Graf R, Schroeter M (2012) Multi-session transcranial direct current stimulation (tDCS) Elicits inflammatory and regenerative processes in the rat brain. PLoS One 7:e43776.

Ruffini G, Fox MD, Ripolles O, Miranda PC, Pascual-Leone A (2014) Optimization of multifocal transcranial current stimulation for weighted cortical pattern targeting from realistic modeling of electric fields. Neuroimage 89:216–225.

Salehinejad MA, Wischnewski M, Nejati V, Vicario CM, Nitsche MA (2019) Transcranial direct current stimulation in attention-deficit hyperactivity disorder: A meta-analysis of neuropsychological deficits. PLoS One 14:1–26.

Sánchez-León CA, Ammann C, Medina JF, Márquez-Ruiz J (2018a) Using Animal Models to Improve the Design and Application of Transcranial Electrical Stimulation in Humans. Curr Behav Neurosci Reports 5:125–135.

Sánchez-León CA, Sánchez-López Á, Ammann C, Cordones I, Carretero-Guillén A, Márquez-Ruiz J (2018b) Exploring new transcranial electrical stimulation strategies to modulate brain function in animal models. Curr Opin Biomed Eng 8:7–13.

Sarmiento CI, San-Juan D, Prasath VBS (2016) Letter to the Editor: Brief history of transcranial direct current stimulation (tDCS): From electric fishes to microcontrollers. Psychol Med 46:3259–3261.

Sasaki K, Kawaguchi S, Yoneda Y (1969) Responses Evoked By the in the Stimulation Cortex. Jpn J Physiol 19:95–109.

Schmahmann JD (2001) The cerebrocerebellar system: Anatomic substrates of the cerebellar contribution to cognition and emotion. Int Rev Psychiatry 13:247–260.

Schmahmann JD, Sherman JC (1998) The cerebellar cognitive affective syndrome. Brain 121:561–579.

Shinoda Y, Sugiuchi Y, Futami T (1987) Excitatory inputs to cerebellar dentate nucleus neurons from the cerebral cortex in the cat. Exp Brain Res 67:299–315.

Spampinato D, Celnik P (2017) Temporal dynamics of cerebellar and motor cortex physiological processes during motor skill learning. Sci Rep 7:1–12.

Stafford J, Brownlow ML, Qualley A, Jankord R (2018) AMPA receptor translocation and phosphorylation are induced by transcranial direct current stimulation in rats. Neurobiol Learn Mem 150:36–41.

Stagg CJ, Antal A, Nitsche MA (2018) Physiology of Transcranial Direct Current Stimulation. J ECT 34:144–152.

Stagg CJ, Best JG, Stephenson MC, O'Shea J, Wylezinska M, Kincses ZT, Morris PG, Matthews PM, Johansen-Berg H (2009) Polarity-Sensitive Modulation of Cortical Neurotransmitters by Transcranial Stimulation. J Neurosci 29:5202–5206.

Stoodley CJ, D'Mello AM, Ellegood J, Jakkamsetti V, Liu P, Nebel MB, Gibson JM, Kelly E, Meng F, Cano CA, Pascual JM, Mostofsky SH, Lerch JP, Tsai P (2017) Altered cerebellar connectivity in autism and cerebellar-mediated rescue of autism-related

behaviors in mice. Nat Neurosci 20:1744–1751.

Sugawara K, Onishi H, Yamashiro K, Kojima S, Miyaguchi S, Kirimoto H, Tsubaki A, Tamaki H, Shirozu H, Kameyama S (2015) The effect of anodal transcranial direct current stimulation over the primary motor or somatosensory cortices on somatosensory evoked magnetic fields. Clin Neurophysiol 126:60–67.

Sun Y, Lipton JO, Boyle LM, Madsen JR, Goldenberg MC, Pascual-Leone A, Sahin M, Rotenberg A (2016) Direct current stimulation induces mGluR5-dependent neocortical plasticity. Ann Neurol 80:233–246.

Swenson RS, Sievert CF, Terreberry RR, Neafsey EJ, Castro AJ (1989) Organization of cerebral cortico-olivary projections in the rat. Neurosci Res 7:43–54.

Vaseghi B, Zoghi M, Jaberzadeh S (2015) Differential effects of cathodal transcranial direct current stimulation of prefrontal, motor and somatosensory cortices on cortical excitability and pain perception - a double-blind randomised sham-controlled study. Eur J Neurosci 42:2426–2437.

Voogd J, Glickstein M (1998) The anatomy of the cerebellum. Cerebellum 21:370–375.

Vöröslakos M, Takeuchi Y, Brinyiczki K, Zombori T, Oliva A, Fernández-Ruiz A, Kozák G, Kincses ZT, Iványi B, Buzsáki G, Berényi A (2018) Direct effects of transcranial electric stimulation on brain circuits in rats and humans. Nat Commun 9.

Watson TC, Jones MW, Apps R (2009) Electrophysiological mapping of novel prefrontal – cerebellar pathways. Front Integr Neurosci 3:1–11.

Wexler A (2017) Recurrent themes in the history of the home use of electrical stimulation: Transcranial direct current stimulation (tDCS) and the medical battery (1870–1920). Brain Stimul 10:187–195.

Woodman GF (2010) A brief introduction to the use of Event-Related Potentials (ERPs) in studies of perception and attention. Attention, Perception, Psychophys 72:1–29.

Woolsey TA, Van der Loos H (1970) The structural organization of layer IV in the somatosensory region (SI) of mouse cerebral cortex. The description of a cortical

field composed of discrete cytoarchitectonic units. Brain Res 17:205–242.

Wu CH (1984) Electric fish and the discovery of animal electricity. Am Sci 72:598–607.

Yamashita T, Petersen CCH (2016) Target-specific membrane potential dynamics of neocortical projection neurons during goal-directed behavior. Elife 5:1–11.

Yosephi MH, Ehsani F, Zoghi M, Jaberzadeh S (2018) Multi-session anodal tDCS enhances the effects of postural training on balance and postural stability in older adults with high fall risk: Primary motor cortex versus cerebellar stimulation. Brain Stimul 11:1239–1250.

Zembrzycki A, Chou SJ, Ashery-Padan R, Stoykova A, O'Leary DDM (2013) Sensory cortex limits cortical maps and drives top-down plasticity in thalamocortical circuits. Nat Neurosci 16:1060–1067.

Zuchowski ML, Timmann D, Gerwig M (2014) Acquisition of conditioned eyeblink responses is modulated by cerebellar tDCS. Brain Stimul 7:525–531.

Zucker RS, Regehr WG (2002) Short-Term Synaptic Plasticity. 64:355–405.